Impurity Physics in Resonant X-Ray Scattering and Ultracold Atomic Gases

Impurity Physics in Resonant X-Ray Scattering and Ultracold Atomic Gases

a dissertation presented
by
David Isaiah Benjamin
to
The Department of Physics

in partial fulfillment of the requirements
for the degree of
Doctor of Philosophy
in the subject of
Physics

Harvard University
Cambridge, Massachusetts
September 2014

Thesis advisor: Professor Eugene Demler David Isaiah Benjamin

Impurity Physics in Resonant X-Ray Scattering and Ultracold Atomic Gases

Abstract

This thesis presents work on theoretical tools used to study transient and quantum-fluctuating impurity potentials that arise in resonant x-ray scattering and ultracold atomic gases. These tools fall under two main classes, functional determinants for exact evaluation of many-fermion matrix elements, and the variational polaron transformation. The following work carefully introduces both approaches and compares theoretical predictions to known experimental and computational results. In several cases this thesis presents arguments that experiments on high-temperature superconducting cup rates must be reinterpreted in terms of a quasiparticle picture. Where no experimental data exist, predictions are made and suggestions given for new uses for simple experimental techniques. For example, indirect resonant inelastic x-ray scattering turns out to be a versatile pseudo gap probe, and radio frequency absorption of a fermi gas with an impurity can detect a repulsively-bound state.

Contents

Citations to Previously Published Work

Chapter 1 is based on
"Microscopic Theory of Resonant Soft-X-Ray Scattering in Materials with Charge Order: The Example of Charge Stripes in High-Temperature Cuprate Superconductors",
David Benjamin, Dmitry Abanin, Peter Abbamonte, and Eugene Demler
Phys. Rev. Lett. **110**, 137002 (2013)

Chapter 2 is based on unpublished work submitted to Phys. Rev. X:
"Probing Competing and Intertwined Orders with Resonant Inelastic x-ray Scattering in the Hole-Doped Cuprates",
David Benjamin, Israel Klich, and Eugene Demler
arXiv:1407.3843

Chapter 3 is based on:
"Single-Band Model of Resonant Inelastic X-Ray Scattering by Quasiparticles in High-T_c Cuprate Superconductors",
David Benjamin, Israel Klich, and Eugene Demler
Phys. Rev. Lett. **112**, 247002 (2014)

Chapter 4 is based on:
"Variational polaron method for Bose-Bose mixtures",
David Benjamin and Eugene Demler
Phys. Rev. A **89**, 033615 (2014)

Acknowledgments

I owe my career in science to my parents, who gave me many tools of the physicist's mind and a distaste for knowledge without understanding. Camping knots, soldering copper pipe, history conversations on evening dog walks, pitching mechanics, and a wonderful three-year experiment with home-schooling all led me to pursue physics. Above all, though, they taught me that one's abilities must be used to doing something good for the world.

More recently, I am indebted to my advisor, Eugene Demler. He steadily believed in me while I slowly became a competent scientist and endured much aggravation trying (successfully, I think) to extinguish my bad habits. In addition to his immense knowledge of physics, Eugene taught me to place intuition at the core of an argument and to be skeptical of heavy theoretical machinery when a simple calculation will do. I will never forget his rule to limit presentations to one equation, zero if possible. Thanks to Eugene I don't think I could ever tolerate working conditions without long conversations at a chalkboard. I carry all of his lessons with me as I begin a career in computational biology.

In addition to Eugene I am grateful to my collaborators Dima Abanin, Peter Abbamonte, Israel Klich, Emmanuele Dalla Torre, and Richard Schmidt. I especially thank Dima for teaching me the method of functional determinants after realizing that it provided the missing link to my project on REXS. His help led to my first publication and to several chapters of this thesis.

I am grateful to David Morin for coordinating the Harvard physics department's teaching and and for assigning me to courses with fresh challenges whenever I asked. He takes seriously requests to teach graduate solids one year and undergraduate quantum mechanics the next. He helped me stay afloat by repeating courses while my son was an infant. I have learned a lot about teaching from the professors with whom I taught. Logan McCarthy and Vinothan Manoharan showed me how to respect non-scientists' efforts in physics and to enjoy helping them. Subir Sachdev showed me that one can teach quantum field theory to undergraduates. From Howard Georgi I learned how to entertain students without wasting their time and to teach better by lecturing less. I completed my teaching career at Harvard with Eugene's very successful and very fun new course on group theory and topology.

In addition to those who helped me make the most of my time at Harvard, Jacob Barandes has helped me continually in the last year in my job search. I got in touch with everyone he ever mentioned to me and received an enormous amount of advice about all the options I considered. Thanks to this help, I begin the next step in my scientific career at the Broad Institute confident that I have chosen correctly.

Finally, I thank my wife Irina for her support during the long road of graduate school. As much I might sometimes wish for superhuman capacity for work, the fact is that I do not, and her companionship has maintained my sanity. She has encouraged me for seven years, one year past the end of her own PhD that she finished while raising our son Aron. And, if I make a name for myself in my new career, I learned about SNPs and GWAS studies first from her.

0

Introduction

Problems involving the behavior of an impurity embedded in a larger system, such as a Fermi sea or a Bose superfluid, have a long history in condensed matter physics. In addition to their practical importance they are a fertile source of toy models and test cases for theoretical techniques. In this thesis I present several examples where I have applied theoretical machinery with an "impurity physics" flavor to problems that (with one exception) would not be considered impurity problems.

We begin with several chapters on the formalism of resonant elastic x-ray scattering (REXS) and resonant inelastic x-ray scattering (RIXS). Although the experiments we seek to describe are performed on homogeneous systems, resonant x-ray scattering inherently involves a transient impurity in the form of a hole left behind when an energetic photon excites a core electron into a conduction band. In each of these chapters I advance several goals in parallel.

First, I am interested in developing theoretical formalism to describe RIXS and REXS. In all types of resonant x-ray experiments, experimental progress has far outpaced theoretical analyses due to the rapid improvement of instrumentation. In fact, it is only in the last fifteen years that has energy resolution has shrunk below 1 eV. Consequently it is very common to find analyses of RIXS and REXS that attempt to exploit analogies to other experimental probes. Unfortunately, such analogies often turn out to be non-existent when one actually calculates the intensity of scattered x-rays. For example, it is common in studies of direct RIXS to calculate the structure factor $S(\mathbf{k}, \omega)$ in some proposed model and compare it to the RIXS intensity at momentum transfer $\mathbf{k}$ and energy transfer ω. As we will see, however, RIXS is not neutron scattering and its intensity is not a structure factor.

Second, I want to find general qualitative patterns exhibited in resonant x-ray scattering data and discover the intuitive theoretical reasons for these patterns. Such a vocabulary of phenomena related to resonant x-ray scattering is of great interest to experimentalists who need to know how to interpret their data. It will also prove useful in predicting what sort of information an experiment can, in principle, reveal. The work presented in this thesis therefore addresses the question of what REXS and RIXS can do that neutron scattering and ARPES cannot. One example of a pattern whose origin is revealed by quantitative analysis, in chapter 1 I discuss the presence of peaks in REXS

data and relate it to nesting of isoenergy contours of the quasiparticle dispersion. Another, discussed in chapter 3, is a polarization-dependent shift in direct RIXS spectra that turns out to come from the combination of a core hole potential and the Pauli exclusion principle. It is important to realize that both these interpretations are not only filling a void of intuition about resonant x-ray scattering. Rather, they supplant extremely tempting interpretations that are apparently obvious – until one actually performs a calculation of REXS or RIXS intensities. These prevailing interpretations of data will be discussed in chapters 1 and 3. The content of chapter 2, on indirect RIXS, is relatively uncontroversial as it attempts to provide guidance about experiments that have yet to be performed and have not yet developed an orthodox opinion.

In contrast to the first two goals, which were related to bringing the field of resonant x-ray scattering closer to maturity, the third goal of these chapters is to use REXS and RIXS to answer questions about the high-temperature cuprate superconductors. One major theme in the last decade of work on the cuprates has been the emergence of experiments that in some respects they behave more like Fermi liquids than had previously been thought. Most dramatically, magnetic oscillations experiments have revealed incontrovertible signatures of a Fermi surface. This is not to say that the cuprates *are* Fermi liquids (except at large overdoping), but rather that weakly-coupled approaches may be a reasonable starting point for describing these materials, at least as far as some experiments are concerned. It also must be remembered that strongly-coupled models may yield effective weakly-coupled physics. In this thesis I will argue that data from resonant x-ray experiments support a quasiparticle interpretation of cuprate phenomenology. Having said that, REXS and RIXS remain in their adolescence, each with only a handful of significant experiments that still have not nearly mapped out the entire phase diagram. Despite my own opinions, my aim in this thesis is to

convince skeptics that a quasiparticle interpretation of cuprate experiments should not be dismissed *a priori* as outlandish. I hope that future experiments, along with analyses that calculate the scattered intensity itself and not some (assumed) proxy, will help to settle debates about the cuprates.

After the discussion of resonant x-ray scattering, we continue in chapter 4 with a treatment of the variational polaron transformation and its application to mixtures of two atomic Bose gases. The polaron transformation is well known to most condensed matter physicists. It is, however, not applicable for a wide range of parameters because it is inflexible – it yields polarons with a constant shape. As shown in chapter 4, this is not an inherent deficiency of the polaron transformation and a variational extension of the method is fairly straightforward. Previous work has used a variational polaron tranformation to analyze a single impurity in a bath, but to my knowledge such formalism has never before been applied to a mixture, in which case the variational polarons must be optimized self-consistently among many particles. It turns out, however, that this procedure is actually not much harder than the single polaron case.

Finally, we conclude with the problem of RF absorption of a mobile impurity particle in an ultracold atomic gas, in which only the final state of the impurity interacts with the bath. This is the famous othogonality catastrophe problem of x-ray absorption, but with a finite-mass particle rather than a static potential. After several transformations we recast the problem as one of a single Hubbard-Stratonovich field and fermion bath with a field-dependent potential. The thesis comes full circle when we exploit the method of functional determinants previously used to describe resonant x-ray scattering to integrate out the fermions. We thereby obtain an effective field theory of the Hubbard-Stratonovich field that can be integrated analytically.

Before we proceed with the work described above, a brief summary of the different

types of resonant x-ray scattering will prove useful.

0.1 Resonant x-ray scattering

Like any photon scattering experiment, resonant x-ray scattering involves an incoming photon with momentum $\mathbf{k}_i$, energy ω, and polarization η_i; and an outgoing photon with momentum $\mathbf{k}_f = \mathbf{k}_i - \Delta\mathbf{k}$, energy $\omega - \Delta\omega$, and polarization η_f. By conservation of momentum and energy, $\Delta\mathbf{k}$ and $\Delta\omega$ are the momentum and energy of excitations left behind in the system. To appreciate resonant x-ray scattering, we must first briefly consider non-resonant x-ray scattering. There the intensity of scattered radiation is given by the first-order Thompson formula

$$I \propto \sum_f |\langle f|\rho_{\Delta\mathbf{k}}|i\rangle(\eta_f \cdot \eta_i)|^2 \, \delta(E_f - E_i - \Delta\omega), \tag{1}$$

where $|i\rangle$ and $|f\rangle$ are the initial and final electron states, with energies E_i and E_f, and ρ is the electron density operator. In addition to an uninteresting dependence on the final state, the Thompson scattering formula is sensitive to the total density of electrons and therefore receives its main contribution from core electrons by virtue of their quantity. Resonant x-ray scattering is achieved when the incident photon energy ω is near the energy of a transition from a core state to an unoccupied state near the Fermi level. Under this condition, the second-order amplitude of processes containing an intermediate state, which exists transiently between absorption and re-emission, with an added x-ray photoelectron above the Fermi level can exceed that of first-order scattering. The resonance from this intermediate state is often sufficiently strong to dominate the first order amplitude, whence straightfroward perturbation theory gives

the Kramers-Heisenberg formula for the scattered intensity:

$$I \propto \sum_f \left| \sum_n \frac{\langle f|\mathbf{p}(\mathbf{k}_f)\cdot\eta_f|n\rangle\langle n|\mathbf{p}(-\mathbf{k}_i)|i\rangle}{E_n - E_i - \omega} \right|^2 \delta(E_f - E_i - \Delta\omega - i\Gamma), \tag{2}$$

where the new ingredients are the intermediate state $|n\rangle$, the core-hole decay rate Γ, and the momentum operator (in first-quantized notation) $\mathbf{p}(\mathbf{k}) = \sum_m \mathbf{p}_m e^{-i\mathbf{k}\cdot\mathbf{r}_m}$. Note that the intermediate state energy E_n includes the interaction between valence electrons and a core hole left behind by the photoexcited electron. Projecting out all but the resonant contribution*, we have, up to a polarization-dependent prefactor (see Appendix E for an explicit calculation),

$$I \propto \sum_f \left| \sum_n \frac{\langle f|T^\dagger(\mathbf{k}_f)|n\rangle\langle n|T(\mathbf{k}_i)|i\rangle}{E_n - E_i - \omega - i\Gamma} \right|^2 \delta(E_f - E_i - \Delta\omega), \tag{3}$$

where $T(\mathbf{k}) = \sum_m e^{-i\mathbf{k}\cdot\mathbf{r}_m} d_m^\dagger c_m$ is a dipole transition operator in which c_m annihilates a core electron and $d_m^\dagger$ creates an excited photoelectron at site m, that is, it is the creation operator corresponding to a Wannier orbital at position $\mathbf{r}_m$. For the case of multiple excited bands, one must also sum over bands, with each band weighted by its own dipole matrix element. We will not consider the case of multiple bands in this thesis, although the formalism developed below extends in an obvious way. Although the core-to-valence band resonance can amplify the intensity of second-order scattering by over three orders of magnitude, this amplification does not suffice to make dipole-forbidden resonant transitions detectable over Thompson scattering. Thus the only possibilities we consider are those that are realized in experiments on the cuprates: $1s \to 4p$ and

*A non-elemental material will have several possible core level resonances, but barring coincidence their energies ω will not overlap.

$2p \rightarrow 3d$ transitions. Finally, the core hole is generally immobile, so absorption and re-emission must occur at the same site. This causes the Kramers-Heisenberg formula to simplify to

$$I \propto \sum_f \left| \sum_n \sum_m e^{-i\Delta\mathbf{k}\cdot\mathbf{r}_m} \frac{\langle f|d_m c_m^\dagger|n\rangle\langle n|d_m^\dagger c_m|i\rangle}{E_n - E_i - \omega - i\Gamma} \right|^2 \delta(E_f - E_i - \Delta\omega), \tag{4}$$

Having introduced the basic equation describing resonant x-ray phenomena, we now discuss the different flavors of experiments.

0.2 REXS and Direct RIXS

In direct scattering, the resonance is chosen so that the core electron is photoexcited to a valence band intersecting the Fermi level, or to a band just above the Fermi level. The essential feature is that the electron is injected into the band in which most of the interesting physics of the system is expected to occur. Although the distinction between elastic scattering (REXS) (which is always performed under direct RIXS conditions) and inelastic scattering (RIXS) is quantitatively a matter of adjusting $\Delta\omega$, they serve qualitatively distinct purposes. Fig. 1 shows the simplest possible RIXS process containing only absorption and re-emission, i.e. with trivial transient state dynamics. The process shown is inelastic because the photoelectron added to the system is more energetic than the electron that re-fills the core hole. That is, a particle-hole excitation is added to the system. It is also possible for the photoelectron to scatter during the transient state, a process that also yields inelastic scattering. Similarly, one can have elastic scattering if the photoelectron scatters elastically. This can occur if the scattering is due to period order, such as a charge density wave. Therefore, with slight modification Fig. 1 also describes REXS.

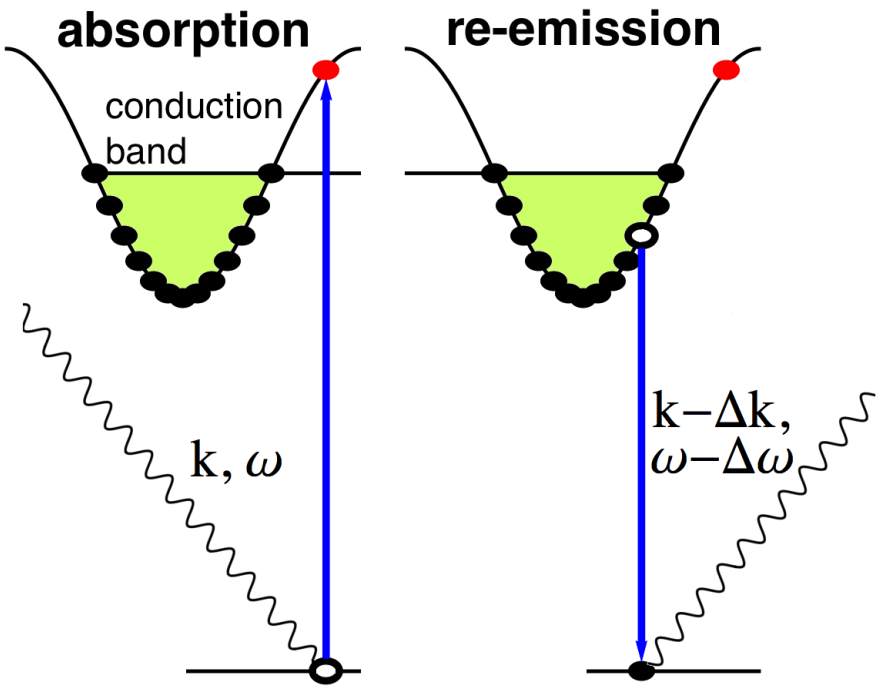

Figure 1: Simple schematic of RIXS. A photon is absorbed, promoting a core electron to the conduction band. Subsequently, another conduction electron re-fills the core hole and emits a photon.

If we could ignore the core hole potential, we could drop the operators $c^\dagger$ and c and absorb the constant core hole energy into ω. Furthermore, $|i\rangle$ and $|n\rangle$ are, in this case, eigenstates of the same valence electron Hamiltonian H. The matrix elements of elastic scattering in this approximation correspond to a thought experiment in which an electron is added to site m and some time later destroyed at the same site. To see this more explicitly, we apply the identity

$$\frac{1}{z} = \int_0^\infty e^{-itz}\, dt \tag{5}$$

to the resonant denominator of the Kramers-Heisenberg formula to obtain

$$\sum_n \frac{\langle i|d_m c_m^\dagger|n\rangle\langle n|d_m^\dagger c_m|i\rangle}{E_n - E_i - \omega - i\Gamma} \rightarrow \sum_n \frac{\langle i|d_m|n\rangle\langle n|d_m^\dagger|i\rangle}{E_n - E_i - \omega - i\Gamma} \tag{6}$$

$$= \sum_n \int_0^\infty e^{-i(E_n - E_i - \omega)t} e^{-\Gamma t} \langle i|d_m|n\rangle\langle n|d_m^\dagger|i\rangle\, dt \tag{7}$$

$$= \int_0^\infty e^{i\omega t} e^{-\Gamma t} \langle i|d_m e^{-iHt} \sum_n |n\rangle\langle n| d_m^\dagger e^{iHt}|i\rangle\, dt \tag{8}$$

$$= \int_0^\infty e^{i\omega t} e^{-\Gamma t} \langle i|d_m e^{-iHt} d_m^\dagger e^{iHt}|i\rangle\, dt, \tag{9}$$

which is precisely the Green function at frequency ω for an electron introduced to site m to propagate back to the same site m, modified by a decay rate Γ. To obtain the REXS intensity, this Green function is squared, and *then* Fourier-transformed via $\sum_m e^{-i\Delta\mathbf{k}\cdot\mathbf{r}_m}$. If these two operations, taking the square and Fourier-transforming, could be commuted, REXS would, in the limit of no core hole potential, measure a single-electron Green function as directly as angle-resolved photoemission spectroscopy (ARPES) measures a spectral function. Although this is, of course, not possible, it remains true that REXS is the Fourier-transform of some site-dependent quantity –

the squared frequency-dependent Green function for an electron created at that site to be found later at the same site – and therefore translational symmetry breaking is a necessary condition for a non-vanishing REXS signal. In fact, REXS can be thought of as valence-selective diffraction, and has been used to detect charge and orbital order in correlated materials. This qualitative picture is not changed much by the core hole potential. The difference is that a core hole potential must be added to the Hamiltonian H in the transient state propagator. However it remains true that only translational symmetry breaking produces a signal at non-zero momentum.

While the primary purpose of REXS is to reveal properties of the ground state in the form of translational symmetry breaking, direct RIXS measures the energy and momentum of excitations. Two broad categories of excitation are possible. First, there can be particle-hole pairs left behind by zeroth-order processes in which the core hole is filled by an electron from an unoccupied state lower in energy than the excited photoelectron state. Secondly, the photoelectron may interact with other valence electrons and create an excitation. The range of excitations that direct RIXS can produce is very promising, but it is also a complication that has so far been unappreciated in the literature. In this sense, indirect RIXS is superior because it decouples the photoexcited electron from the excitations that it measures. However, it is wholly dependent of the core hole interaction and does not exhibit the variety of direct RIXS. While the work in this thesis only explores direct RIXS and indirect RIXS separately, it would be interesting for future work to examine to what extent indirect RIXS could complement direct RIXS as a means of disentangling different contributions.

0.3 Indirect RIXS

In this last form of resonant x-ray scattering the photon energy is tuned to a resonant transition from a core level to a highly-dispersive band 10 eV or so above the Fermi energy. In practice the interaction of an electron in this band with any other electron can be neglected. Unlike the case of REXS and direct RIXS, in indirect RIXS the core hole is indispensable as nothing else is available to excite the valence electrons. Since the core hole behaves as a static potential in the intermediate state its main effect, and the only one that will be discussed in this thesis, is to excite particle-hole "shake-up" pairs. In a non-conducting system, where there are no low-energy particle-hole pairs, another effect in which the core hole potential creates spin excitations via local modulation of exchange interactions. Fig. 2 illustrates the formation of shale-up pairs in indirect RIXS performed on a conducting system.

0.4 Functional Determinants

Finally, we introduce a versatile method for calculating expectation values in fermion systems that underlies much of the work in this thesis. Here we will demonstrate a few simple examples, giving a flavor of what is possible and building intuition for the meaning of the formula. Chapters 1, 2, and 3 involve extensions of these basic formulas with varying degrees of sophistication, while chapter 5 uses the simplest version but couples it to field-theoretic techniques. Appendix A presents an ingenious method devised by Israel Klich for applying functional determinants to more general Hamiltonians.

Consider a time-dependent problem starting from an initial many-body state $|\Psi(0)\rangle$, which is an eigenstate of Hamiltonian H_0, which then time evolves under a different Hamiltonian H_1. This describes quench experiments in ultracold atom systems and the

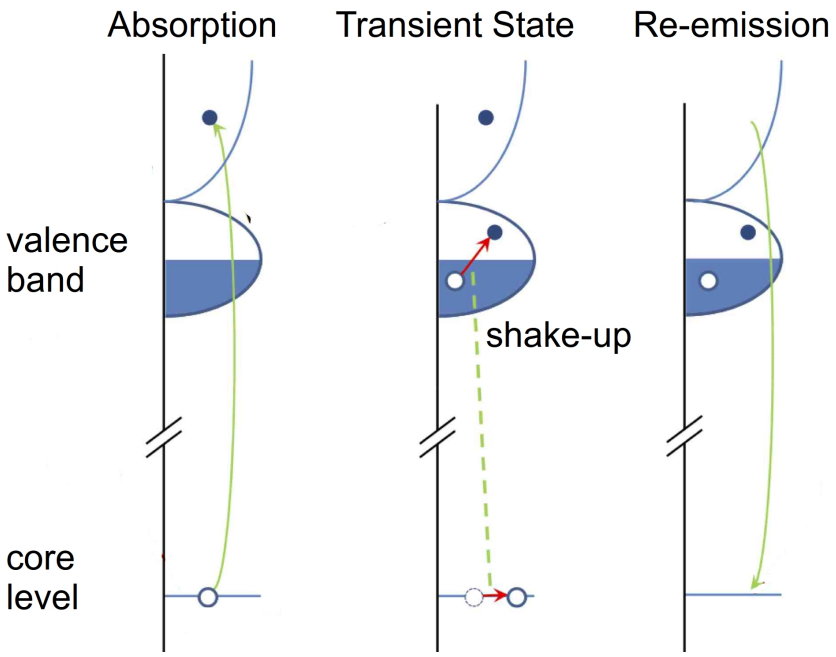

Figure 2: Simple schematic of indirect RIXS. A photon is absorbed, promoting a core electron to a higher conducting band. In the transient state, the positively-charge core hole scatters electrons in the valence band. Finally, the photoelectron re-fills the core hole and emits a photon.

transient state of resonant x-ray scattering, in addition to many other non-equilibrium problems. Expectation values of operator X at time t are given by

$$\langle X \rangle (t) = \langle \Psi(0) | e^{iH_1 t} X e^{-iH_1 t} | \Psi(0) \rangle, \tag{10}$$

which generalizes at arbitrary temperature $T = 1/\beta$ to

$$\langle X \rangle (t) = \frac{\mathrm{tr}\left[e^{iH_1 t} X e^{-iH_1 t} e^{-\beta H_0}\right]}{\mathrm{tr}\left[e^{-\beta H_0}\right]}. \tag{11}$$

It is crucial to note that, as the expectation is with respect to a many-body state, the traces above are taken with respect to many-body Fock space. Suppose, however, that H_0 and H_1 are quadratic (i.e. non-interacting) operators. We might suspect that we are not dealing with a true many-body problem and that somehow formulas must decompose into tractable single-body parts. As we shall see, such a decomposition is possible and we can reduce Eq. (2.6) to an expression involving only single-particle matrices. That is, we recast a trace over 2^N-dimensional Fock space into a manageable operation (a determinant, as it turns out), in N-dimensional Hilbert space.

The precursor to all further determinantal formulas we shall derive is the denominator of Eq. (2.6). Consider in general the Fock space trace

$$A = \mathrm{tr}\left[e^{Z}\right], \tag{12}$$

where $Z = z_{ij} c_i^\dagger c_j$ is a quadratic operator. Here and below, we use the convention that lowercase, eg 'z', indicates the matrix elements of an operator, while uppercase, eg 'Z' denotes the operator itself. The former can be thought of as a single-particle Hilbert space operator simply by mapping it to a matrix (or equivalently, by projecting Z to the

single-particle sector of Fock space). This convention sacrifices some amount of clarity for convenience, an acceptable trade-off given that the distinction between Z and z is always obvious from context.

Suppose we have diagonalized Z as $Z = \sum_\alpha \omega_\alpha c_\alpha^\dagger c_\alpha$, where the basis $\{\alpha\}$ is obtained from the original basis via a unitary transformation. The Fock space trace is much easier to evaluate with respect to this basis, where it becomes the product of independent traces over the 2-dimensional phase space – occupied or unoccupied – of each state α:

$$A = \mathrm{tr}\left[\exp(\sum_\alpha \omega_\alpha c_\alpha^\dagger c_\alpha)\right] = \sum_{\{n_\alpha\}} \left(\prod_\alpha e^{\omega_\alpha n_\alpha}\right) = \prod_\alpha \left(\sum_{n_\alpha=0,1} e^{\omega_\alpha n_\alpha}\right) = \prod_\alpha (1 + e^{\omega_\alpha}) \tag{13}$$

Finally, since the eigenvalues of z – the *single*-particle operator – are ω_α, it follows that $1 + e^{\omega_\alpha}$ are the eigenvalues of $1 + e^z$. Hence

$$A = \text{product of eigenvalues of } 1 + e^z = \det(1 + e^z) \tag{14}$$

In addition to the aforementioned fact that this approach results in a relatively single-particle expression, it has the additional virtue of yielding a manifestly basis-independent expression. Therefore, though we appeal to the *existence* of a basis that diagonalizes Z, we never need to know this basis.

A next level of complexity, and one that brings us significantly closer to calculating the numerator of Eq. (2.6), is a trace of the form

$$B = \mathrm{tr}\left[e^{Z_1} e^{Z_2}\right] \tag{15}$$

where Z_1 and Z_2 are both quadratic. By the Baker-Campbell-Haussdorff lemma there

exists another quadratic operator Z such that $e^Z = e^{Z_1}e^{Z_2}$. Explicitly, one has the formula

$$Z = Z_1 + Z_2 + \frac{1}{2}[Z_1, Z_2] + \frac{1}{12}\left([Z_1, [Z_1, Z_2]] + [Z_2, [Z_2, Z_1]]\right) - \frac{1}{24}[Z_2, [Z_1, [Z_2, Z_1]]] \ldots \tag{16}$$

which contains only terms involving Z_1, Z_2, and commutators. Since the commutator of two quadratic operators is quadratic, Z is also quadratic. Alternatively, since the space of all quadratic operators is closed under commutation, it forms a Lie algebra, which naturally maps to a Lie group via the exponential map. By the group property, $e^{z_1}e^{z_2}$ belongs to the group and thus it has the form e^z for some z in the Lie algebra. Finally, a common physical situation is where $Z_{1,2} = iH_{1,2}$ for Hermitian $H_{1,2}$, in which case Z exists simply because the product of unitary operators in unitary, hence the exponential of i times a Hermitian operator. In any case, the previous result carries over:

$$B = \mathrm{tr}e^Z = \det(1 + e^z) = \det(1 + e^{z_1}e^{z_2}). \tag{17}$$

By induction, this works for an arbitrary product:

$$\mathrm{tr}\left[e^{Z_1}e^{Z_2}\ldots e^{Z_n}\right] = \det\left(1 + e^{z_1}e^{z_2}\ldots e^{z_n}\right). \tag{18}$$

These derivations form the foundation of the more-complicated determinantal formulas we will encounter later. In fact, we apply Eq. (18) without elaboration in Chapter 2, when we study indirect RIXS. In Chapter 1 on REXS and Chapter 3 on direct RIXS we will insert non-exponentiated operators into the traces. Finally, in Chapter 5 we will deal with interacting Hamiltonians.

1

Resonant Elastic X-Ray Scattering and Charge Density Waves in the Cuprates

1.1 Introduction

As discussed in the introduction, resonant elastic x-ray scattering (REXS) is a powerful technique for exploring strongly-correlated quantum materials[6,116,5]. While neutron

and non-resonant x-ray scattering cross sections are dominated by the contributions of nuclei and core electrons, REXS couples selectively to conduction band electrons and is extremely sensitive to many-body correlations[6,116,30,41,3,122,92,5,32,46,98,99,38]. For this reason one can think of REXS as "valence-selective diffraction." However, this description may actually understate the versatility of REXS, for unlike traditional, non-resonant, x-ray diffraction, REXS does not couple only to the charge density. Rather, it couples to essentially *any* perturbation of valence electrons, and elastic (diffraction) peaks in REXS accompany many types of translational symmetry breaking, including those such as orbital order that do not entail charge order. As an example of the extent of the resonant behavior, in the case of the oxygen K edge in LBCO and LSCO the cross section for charge carriers is four orders of magnitude greater at resonance than away from resonance[99]. Further promise of REXS comes from its ability to study a wide class of materials, including those available only in small samples and those with buried interfaces [98,97,99]. This is in stark contrast to neutron scattering, which due to small cross sections generally requires large single crystals for samples. REXS has recently been used to observe orbital order in manganites[116,30,41] and ruthenates[122], hole crystallization in spin ladders[3], and charge order in cuprates[5,32,38], nickelates[92], and manganites[46,75].

Although qualitative interpretation of REXS data has already provided valuable insight into a variety of strongly correlated materials, detailed quantitative understanding of these experiments is still lacking, and there exist no reliable tools for connecting measured REXS spectra to microscopic models. It is obvious that an elastic peak at momentum $\mathbf{Q}$ implies some sort of ordering with wavevector $\mathbf{Q}$, but aside from this few attempts have been made to extract information from REXS spectra. As an example of REXS data (examined in detail below), consider in Fig. 1.2 data from Ref. [5] showing

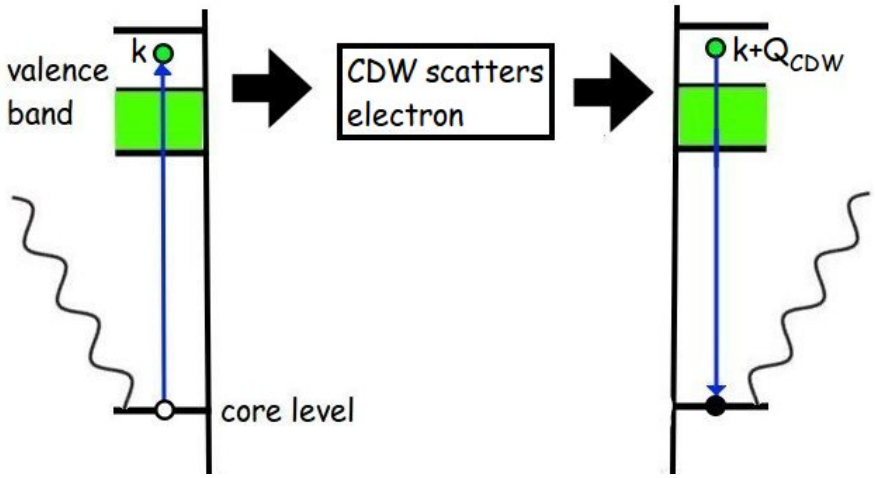

Figure 1.1: Outline of REXS experiments for detecting charge density wave order. A photon is absorbed, exciting a core electron to the valence band. This photoelectron is scattered elastically by the charge density wave potential, imparting a momentum $\mathbf{Q}$. The photoelectron re-fills the core hole and a photon is re-emitted. The process imparts a momentum $-\mathbf{Q}$ to the scattered photon.

the REXS intensity as a function of incident photon energy ω taken at the constant momentum – the charge density wave wavevector of underdoped LBCO, given by the peak in momentum space. Data are shown for two resonances, one for each type of atom, copper and oxygen, in the CuO_2 conducting layers. The obvious question is: why are there two peaks in the oxygen spectrum? However, one should also wonder what their separations and relative heights mean, and why the copper resonance exhibits only one peak. Furthermore, one should wonder why there need be any peaks at all! Due to (too much) experience with non-resonant x-ray scattering and absorption, it is usually assumed that the lower-energy peak comes from the Fermi edge. However, there is no reason to believe that resonant x-ray scattering at a particular momentum has analogous phenomenology. In fact, we will see below that neither peak is related to the Fermi level.

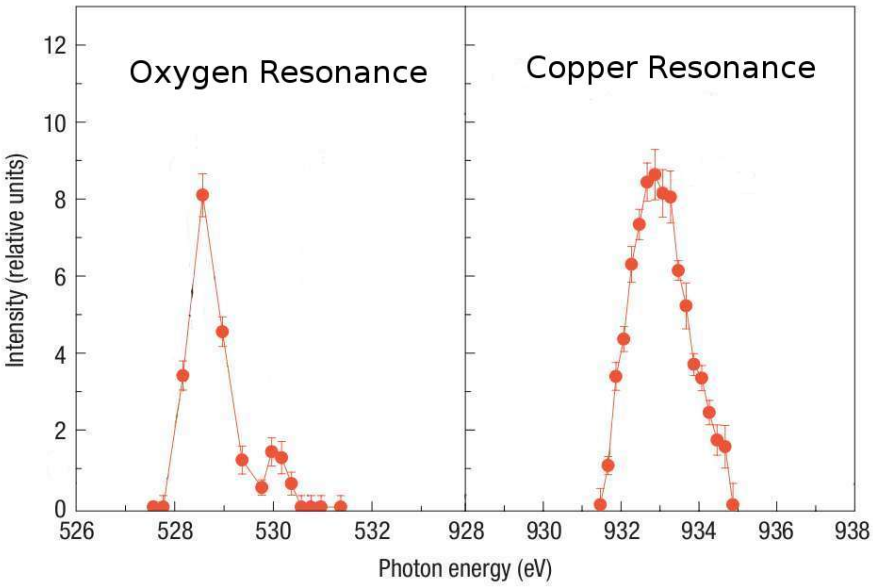

Figure 1.2: REXS data, intensity versus incident photon energy at constant momentum, from underdoped LBCO[5] exhibiting non-trivial peak structure.

Up to now, most efforts to interpret resonant x-ray diffraction (RXD) experiments have adapted the use of atomic form factors from x-ray crystallography[6,5,46,32]. The form factor concept assumes optical locality, which is valid for ordinary x-ray diffraction where immobile core electrons dominate, but breaks down in the resonant case if valence states are delocalized. Some authors have attempted to account for this nonlocality by defining the form factor in terms of a cluster, rather than a single atom[92,30]. But even this approach should break down if valence states are propagating quasiparticles. Basically, the form factor approach assumes that electrons can not move and behave as static dipole oscillators, a dubious approximation when dealing with conducting materials. Recent work of Abbamonte et al.[4] showed that neglecting the finite lifetime of core holes and interaction of conduction electrons with core holes allows one to relate REXS spectra to the local electron Green's function measured in STM. How-

ever, these neglected effects are expected to play an important role and it is not clear how accurately such a simplified analysis can explain REXS spectra in real materials. An approach based on the Bethe-Salpeter equation[84] captures excitonic effects of the core hole but ignores the full many-body character of the core hole-Fermi sea interaction, including the orthogonality catastrophe. The state of affairs in REXS should be contrasted to the more established probes of conduction electrons, ARPES[24,67,18] and STM[33,48,72,110,49,119], where it is often possible to read off spectral functions directly from measurements, facilitating the comparison of theoretical models with experimental results.

In this chapter we present the first microscopic model of REXS in systems with charge order in the conduction band, such as striped high-T_c cuprates[103,115,48,55,73,112,14,120]. We develop a theoretical approach that allows us to analyze REXS spectra in the case of itinerant conduction electrons and include realistic band structures. Our formalism *treats exactly* excitonic effects and the orthogonality catastrophe arising from the interaction of conduction electrons with core holes as well as finite lifetime of core holes. We show that the two-peak spectrum observed in experiments at the O K edge of $La_{1.875}Ba_{0.125}CuO_4$[5,32] can be explained by dynamical nesting of the "standard" band structure of cuprates (see Figures (1.3) and (1.4)). We find that interaction of conduction electrons with the core hole changes the spectrum significantly. For a physically reasonable core hole potential we obtain quantitative agreement with the experimental data on underdoped $La_{1.875}Ba_{0.125}CuO_4$ (LBCO) near the 1/8-anomaly[5] (similar spectra were observed for $La_{1.8-x}Eu_{0.2}Sr_xCuO_4$(LESCO) in[32]). Our results suggest that REXS at the O K edge can be directly connected to the known quasiparticle band structure, providing a new, bulk-sensitive measure of the spectral function that is complementary to ARPES and STM techniques.

This chapter is organized as follows. We develop a general formalism for analyzing elastic REXS in systems with charge order in the conduction band. We then apply our formalism to the period-4 charge modulation of underdoped cuprate superconductors. We give a simple qualitative disccussion of the calculated spectra and compare them to experiments.

1.2 Theoretical formalism

Following Ref. [4] we consider an effective single band model describing resonant absorption and emission of photons

$$H_{\text{int}} = \sum_{j,\mathbf{k},\lambda} V(\mathbf{k},\lambda) \left(d_j^\dagger c_j a_{\mathbf{k},\lambda} e^{i\mathbf{k}\cdot\mathbf{r}} + \text{h.c.} \right) \tag{1.1}$$

Here c_j and d_j are annihilation operators of electrons on site j in the core orbital and conduction band respectively, $a_{\mathbf{k},\lambda}$ annihilates a photon with momentum $\mathbf{k}$ and polarization $\hat{\varepsilon}_{\mathbf{k},\lambda}$, and $V(\mathbf{k},\lambda)$ are matrix elements whose precise form is not important to us. Resonant scattering is a second order process in H_{int}

$$I(\omega) = \sum_f \left| \sum_n \frac{\langle f|H_{\text{int}}|n\rangle\langle n|H_{\text{int}}|i\rangle}{E_i - E_n + \omega + i\Gamma} \right|^2 \tag{1.2}$$

Here $|i\rangle$ is the initial state of the system with N electrons in the conduction band, no core holes, and one incoming photon with momentum $\mathbf{k}_i$; $|n\rangle$ is the intermediate state with one core hole and one extra electron in the conduction band, and no photons; $|f\rangle$ is the final state with the core levels filled again, N electrons in the conduction band and one outgoing photon with momentum $\mathbf{k}_f$. E_i and E_n are energies of the initial and intermediate electron states, respectively. Note that the latter includes the potential of

the core hole. Γ is the decay rate of the core hole, including radiative and non-radiative processes. We focus on elastic scattering by ordering wavevector $\mathbf{Q}$ where we can take $|f\rangle = |i\rangle$ and $\mathbf{k}_f = \mathbf{k}_i + \mathbf{Q}$.

Because the core hole is immobile it must be re-filled on the same site j on which it is created and it may be subsumed into a static potential that acts on the conduction electrons of the intermediate state. The core hole contributes the trivial matrix element $\langle 1|c_j^\dagger|0\rangle\langle 0|c_j|1\rangle = 1$ and we can perform the same manipulations as in the introduction to pass from the energy domain to the time domain, which is convenient since transient state eigenstates are not eigenstates of $\mathcal{H}_0$.

$$I(\omega, \mathbf{Q}) \propto \left| \sum_{j,n,\sigma} e^{-i\mathbf{Q}\cdot\mathbf{r}_j} \frac{\langle i|d_{j\sigma}|n\rangle\langle n|d_{j\sigma}^\dagger|i\rangle}{E_i - E_n + \omega + i\Gamma} \right|^2 \tag{1.3}$$

$$= \left| \sum_{j\sigma} e^{-i\mathbf{Q}\cdot\mathbf{r}_j} \int_0^\infty e^{-(i\omega+\Gamma)t} S_{j\sigma}(t) dt \right|^2 , \tag{1.4}$$

where $S_{j\sigma}(t) = \langle i|d_{j\sigma} e^{-iH_1(j)t} d_{j\sigma}^\dagger e^{-iH_0 t}|i\rangle$. Without a core hole potential, $H_1(j) = H_0$ and $S_{j\sigma}(t)$ reduces essentially to the retarded Green's function[4]. Here the matrix elements and operators refer only to the conduction electron Fock space. If we measure photon frequencies relative to the difference between the chemical potential of the conduction band μ and the energy of the core state electron ξ_c, $\omega' = \omega - (\mu - \xi_c)$, we can set $E_i = 0$ so that $H_0|i\rangle = 0$. The intermediate states $|n\rangle$ are eigenstates of

$$H_1(j) = H_0 + U(\mathbf{r} - \mathbf{r}_j), \tag{1.5}$$

where U is the potential due to the core hole at site j and H_0 is given in the grand canonical ensemble. Equation (3.2) also applies to a thermal ensemble at temperature

$T = 1/\beta$, provided that we use

$$S_{j\sigma}(t) = \frac{\mathrm{tr}\left[d_{j\sigma} e^{-iH_1 t} d^{\dagger}_{j\sigma} e^{-\beta H_0}\right]}{\mathrm{tr}\left[e^{-\beta H_0}\right]}. \tag{1.6}$$

We stress that the trace here is taken with respect to Fock space.

We emphasize that equations (3.2) - (1.6) are very general and apply for an arbitrary interacting Hamiltonian of conduction band electrons H_0. While Eq. 1.6 was formulated for the single band case, it can be generalized to the multi orbital case by adding orbital indices to electron operators and restoring orbital-dependent matrix elements for absorption and emission. In the remainder of this chapter we will limit our discussion to the model of non-interacting electrons. This simplifying assumption is justified as long as the lifetime of electron states in the conduction band is longer than the lifetime of the core hole Γ^{-1} (see also the discussion below).

The trace in Eq. (1.6) is reminiscent of the orthogonality catastrophe of x-ray absorption[68,79] and the Fermi edge singularity of mesoscopic transport[74,2]. It expresses the many-body overlap of the initial Fermi sea with the perturbed Fermi sea that time evolves under H_1 and the single-particle dynamics of the extra electron injected into the conduction band at site j. It is of the same form as the elementary formulas we examined in the introduction, but with the insertion of one electron creation operator and one annihilation operator. As mentioned above, the functional determinant formalism extends to the case of fermion insertions with no great difficulty or increase in complexity[23,57]. Leaving the derivation of this generalized formula to Appendix C, we obtain

$$S_j(t) = \det\left((1-\hat{N}) + e^{-ih_1 t}\hat{N}\right)^2 \left(\frac{\hat{N}}{1-\hat{N}} + e^{ih_1 t}\right)^{-1}_{jj}, \tag{1.7}$$

where $\hat{N} \equiv (1 + \exp(\beta h_0))^{-1}$. (As a reminder, we use throughout this thesis the convention that lowercase letters denote the matrix elements corresponding to a quadratic many-body operator, denoted in uppercase). The determinantal factor corresponds to the many-particle dynamics of the Fermi sea and is squared due to the presence of two spin species regardless of the spin of the photo-excited electron. One can interpret it as follows: the argument inside the determinant is an operator that time-evolves only those states that are initially occupied, and taking the determinant computes an overlap of Slater states. The matrix element part corresponds to single-particle dynamics of the intermediate photoelectron. It is a local Green's function for propagation of a single electron from site j to site j, modified by the Pauli-blocking term $N/(1-N)$. For period-p order, one needs to sum over p inequivalent sites j. The determinant can be evaluated efficiently for a finite system, converging by a system size of 25×25 (an average personal computer can handle system sizes of 40×40 in less than an hour). Eqs. (3.2) and (1.7) constitute a convenient formula for calculating REXS spectra in the approximation of noninteracting electrons. They treat exactly interaction of electrons with the core hole potential and finite lifetime of the core hole.

1.3 REXS of cuprate superconductors

Before we apply the above formalism to the cuprate superconductors, it is worth mentioning previous attempts to interpret the data presented in Fig. 1.2. This summary is necessarily rather brief – despite the significance of these data as the first direct proof of CDW order in the cuprates, there was no serious quantitative analysis of them for eight years, when the work of this chapter was done. There was, however, a somewhat hand-waving interpretation, which was to ascribe the two peaks in Fig. 1.2 to the lower

and upper Hubbard bands. The fact that these peaks occurred not in absorption, but in REXS at a non-zero CDW wavevector $\mathbf{Q}$, would imply some translational symmetry breaking related to this Mott insulating physics, and thus the idea was that the samples in question exhibited "spatially-modulated Mottness." Due perhaps to the lack of any better explanation, most of a decade passed before an obvious problem with this explanation was pointed out in the literature: the separation between peaks in the REXS experiments on LBCO and LESCO is slightly less than 1.5 eV, while the smallest Mott gaps in cuprates are around 2.0 eV. In particular, x-ray absorption data performed on the same samples do not contain two peaks separation by a gap matching that of REXS. In addition to this inconsistency, one could also point out that in the cuprates, Mott-Hubbard physics is primarily related to double occupancy of a copper site, and thus in a model of spatially-modulated Mottness one would expect the copper REXS resonance to show a more pronounced double peak structure than the oxygen resonance, in contrast to the actual data. Given what were, in our opinion, fundamental defects of this interpretation, we wondered how well a simple quasiparticle model could explain the data.

We apply Eqs. (3.2) and (1.7) to charge order in an effective one-band model of the cuprates

$$H_0 = \sum_{\mathbf{k}} \xi_{\mathbf{k}} d^\dagger_{\mathbf{k}} d_{\mathbf{k}} + V \sum_{\mathbf{k}} \left(d^\dagger_{\mathbf{k}+\mathbf{Q}} d_{\mathbf{k}} + d^\dagger_{\mathbf{k}} d_{\mathbf{k}+\mathbf{Q}} \right). \tag{1.8}$$

Eq. 1.8 is a mean-field description of a state with charge order[83,55,44,112,93,117,71] It provides a phenomenological description of charge ordered states regardless of its microscopic origin. Possible mechanisms may include electron-electron interactions, in which case charge order is often referred to as stripes[120,91], or it may be due to nesting

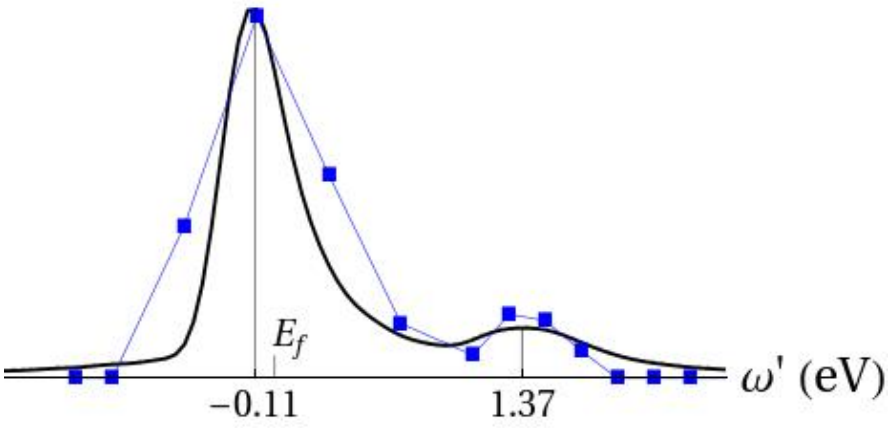

Figure 1.3: Calculated REXS spectrum for period-4 charge order for the canonical cuprate band-structure (parameters given below Eq. (1.8)) and core hole potential $U_0 = -250$ meV. Horizontal axis shows shifted energy ω' of scattered photons, where $\omega' = 0$ is the energy required to excite a core electron to E_f in the absence of a core hole potential, vertical axis is intensity of elastic scattering (arbitrary units). Squares give experimental data for LBCO from Ref. [5]. Note that the position of the first peak is not E_f. It is determined by both the dynamic nesting and the core hole potential.

of the Fermi surface and electron-phonon interactions[66,95,9].

We use the tight-binding dispersion $\xi_{\mathbf{k}} = -\sum_{\mathbf{r}} e^{i\mathbf{k}\cdot\mathbf{r}} t_{\mathbf{r}} - \mu$ and parameters $t_{(1,0)} = 340$, $t_{(1,1)} = -32$, $t_{(2,0)} = 25$, $t_{(2,1)} = 31$ meV characteristic of LBCO[69]. For simplicity we ignore k_z dispersion, which would at most smear energy peaks by an amount $t_z \lesssim 50$ meV[69]. Figure (1.3) presents a REXS spectrum for a contact core hole potential $U(\mathbf{r}-\mathbf{r}_j) = U_0\delta_{\mathbf{r},\mathbf{r}_j}$. We have also calculated spectra using Yukawa potentials of various ranges and found similar results (see appendix B). We have chosen a realistic core hole lifetime $\Gamma = 250$ meV.

Figure 1.3 shows calculated intensity of REXS as a function of initial photon energy. The two peak structure of the spectrum is in good agreement with experimental findings[5,32]. There is a simple physical argument which shows that the two peak structure

is a robust feature of the canonical band structure of high Tc cuprates. Let us consider the simplifying limit of zero core hole potential. In this case the intermediate eigenstates are obtained by adding an electron in some eigenstate $|\phi\rangle$ of H_0 to the Fermi sea, and the energy domain expression Eq. (1.3) reduces to

$$I(\omega, \mathbf{Q}) \propto \left| \sum_{j,\phi} e^{-i\mathbf{Q}\cdot\mathbf{R}_j} \frac{(1 - n_F(E_\phi)) \left|\langle\phi|j\rangle\right|^2}{E_i - E_\phi + \omega + i\Gamma/2} \right|^2 . \tag{1.9}$$

Unoccupied states ϕ contribute strongly when their energy is in resonance and the Fourier transform of their density at wavevector $\mathbf{Q}$ is large. In the presence of a CDW potential, Bloch states separated by wavevector $\mathbf{Q}$ hybridize to form eigenstates with non-trivial density. This occurs most readily when $\xi_{\mathbf{k}}$, $\xi_{\mathbf{k}+\mathbf{Q}}$ are nearly degenerate. The REXS intensity at energy E comes from points on the surface of constant energy E that are separated by wavevector $\mathbf{Q}$[83]. Usually these are isolated pairs of points, but at certain energies the surfaces are nested so that sections separated by $\mathbf{Q}$ move in parallel (see Figure (1.4)). At these energies there is a large density of hybridized states. This is the phenomenon of dynamic nesting. While Fermi surface nesting, which is just dynamic nesting at $E = E_f$, is uncommon, dynamic nesting is a generic consequence of symmetry. Consider the two-dimensional cuprate Brillouin zone and period-4 CDW wavevector $\mathbf{Q} = (\pi/2, 0)$. Any Bloch state $|\mathbf{k}\rangle$ on the lines $k_x = -\pi/4$ and $k_x = 3\pi/4$ is degenerate with $|\mathbf{k} + \mathbf{Q}\rangle$. Constant energy contours with segments tangent to the line $k_x = -\pi/4\,(-3\pi/4)$ also have segments tangent to $k_x = \pi/4\,(3\pi/4)$; these symmetry-equivalent segments are dynamically nested. Fermi surface nesting is not generic because there is no particular reason why the particular contour $E = E_f$ should be tangent to the lines (or, in three dimensions, a plane). Dynamic nesting, on the other hand, occurs when *some* energy contour is tangent to the lines. For our choice of LBCO hopping

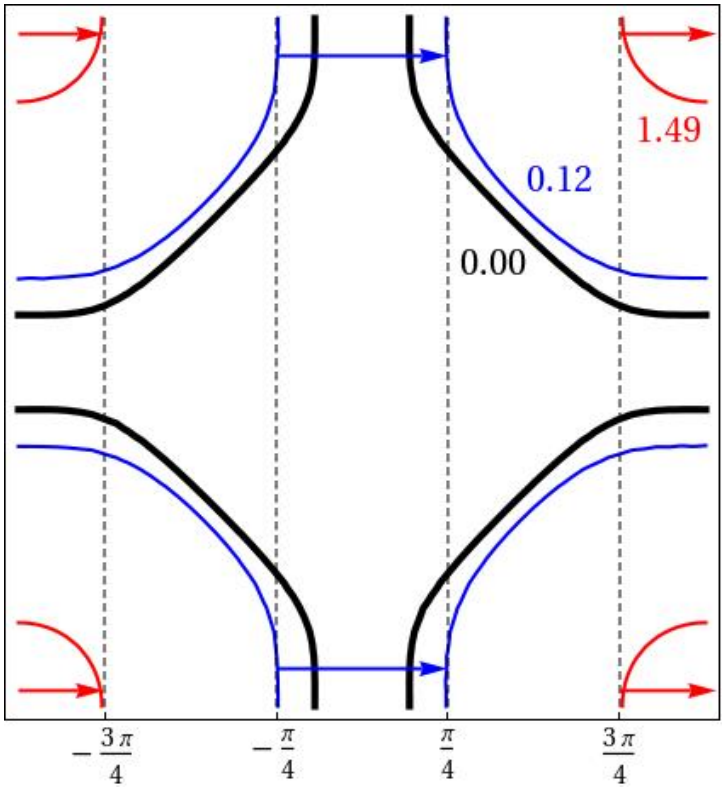

Figure 1.4: Dynamic nesting in the cuprate band structure. Nested segments of the $E = E_f + 0.12$ eV and $E = E_f + 1.49$ eV contours are shown in blue and red. The Fermi surface is shown in black. The lines $k_x = -3\pi/4, -\pi/4, \pi, 4, 3\pi/4$ (dashed) are a visual guide.

strengths the energy contours exhibiting dynamic nesting correspond to energies 0.1 eV and 1.5 eV above the Fermi level– which are separated by nearly the same amount as REXS peaks. The small discrepancy is due to the tendency of the core hole potential to widen the distance between peaks and vanishes when we set $U_0 = 0$ (see appendix B).

A simplified model neglecting the core hole potential explains the spectrum and its two peaks qualitatively but does not give the correct relative weights of the two peaks. Including the core hole potential yields quantitative agreement with experiments. The

core hole potential has a weak effect on the energy separation between the two peaks but dramatically decreases the intensity of the high-energy peak. A core hole potential strength $U_0 = -250$ meV, which is reasonable for a screened core hole interacting with conduction electrons, reproduces the experimental ratios of peak intensities. A non-physical repulsive core hole decreases the intensity of the low-energy peak. The discussion of Ref. [4] connecting the REXS spectrum to the electron spectral function thus remains largely accurate in the presence of a weak core hole potential. However, strong core hole potentials yield spectra with qualitative features, such as a lack of a high-energy peak, that give misleading conclusions in analyses based only on the spectral function. For example, we attribute the absence of a second peak in REXS at the Cu $L_{3/2}$ edge[5] to a strong Cu core hole potential. The spectrum is robust to changes in the core hole lifetime Γ, which broadens the peaks, and the CDW strength V, which scales the overall intensity. Small changes in the hopping strengths have little effect; multiplying them by a uniform factor affects the distance between peaks.

Our calculations provide the first quantitative explanation for the two peak structure observed in LBCO and LESCO [5,32]. An earlier interpretation of the two peaks as arising from the lower and upper Hubbard bands, the so-called "spatially-modulated Mottness", was not supported by quantitative analysis. Moreover, a separation of $\sim$ 1.9 eV between peaks is found in x-ray absorption spectroscopy (XAS) of LBCO and LSCO[81,5]. According to the lower/upper Hubbard band interpretation, in which between peaks there is a gap, the separation between peaks in REXS must be at least as large as the separation in XAS. Thus we think that dynamical nesting of the band structure provides a more natural interpretation of the two peak structure observed in LBCO and LESCO.

1.4 Discussion

We now comment on the specific values of the band structure that we used in our analysis. Ab-initio LDA calculations on LSCO give $t_{(1,0)} = 430$, $t_{(1,1)} = -40$, $t_{(2,0)} = 30$, $t_{(2,1)} = 35$ meV[69] while fitting of the ARPES spectra gives $t_{(1,0)} = 250$, $t_{(1,1)} = -25$, $t_{(2,0)} = 20$, $t_{(2,1)} = 28$[69]. The ratios among tight-binding parameters are nearly identical for both cases, so the band structure is well-known up to an overall truncation factor. The two peak character of the REXS spectra appears for both band structures with nearly the same relative intensities of the two peaks. We find that taking either the LDA or ARPES dispersions gives peaks separated by 1.7 and 1.3 eV. We obtain the best fit to REXS data by choosing parameters halfway between the two. We point out that it is not so surprising that band structure obtained from the ARPES data does not provide the best agreement with the REXS spectra. ARPES data only exist within 200 meV of the Fermi surface[51], where the renormalization effect due to interactions is strongest, while we are interested in features at much higher energy. Additionally, it has been suggested that ARPES tends to underestimate electron dispersion relative to x-ray experiments[50,69]. Another important issue is our approximation of non-interacting electrons. The key quantity entering our analysis is a generalized propagator (1.6) . The effect of many-body correlations is to introduce decay of an electron into other excitations, but as far as the Green's function is concerned this simply contributes an imaginary part to the electron's self-energy (we assume that the effective one-band model we use has already incorporated renormalization via the *real* part of self-energies). Furthermore, if the decay of the electron is slow compared to the decay of the core hole, any broadening introduced by electron interactions will be hidden within the width Γ. Conversely, if the electron decays very rapidly, REXS peaks will be broadened into oblivion.

Therefore, the presence of peaks in an REXS spectrum puts an upper bound on the imaginary self-energy and implies that excitations resemble well-defined quasiparticles. Thus REXS, which probes high energy excitations, complements magnetic oscillation experiments[65,31,111], which have given evidence for well defined quasiparticles close to the Fermi energy.

1.5 Outlook

We have developed a microscopic model of REXS that takes into account the itinerant character of conduction band electrons and excitonic effects. We showed that a simple physical picture of dynamical nesting found in the canonical band structure of cuprates gives rise to a two peak structure, while the core hole potential is necessary for quantitative agreement with the data. Our analysis shows that even at high energies electronic excitations behave like sufficiently well-defined quasiparticles described by the canonical band structure.

Beyond providing a general framework for interpreting experimental data, our analysis also points to specific measurements to be made. Recent work on charge order in underdoped YBCO[38], which was performed at energies corresponding to Cu L edges, could be repeated at the O K edge. We would expect to find, as in LBCO, a two-peak energy dependence with peaks determined by band structure. Another prediction of our formalism is that REXS should be able to distinguish between uniaxial and biaxial (or stripe and checkerboard in the case of cuprates) order. In the latter case, coexisting Fourier components at wavevectors $\mathbf{Q}_x$ and $\mathbf{Q}_y$ generate a harmonic $\mathbf{Q}_x + \mathbf{Q}_y$. REXS measurements at this wavevector should exhibit a peak at energy determined by its corresponding dynamic nesting.

2

Indirect RIXS and the Cuprate Pseudogap Phase

2.1 Introduction

Unlike the cases of REXS, where we saw that over-reliance on the analogy with non-resonant x-ray scattering can be misleading, and direct RIXS, where we will see the

pitfalls of a tempting analogy to neutron scattering, there is no obvious naive comparison to be made with indirect RIXS. Unlike the other probes, in which the presence of the core hole potential is a complication, indirect RIXS relies on the core hole. As there is no other way in condensed matter physics (ouside of ultracold atoms) to introduce a transient local potential, indirect RIXS has not been inaccurately pigeonholed as the other techniques have. For this reason, this chapter need not focus on clarifying misconceptions about indirect RIXS, of which there are no notable ones, and will instead focus on proposing experiments. Of course, the other side to the lack of facile comparisons is that it is not generally known what one should do with indirect RIXS, hence little experimental and theoretical work has been done in this area. In this chapter we put forward a very simple idea: since indirect RIXS measures the spectrum of particle-hole pairs, it must be sensitive to any perturbation that reconstructs the Fermi surface. In other words, one should be able to use indirect RIXS to detect essentially any order parameter. As a concrete example we will consider the case of the pseudogap in the high-temperature cuprate superconductors. This choice has two great advantages. First, the pseudogap energy scale is very large, as much as several hundred meV, and is therefore not limited by current resolutions of 50 meV or so. Second, it is unknown what type of order (or orders) produces the pseudogap, which permits us to test our formalism on several types of order without veering into irrelevant speculation.

The state of the underdoped cuprates above the superconducting transition temperature is an outstanding puzzle in the field of high-temperature superconductivity. Many different types of order[102,56,86,21,55,77,107,112,14,11,25,35] have been hypothesized to coexist or compete with superconductivity and to explain pseudogap behavior in which the density of states is depleted around the Fermi energy. These potential phases are difficult to detect because, with the exception of charge density wave (CDW) and spin density

wave (SDW) in certain cuprates at specific dopings, they exhibit dynamic fluctuations and spatial inhomogeneity[55,87]. These fluctuations smear the signatures of potential order parameters and render them undetectable by quasistatic probes that effectively average over time scales longer than those of fluctuations. Resonant inelastic x-ray scattering (RIXS) can overcome this obstacle because its time scale is bounded by the finite lifetime (roughly $(250\,\mathrm{meV})^{-1} \approx 1\,\mathrm{fs}$) of an intermediate state core hole due to Auger decay and other processes. Essentially, RIXS can take instantaneous snapshots of fluctuating short-range order. However, there exists little theory for RIXS in systems with itinerant electrons; in particular, it is not clear how RIXS can be used to probe competing orders, such as those that appear (and are hypothesized to exist) in the normal phase of the cuprate superconductors*. In this chapter we show that indirect RIXS, in which one measures the effect of a positively-charged transient core hole on the valence band Fermi sea, is sensitive to changes in the particle-hole excitation spectrum induced by many of the most commonly considered order parameters proposed for the peudogap phase. We show that it is possible to detect and distinguish different order parameters, for example charge density waves, antiferromagnetism, and the hypothesized d-density wave[21]. We derive a formula for indirect RIXS in systems with itinerant electrons, accounting exactly for the core hole potential acting on valence electrons.

2.2 Theoretical Formalism

In indirect RIXS a photon is absorbed and causes a transition of a core electron to an excited band *above* the valence band, leaving behind a positively-charged core hole.

*Partial exceptions to this statement include our previous work[13] on direct RIXS, which did not consider ordered states, and an analysis of direct RIXS[70] that considered different pairing order parameters.

In the cuprates, the most commonly-used transition is $1s \rightarrow 4p$. The excited band is generally weakly-interacting; in cuprates this occurs because it is derived from a delocalized $4p$ orbital. Thus the excited electron does very little in indirect RIXS except re-fill the core hole and emit a scattered photon. The interesting action is the effect of the core hole on the electrons in the valence band, which in a conducting system is to generate particle-hole "shake-up" pairs. When one measures the energy difference $\Delta\omega$ and momentum difference $\Delta\mathbf{q}$ between the incident and scattered photons, one is measuring the dispersion of shake-up pairs. The spectral weights of shake-up processes at different energy and momenta reveal the joint density of states of particles and holes, which in turn sheds light on quasiparticle dispersions modified by different types of order.

The intensity for incident x-rays of momentum $\mathbf{q}_i$ and energy ω_i to be scattered into outgoing momentum $\mathbf{q}_f = \mathbf{k}_i + \Delta\mathbf{k}$ and energy $\omega_f = \omega_i - \Delta\omega$ is calculated from the familiar Kramers-Heisenberg formula[60]

$$I \propto \sum_f \left| \sum_n \frac{\langle f|T|n\rangle\langle n|T^\dagger|i\rangle}{\omega_i + E_n - E_i + i\Gamma} \right|^2 \delta(E_f - E_i - \Delta\omega), \tag{2.1}$$

where $|i(n,f)\rangle$ are the initial (intermediate, final) states with energies $E_{i(n,f)}$, $1/\Gamma$ is the lifetime of the intermediate state core hole, and $T^\dagger = \sum_m e^{\mathbf{q}_i\cdot\mathbf{R}_m} s_m p_m^\dagger$, $T = \sum_m e^{-\mathbf{q}_i\cdot\mathbf{R}_m} s_m^\dagger p_m$ are transition operators. This notation reflects the $1s \rightarrow 4p$ indirect RIXS in the high-T_c cuprates. We assume momentum-independent dipole matrix elements and leave polarization dependence implicit[4]. The attractive potential due to the core hole is most easily accounted for by switching to the time domain[78,12], where we

have

$$I \propto \sum_{m,n} e^{i\Delta\mathbf{q}\cdot(\mathbf{R}_n-\mathbf{R}_m)} \int_{-\infty}^{\infty} ds \int_0^{\infty} dt \int_0^{\infty} d\tau e^{i\omega_i(t-\tau)-is\Delta\omega-\Gamma(t+\tau)} S_{mn}, \tag{2.2}$$

where

$$S_{mn} = \left\langle e^{iH_0\tau} p_n e^{-iH_n\tau} p_n^\dagger e^{iH_0 s} p_m e^{iH_m t} p_m^\dagger e^{-iH_0(t+s)} \right\rangle. \tag{2.3}$$

Eq. (2.3) is a Keldysh-like integral describing the history of absorption and emission events separated by time evolution operators. Since the core hole is immobile and has a constant energy that can be absorbed into ω_i we are able to remove via $H \to H_{m(n)} \equiv H_0 + V_{m(n)}$, where $H_0 = H_d + H_p$ is the Hamiltonian of valence d electrons and the p band and V_m is the potential due to the core hole at site m that acts on valence electrons. As the $4p$ band is highly dispersive we assume that $4p$ electrons do not interact with the core hole or the valence band; this is the usual "spectator" approximation[105]. Therefore, the d and p bands are separable and the $4p$ contribution to Eq. (2.3) reduces to a product of Green functions:

$$S_{mn} = G_p^{nn}(\tau) G_p^{mm}(-t) \left\langle e^{iH_d\tau} e^{-iH_{d,n}\tau} e^{iH_d s} e^{iH_{d,m}t} e^{-iH_0(t+s)} \right\rangle, \tag{2.4}$$

where $G_p^{nn}(t) = \langle 0|p_n(t) p_n^\dagger(0)|0\rangle$ is an easily-calculated single-particle quantity. We note that by Eq. (3.2) S_{mn} is measurable as the Fourier transform of the intensity. Given the form of S_{mn} as a Keldysh-like correlator it is intuitively clear that it may reveal the real-space structure of H. We will discuss this point further below.

Following a recent analysis of direct RIXS[13] we treat the valence band as a system of non-interacting quasiparticles, which is valid when the quasiparticle lifetime is long compared to the core hole lifetime $1/\Gamma$. In the cuprates $\Gamma \geq 250$ meV, which exceeds

quasiparticle widths even quite far from the the Fermi surface. Many-body averages of products of exponentiated quadratic operators such as in Eq. 2.4 have been discussed in numerous works[88,90,57,2,12]. The standard formula $\left\langle e^{Z}\right\rangle = \det\left[(1-\hat{N}) + e^{z}\hat{N}\right]$, where uppercase '$Z$' denotes a quadratic many-body operator and lowercase 'z' denotes its matrix elements $Z = d_i^\dagger z_{ij} d_j$ and $\hat{N}$ is the Fermi occupation operator, gives

$$S_{mn}(t,s,\tau) = G_p^{mn}(\tau)G_p^{mm}(-t)\det\left[\left(1-\hat{N}\right) + e^{ih_d\tau}e^{-ih_{d,n}\tau}e^{ih_d s}e^{ih_{d,m}t}e^{-ih_0(t+s)}\hat{N}\right], \tag{2.5}$$

where $\hat{N} \equiv \left(1+e^{H_0/k_BT}\right)^{-1}$ and $H_d = d_i^\dagger\left(\hat{H}_d\right)_{ij} d_j$. To handle spin, we let $m \to (m,\sigma)$ represent a combined site and spin index and replace the basis $\{i\}$ of Wannier orbitals with a spin-Wannier basis $\{(i,\sigma)\}$. The above determinant formula requires a quadractic Hamiltonian of the form $H = d_i^\dagger h d_j$. We map singlet pairing Hamiltonians with terms of the form $d_\uparrow^\dagger d_\downarrow^\dagger$ to the necessary form $d_\uparrow^\dagger d_\downarrow$ via a particle-hole transformation $d_\downarrow^\dagger \leftrightarrow d_\downarrow$.

The $4p$ Green functions in Eq. (2.4) appear to complicate the analysis of indirect RIXS but in fact simplify it by restricting the number of particle-hole excitations caused by the core hole. Because the $4p$ band is highly dispersive the same-site Green function $G_p^{mn}(t)$ decays very rapidly – it is unlikely that a $4p$ electron created at site n will return except after very brief times. Therefore the time intervals associated with t and τ are effectively truncated much more than by the core hole lifetime alone. This makes numerical integration less computationally expensive, but more importantly dramatically reduces the contribution of processes in which the core hole potential generates multiple particle-hole "shake-up" pairs. Therefore (see below) indirect RIXS spectra can be interpreted in terms of single shake-up pairs and are not dominated by complicated processes involving multiple shake-ups. A common source of confusion is the

assumption that short intermediate state timescales t and τ imply poor energy resolution. However, the times t and τ are conjugate to the incident photon energy ω_i, and indeed spectra are virtually featureless as a function of ω_i. However, the energy transfer $\Delta\omega$ is conjugate to the time s, during which there is no core hole and no $4p$ electron. Hence resolution of $\Delta\omega$ is limited only by instrumental resolution. This preserves the dispersion information of $\Delta\omega$ vs. $\Delta\mathbf{k}$ that is fundamental to RIXS.

2.3 Main Results

We are interested in whether indirect RIXS distinguishes different types of short-range order in hole-doped cuprates, particularly those that are hypothesized to exist in the pseudogap phase of underdoped cuprates above T_c. In order to exploit the determinantal formalism, which requires a quadratic Hamiltonian, we will treat these orders as mean-field additions to the band structure Hamiltonian

$$H_0 = \sum_{\mathbf{k},\sigma} \varepsilon_{\mathbf{k}} d^\dagger_{\mathbf{k},\sigma} d_{\mathbf{k},\sigma}, \tag{2.6}$$

For concreteness we will use a single-band tight-binding dispersion

$$\begin{aligned}\varepsilon_{\mathbf{k}} = &-2t_1(\cos(k_x)+\cos(k_y)) - 4t_2\cos(k_x)\cos(k_y) - 2t_3(\cos(2k_x)+\cos(2k_y)) \\ &- 4t_4(\cos(2k_x)\cos(k_y)+\cos(k_x)\cos(2k_y))\end{aligned} \tag{2.7}$$

with parameters fit to ARPES data: $(t_1, t_2, t_3, t_4) = (126, -36, 15, 1.5)$ meV for Bi-2212[69]. We assume an attractive contact potential $V_m = -U_c \sum_\sigma d^\dagger_{m\sigma} d_{m\sigma}$ for the core hole, with $U_c = 5.0$ eV[105,106]. To H_0 we add charge density wave (CDW), d-density

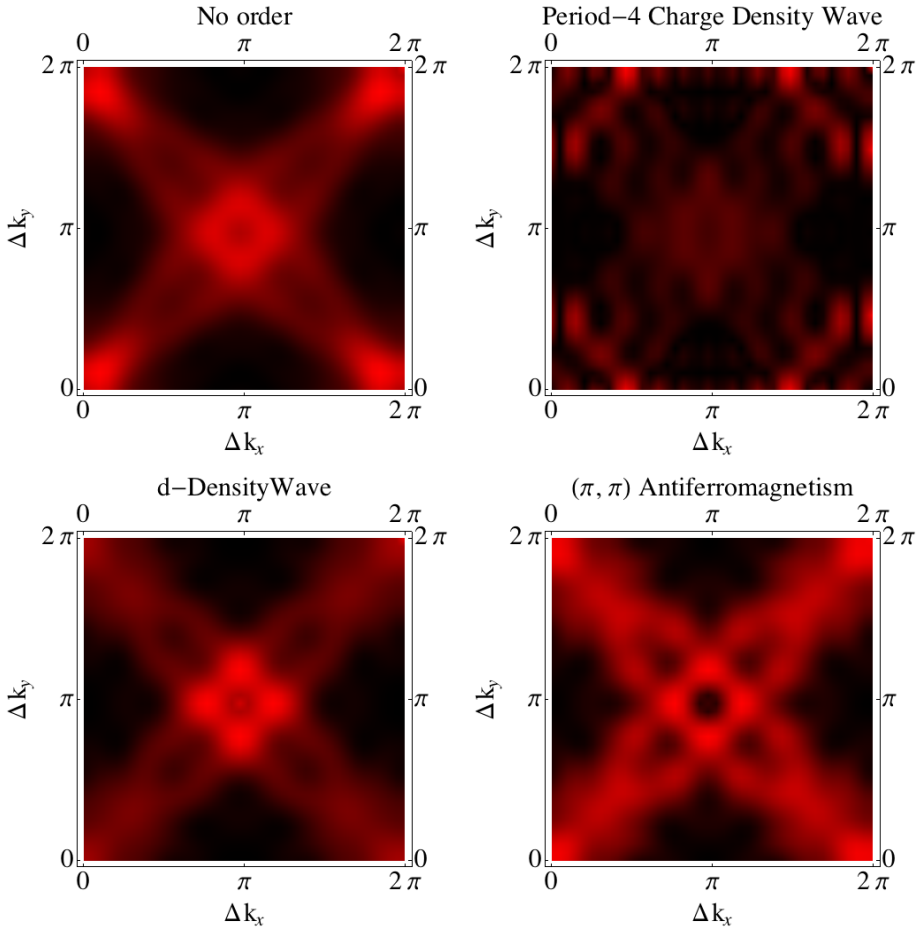

Figure 2.1: Indirect RIXS intensity (arbitrary units) versus momentum over entire Brillouin zone for underdoped Bi-2212 described by Hamiltonians H_0 (upper left) and mean-field Hamiltonians (clockwise from upper right): $H_0 + H_{CDW}$, $H_0 + H_{DDW}$, and $H_0 + H_{AF}$, with mean-field perturbations of amplitude $V_{CDW,DDW,AF} = 100$ meV. Spectra are measured at energy transfer $\Delta\omega = 100$ meV and incident photon energy ω at the $4p$ threshold. Here and elsewhere in this chapter black denotes zero intensity and bright red denotes maximal intensity.

wave, and antiferromagnetic (AF) orders:

$$H_{CDW} = \sum_{\mathbf{k}} V_{CDW} d^{\dagger}_{\mathbf{k}+\mathbf{Q}} d_{\mathbf{k}} \tag{2.8}$$

$$H_{DDW} = \sum_{\mathbf{k}} V_{DDW}(\mathbf{k}) d^{\dagger}_{\mathbf{k}+\mathbf{Q}} d_{\mathbf{k}} \tag{2.9}$$

$$H_{AF} = \sum_{\mathbf{k}} V_{AF} \left[d^{\dagger}_{\mathbf{k}+\mathbf{Q},\uparrow} d_{\mathbf{k},\uparrow} - d^{\dagger}_{\mathbf{k}+\mathbf{Q},\downarrow} d_{\mathbf{k},\downarrow} \right], \tag{2.10}$$

where the ordering wavevectors are $\mathbf{Q} = (2\pi/4, 0)$ (CDW), $\mathbf{Q} = (\pi, \pi)$ (DDW), and $\mathbf{Q} = (\pi, \pi)$ (AF), and $V_{DDW}(\mathbf{k}) = V_{DDW}(\cos k_x - \cos k_y)$. We restrict our attention here to period-4 commensurate CDW order, but the qualitative features of the RIXS signal we present below are not specific to this wavevector. The form of H_{AF} in Eq. (2.10) is that of an alternating sublattice magnetization, which could occur in cuprates if residual local antiferromagnetic correlations persist after long-range antiferromagnetic order is destroyed by hole doping. It is important to compare this form of AF to DDW because they have the same (π, π) wavevector. Thus we are able to study whether indirect RIXS is sensitive not only to the ordering wavevector but also to the form factor $V_{DDW}(\mathbf{k})$. Another important distinction to note is that the DDW is orthogonal to conventional charge order – while DDW is a form of translational symmetry breaking, the charge density due to DDW does not exhibit symmetry breaking. We will therefore be able to reject any naive suspicion that indirect RIXS is only sensitive to order parameters that accompany a density distortion.

In direct RIXS experiments, and indeed in most spectroscopic experiments it is customary to present data in the form of lineshapes, that is, intensity versus $\Delta\omega$ and $\Delta\mathbf{k}$ for momenta along some fixed cut in momentum space. This makes sense for presenting the dispersion of collective modes. However, in indirect RIXS of underdoped cuprates

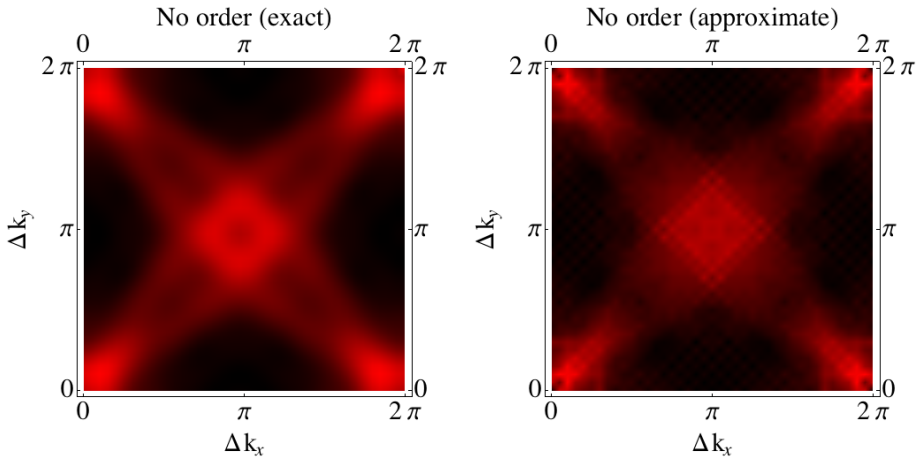

Figure 2.2: Comparison of exact (Eqs. (3.2) and (2.5)) and approximate (Eq. (2.11) formulas for momentum-dependent indirect RIXS intensity of unordered system for doping $p = 0.15$, energy transfer $\Delta\omega = 100$ meV.

the fundamental excitations are a continuum of particle-hole pairs, the dispersion of which is not inherently interesting. Rather, the indirect RIXS intensity measures the joint density of states of particles and holes, which are useful in that they reflect the overall fermiology over the entire Brillouin zone. Thus, the most natural way to present indirect RIXS data is as plots of intensity versus momenta over the entire Brillouin zone for fixed $\Delta\omega$. (In a work complementary to this one, Marra et al have argued that such a presentation of data is also useful for discerning ground state properties via direct RIXS[70]).

In Fig. 2.1 we examine the indirect RIXS spectrum in a state with no terms in H_d other than the band structure H_0 and compare it to states in which various mean-field order parameters are added to H_0. The intensity in the unordered state corresponds closely to the joint density of particle-hole pairs with total momentum Δk and total energy $\Delta\omega$. Besides the peaknear zero momentu transfer, the dominant feature is the

peak at $\Delta k = (\pi, \pi)$ at energies several hundred meV and less. This is due to the large density of states for both particles and holes near antinodal regions $(\pi, 0)$ etc, which is caused by a saddle point in the dispersion. The peak does not occur exactly at (π, π) because the Fermi surface does not cross antinodal momenta $(0, \pi)$ and $(\pi, 0)$, and thus there exists no antinodal-antinodal particle-hole pair with momentum $(\pi, 0) - (0, \pi) = (\pi, \pi)$. In a non-interacting system at half filling and only nearest-neighbor hopping there are van Hove singularities at antinodal momenta and we would expect the diamond-shaped Fermi surface to yield a RIXS maximum at (π, π) for small energy transfers. For the ordered systems we use order parameter amplitudes $V_{DDW} = 100$ meV, $V_{CDW} = 100$ meV, $V_{AF} = 100$ meV, which are typical energy scales for the pseudogap of the cuprates' normal state. These yield distinct changes in the RIXS spectra that allow experiments to distinguish them. Of particular interest is that the d-density wave phase exhibits a clear signature distinct from other phases, including the antiferromagnetic phase which also has a wavevector of (π, π). As seen in Fig. 2.1, indirect RIXS at small $\Delta\omega$ of systems with DDW and AF order follows a similar pattern to unordered systems described by the band structure H_0: intensity maxima at zero momentum and around (π, π), joined by arms running along the nodal directions (k, k). In the DDW system, the maximum near (π, π) is strengthened relative to the maximum near $(0, 0)$, while in the AF system intensity increases along the arms. The behavior of the AF spectrum is directly related to the Fermi surface reconstruction due to ordering at a wavevector of (π, π). As long as V_{AF} is not extremely strong, the bulk of the Fermi surface is replaced by large oval-shaped pockets that overlap the unreconstructed Fermi surface on one side and parallel it on the other. From the point of view of the joint density of states of particle hole pairs, the effect is similar to a broadening of the Fermi surface. In contrast, the d-density wave has the same (π, π) wavevector, but the

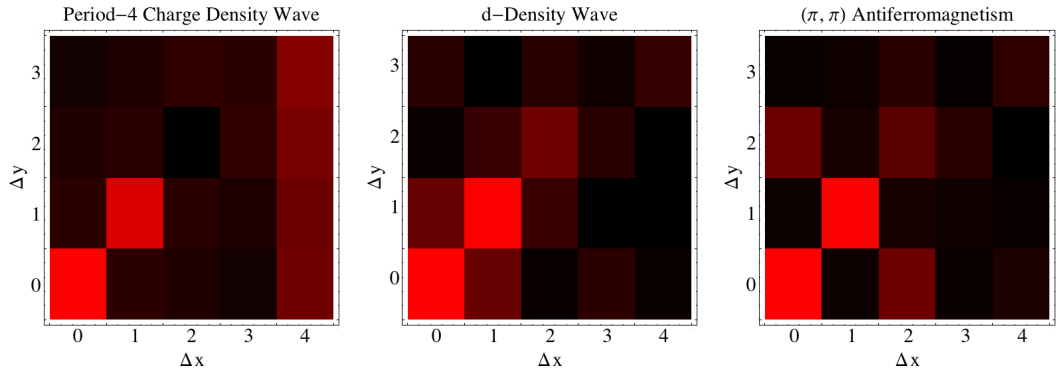

Figure 2.3: Fourier transforms of RIXS intensities from Fig. 2.1 exhibiting clear period-4 periodicity of the CDW system and checkerboard periodicity in the DDW and AF systems.

form factor $V_{DDW}(\mathbf{k})$ vanishes in the nodal direction and is maximal in the antinodal direction. Hence the Fermi surface reconstruction due to DDW order is restricted to the antinodal momenta near $(\pi, 0)$ and $(0, \pi)$. This explains why the "arms" of the indirect RIXS intensity pattern are not broadened as in the system with AF order. The reason the intensity maximum at (π, π) is strengthened is that the antinodal saddle point of the dispersion is buried inside the unreconstructed Fermi surface – there are antinodal holes, but only *near*-antinodal particles. After reconstruction, there are more particles available near the saddle point.

Unlike the previous examples, CDW order strongly modifies the intensity pattern of the orderless system. One distinct feature is the appearance of maxima near $(0, 2\pi/4)$, which is to be expected of Fermi surface reconstruction due to translational symmetry breaking with this wavevector. This is a robust feature of RIXS at low energy transfers; indeed, at zero energy transfer this momentum becomes the elastic peak of the symmetry-broken system. That is, the CDW by definition induces elastic scattering at wavevector Q_{CDW}, which generates low-energy particle hole pairs with total momentum Q_{CDW}. Another obvious feature is the destruction of the intensity near (π, π), which

was a maximum for the unordered system as well as the DDW and AF systems. We observe generally that a perturbation with wavevector $\mathbf{Q}$ does not destroy the density of states of low energy particle-hole pairs with wavevector $\mathbf{Q}$. (Of course, the order yields a gap at energy scales of meV or tens of meV, which are much smaller than current energy scales measured by RIXS). Thus DDW and AF order are in a sense "compatible" with the RIXS spectrum of the unordered system. Ordering at a different wavevector, on the other hand, can and does drastically change the particle-hole joint density of states. The clear qualitative difference between the CDW spectrum and those of DDW and AF systems, along with the maximum at $\mathbf{Q}_{CDW}$, are telltale signs of translational symmetry breaking at a wavevector other than (π, π). However, one can discern different orders even more clearly with a complementary measurement: Recall from above that the Keldysh-like two-site correlator S_{mn} can be measured as the Fourier transform of intensity. Specifically, the Fourier transform of $I(\Delta\mathbf{k}, \omega, \Delta\omega)$ gives $S(\Delta\mathbf{r}, \omega, \Delta\omega) \equiv \sum_{\mathbf{r}_m - \mathbf{r}_n = \Delta\mathbf{r}} S_{mn}(\omega, \Delta\omega)$. It is intuitively clear that $S(\Delta\mathbf{r})$ ought to have a spatial structure corresponding to that of H. In Fig. 2.3, we see that the Fourier transform of RIXS intensity exhibits the spatial periodicity of H, that is, a checkerboard pattern for DDW and AF orders and a stripe at $\Delta x = 4$ for period-4 CDW. (Even though our calculations were performed on 40×40 systems, we show only a few near-neighbor lattice sites in the Fourier-transformed spectra because S_{mn} decays rapidly with separation between $\mathbf{r}_m$ and $\mathbf{r}_n$).

While plots over the entire Brillouin zone are the most efficient way to convey qualitative features of RIXS spectra, a two-dimensional plot of intensity along a cut in momentum space (still at fixed $\Delta\omega$) may more precisely capture certain quantitative features. For example, in the density plots over the full two-dimensional Brillouin zone, the aforementioned difference between DDW and the unordered state is apparent but

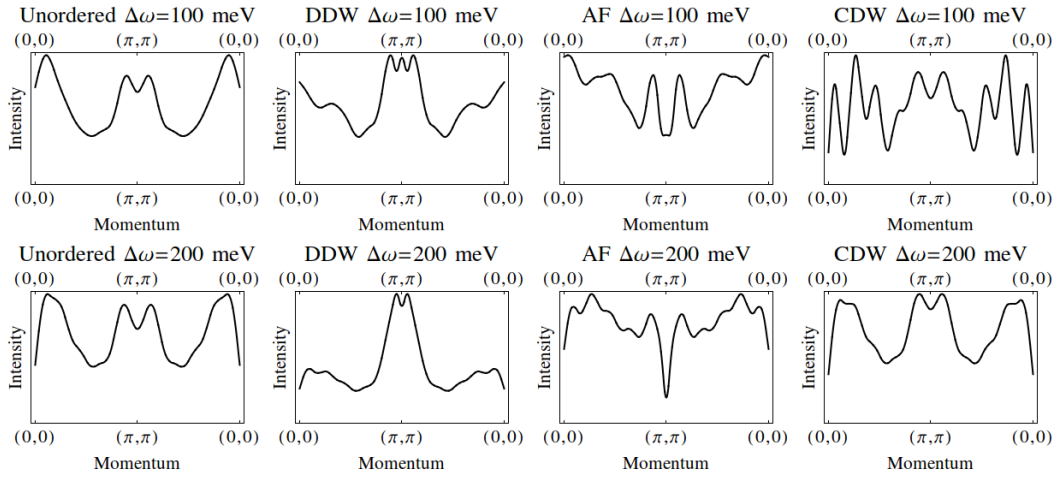

Figure 2.4: One-dimensional plots of intensity along antinodal momenta for fixed $\Delta\omega$ and various types of order.

not overwhelming. In a one-dimensional plot, the quantitative difference is obvious – scattering with momentum transfer near (π, π) is very strongly enhanced relative to near-zero momentum transfers for the DDW case, compared to the unordered state. We show in Fig. 2.4 one-dimensional plots in the antinodal (π, π) direction for alltypes of order considered above.

Thus, each of the orders we have considered have not only distinct patterns of indirect RIXS, but "smoking gun" signatures with simple interpretations. There are, of course, many proposed pseudogap order parameters other than the CDW, DDW, and AF that we have considered here. However, these three examples demonstrate that one can easily obtain robust, falsifiable predictions for the indirect RIXS spectrum of any candidate order. Furthermore, these are among the most widely-proposed orders for the normal state of underdoped cuprates and it is encouraging that they exhibit such distinct patterns.

2.4 Modelling RIXS with a Single Particle-Hole Pair

As mentioned above, our exact results ought to be well-approximated by considering only a single shake-up pair in indirect RIXS. It is straightforward to derive the RIXS intensity under this approximation for arbitrary bilinear Hamiltonians H_d containing any combination of mean-field and impurity potentials. We obtain

$$\begin{aligned} I \propto & \sum_{\alpha,\beta} \left| \tilde{V}_{\alpha,\beta}(\mathbf{k}) \int \frac{g(\varepsilon) d\varepsilon}{(\omega - (\varepsilon_\alpha - \varepsilon_\beta - \varepsilon + i\Gamma)(\omega - \varepsilon + i\Gamma)} \right|^2 \\ & \times n_f(\varepsilon_\alpha)(1 - n_f(\varepsilon_\beta))\delta(\varepsilon_\alpha - \varepsilon_\beta - \Delta\omega), \qquad (2.11) \\ \tilde{V}_{\alpha,\beta}(\mathbf{k}) = & \sum_m e^{i\mathbf{k}\cdot\mathbf{r}_m} \langle \alpha | V_m | \beta \rangle \end{aligned}$$

where $|\alpha\rangle$ and $|\beta\rangle$ are single-particle eigenstates of H_d, $g(\varepsilon)$ is the $4p$ density of states, and $\tilde{V}(\mathbf{k}) = \sum_m e^{i\mathbf{k}\cdot\mathbf{r}_m} V_m$ is the Fourier transform of the core hole potential operator. We show in Fig. 2.2 that Eq. (2.11) gives results very similar to the exact formula Eq. (2.5), which we used to generate the figures in this chapter. In addition to making explicit the connection between RIXS and the joint particle-hole density of states, Eq. (2.11) is also useful for analyzing the dependence of the RIXS signal on the incident photon energy ω. Here the resonance in ω is convoluted with the broad and featureless $4p$ density of states. The intensity is maximal when ω is in resonance to excite the core electron to the $4p$ band minimum, where the group velocity vanishes and the p electron is most likely to return to the core hole site. Other than this feature the resonant factor yields little structure. In particular, the overall shape of the spectrum as a function of $\Delta\mathbf{k}$ and $\Delta\omega$ is unchanged as ω varies (to the point that $\omega = 10$ eV yields figures identical to those shown above, up to an overall scale), although the overall magnitude is strongly ω-dependent. In experiments one should tune ω to maximize the intensity

but varying ω yields no useful information.

2.5 Alternative Analysis of RIXS Data

It is possible that in real samples, with the combined effects of disorder, inhomogeneity, and non-resonant scattering, it may be desirable to increase the statistical power and robustness of measurements. One way to do this is to define appropriate averaged variables. One natural choice is simply to average over a range of $\Delta\omega$:

$$\int_{\Delta\omega_1}^{\Delta\omega_2} I(\Delta\mathbf{k}, \Delta\omega) d\Delta\omega, \tag{2.12}$$

The most useful choice of the interval $[\Delta\omega_1, \Delta\omega_2]$ will be some range of small energy transfers with $\Delta\omega_1$ large enough to avoid the elastic peak but with $\Delta\omega_2$ small enough that the averaged quantity still reflects the redistribution of low-energy particles and holes due to Fermi surface reconstruction. In Fig. 2.5 we plot this integrated intensity in the window 100 meV $\leq \Delta\omega \leq$ 500 meV. The same qualitative distinctions between spectra that appeared for fixed energy transfer $\Delta\omega = 100$ meV are also present in the integrated spectra, namely, concentration of intensity near $\Delta\mathbf{k} = (\pi, \pi)$ for DDW, increase of intensity along the "arms" $\Delta k = (k, k)$, $0 \leq k \leq \pi$ for AF order, and general diffuseness of intensity across the Brillouin zone for CDW. Another measure is the first moment, that is, the averaged energy transfer $\Delta\omega$ weighted by the intensity:

$$1\text{st moment}(\Delta\mathbf{k}) = \int \Delta\omega I(\Delta\mathbf{k}, \Delta\omega) d\Delta\omega \tag{2.13}$$

This measures the shift of particle-hole pairs to higher energies as gaps are opened at parts of the Fermi surface, and to lower energies as new parts of the Fermi surface arise.

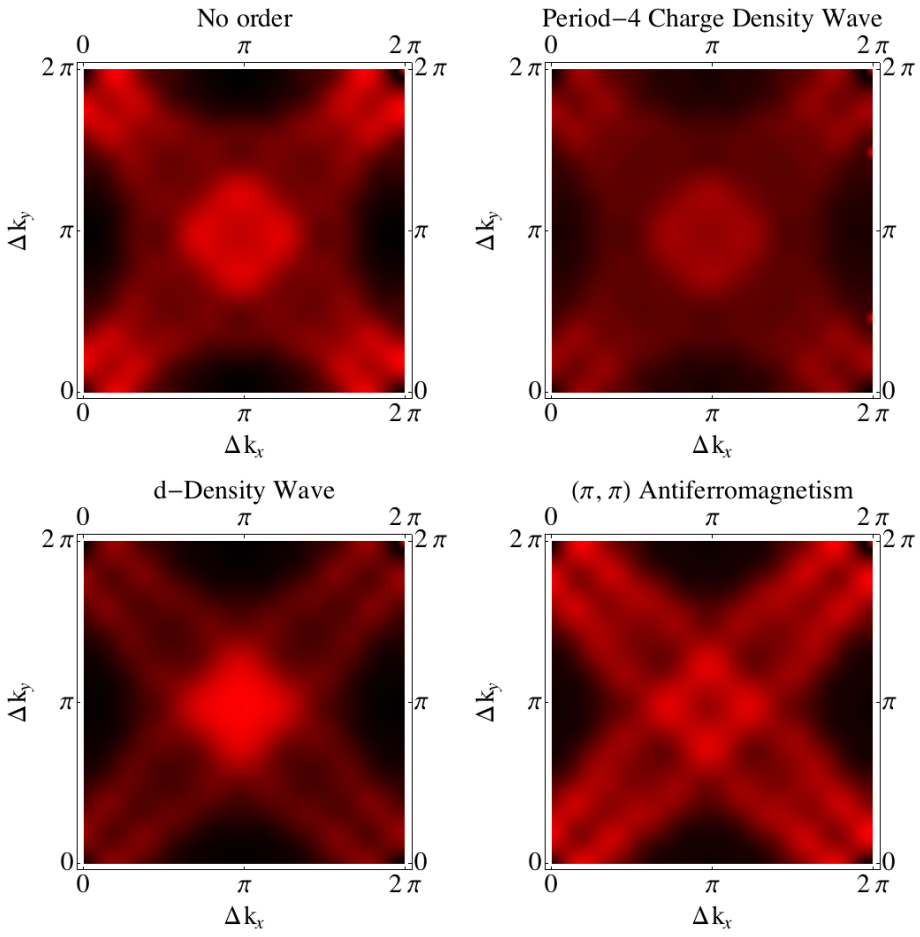

Figure 2.5: Same as Fig. 2.1 but with $\Delta\omega$ integrated from 100 meV to 500 meV. Clockwise from top left: unordered state, CDW, AF, DDW.

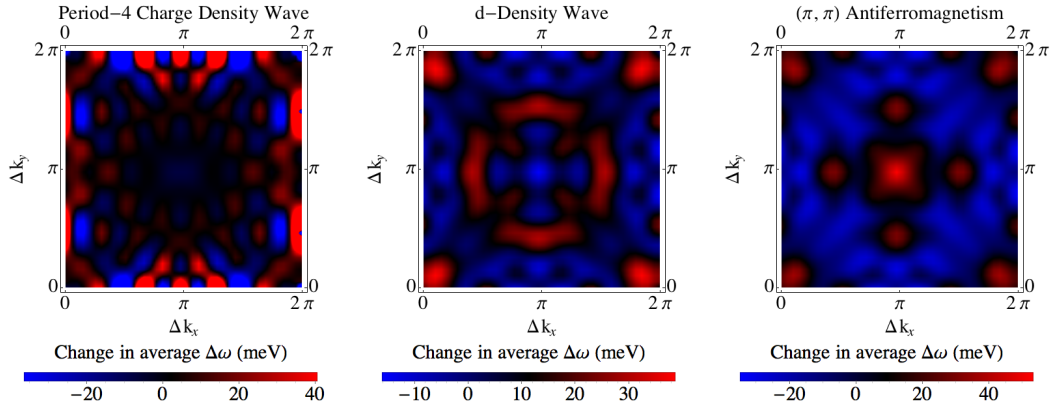

Figure 2.6: Change in first moments integrated over 100 meV $\leq \Delta\omega \leq$ 500 meV relative to unordered first moments as function of momenta across the entire Brillouin zone.

In Fig. 2.6 we show the distinct patterns in the first moments for DDW, CDW, and AF orders relative to the unordered state.

Summary.– We presented a formalism for treating exact band structures and core hole potentials in indirect RIXS. We showed that indirect RIXS measures the joint density of states of particles and holes and is sensitive to perturbations to band structure due to the formation of local ordered states. Furthermore, we showed that it is sensitive even to types of order that do not modulate the electron density.

3

Direct RIXS in Optimally-doped and Over-doped Cuprates

3.1 Introduction

As mentioned above, direct RIXS bears a facile comparison to neutron scattering in that both are momentum- and energy- resolved probes of excitations produced by inelas-

tic scattering. Many direct RIXS experiments in correlated materials are interpreted, without justification, in terms of this comparison. However, some thought reveals very significant difference between direct RIXS and neutron scattering that call into question the validity of their comparison. There is, of course, the defining property that RIXS is resonant while neutron scattering is not. This property is related to the fact that RIXS derives from a second-order process. As a consequence, direct RIXS can exhibit a non-trivial cross section even in the absence of electron interactions – the electron that re-fills the core hole may have a lower energy than the excited photoelectron. Lastly, direct RIXS couples to any excitation involving valence electrons since it is driven by the addition of an electron to the valence system. This is in contrast to neutron scattering, which couples unambiguously to magnetic moments and not to electron charge density. In this chapter we will show in the context of well-known experiments on the cuprate superconductors that the analogy between direct RIXS and neutron scattering is not appropriate and that these experiments must be reinterpreted.

It is widely believed that collective magnetic modes provide the "pairing glue" responsible for high-temperature superconductivity in the doped cuprates[89]. It is therefore extremely important to determine the nature of magnetism in these materials. Recent resonant inelastic x-ray scattering (RIXS) experiments in hole-doped cuprates[63,64,26] find a peak at energy transfers of $\sim 200 - 300$ meV that varies little in location and intensity between the undoped and heavily-overdoped parts of the phase diagram. Previous work[63,64,26] has interpreted this peak as the signature of a collective magnetic mode that evolves with doping from a coherent magnon in the undoped antiferromagnet to a paramagnon with very little loss of spectral weight. This interpretation is troubling for several reasons. First, overdoped cuprates are good metals and well-described by Fermi liquid theory[76]; there is little reason to believe that their propensity for mag-

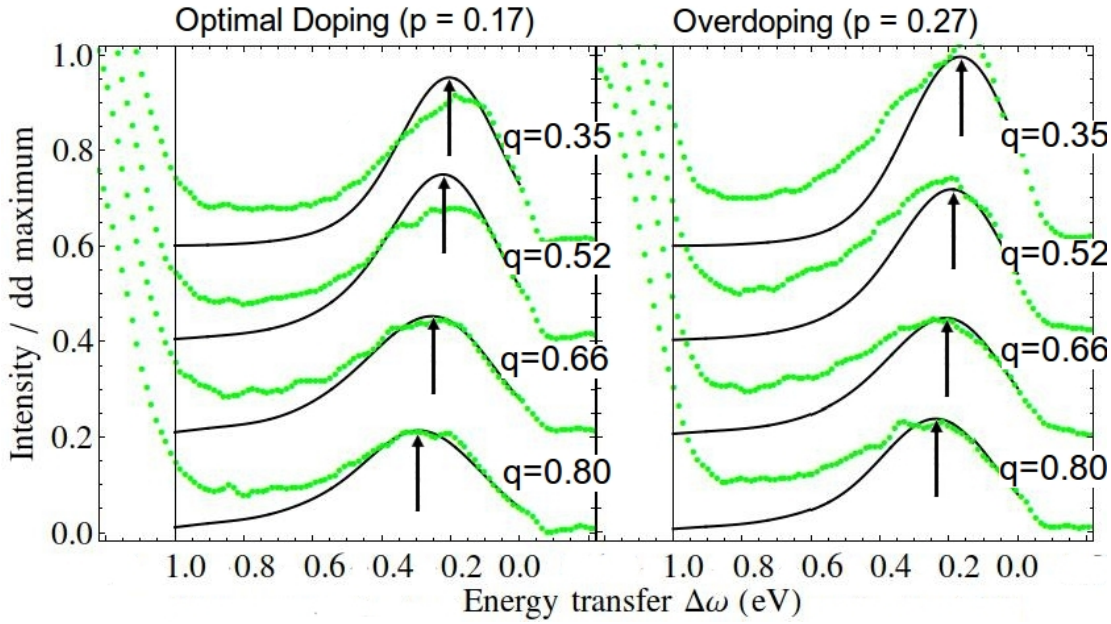

Figure 3.1: Calculated (black curve) and experimental (Ref. [64], green dots) intensity vs. energy transfer for spin-flip RIXS of optimally-doped and overdoped Tl-2201 for antinodal momenta $\mathbf{Q} = q(\pi/a, 0)$ exhibiting identical dispersing peaks. We subtracted a non-resonant elastic peak from the raw experimental data. We did not remove the contribution of dd excitations, which accounts for the discrepancy at large $\Delta\omega$.

netism is comparable to that of the undoped antiferromagnetic Mott insulator. Second, while inelastic neutron scattering experiments detect magnetic collective modes in the undoped cuprates, they find that the spectral weight for magnetic excitations above 100 meV decreases dramatically with doping[53,114,101,104*]. Finally, superconductivity in the cuprates vanishes rapidly with overdoping and it would be difficult to reconcile this with a magnetic pairing glue if the spectral weight of magnetic excitations did not simultaneously decrease.

Despite the wide range of doping in RIXS experiments, most theoretical work has focused on Mott insulating phases[108,109,22] in parent materials and local cluster models

*See, however, Refs. [28] and [27], which argue that the absence of magnetic signatures in neutron scattering is not relevant.

of doped materials[109,54]. Consequently, data from materials with itinerant electrons have been interpreted in terms of models of insulators. In particular, the hypothesis that RIXS data on optimally- and over-doped cuprates exhibit signs of collective magnetic modes is supported by analogy to spin wave theories that apply to undoped Mott-insulating cuprates and not by calculations on a microscopic model with mobile electrons. As even the underdoped cuprates exhibit a Fermi surface[65,31,111], this analogy is likely to fail over much of the cuprate phase diagram. This situation is especially unfortunate because it neglects processes in which one quasiparticle state is filled by photoabsorption and a different quasiparticle hole is left by re-emission (Fig. 3.2), which constitutes the ubiquitous lowest-order contribution to RIXS in any itinerant electron system[60]. In this chapter we analyze RIXS in the doped cuprates with a more appropriate single-band quasiparticle model in order to decide whether one must invoke a higher-order contribution from collective modes to explain experimental data. We find that quasiparticles alone yield excellent quantitative agreement between theory and experiment. We also address the issue of whether our model is not only sufficient but necessary to explain experiments, and propose a simple measurement to conclusively distinguish quasiparticles from collective modes in RIXS.

Below, we calculate RIXS spectra using a model of non-interacting quasiparticles but including an interaction with a positively-charged core hole via an exact determinantal method. We account for spin-orbit splitting of the core level in direct RIXS, in which a Cu $2p$ core electron is photoexcited to the valence band, which opens a spin-flip (SF) channel in addition to the non-spin-flip (NSF) channel[7,8,45]. We apply our formalism to cuprates over a range of doping and achieve quantitative agreement with experimental data (Fig. 3.1). In particular, peaks in the calculated and measured lineshapes disperse identically. As in experiments we also find that NSF lineshapes are broader and higher

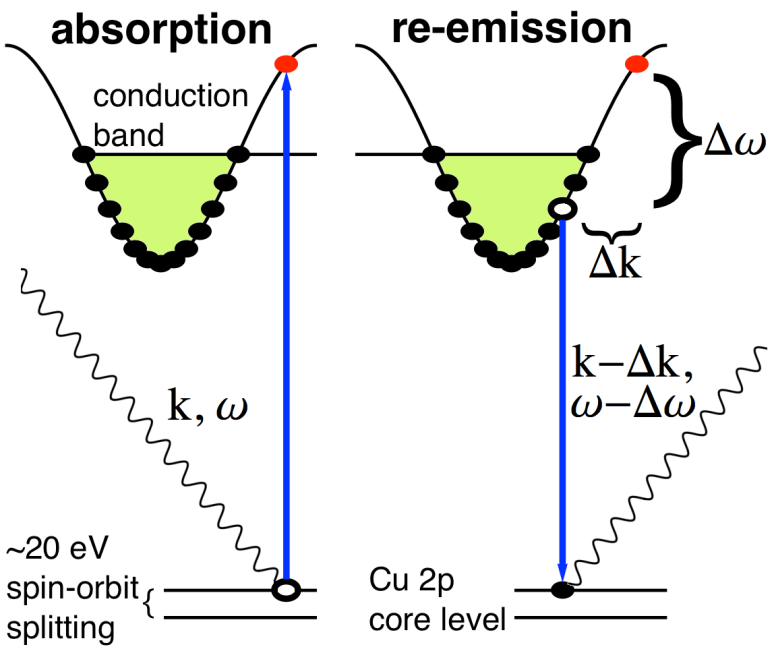

Figure 3.2: Direct RIXS process that leaves behind a single particle-hole pair. The transient core hole potential can excite multiple particle-hole pairs.

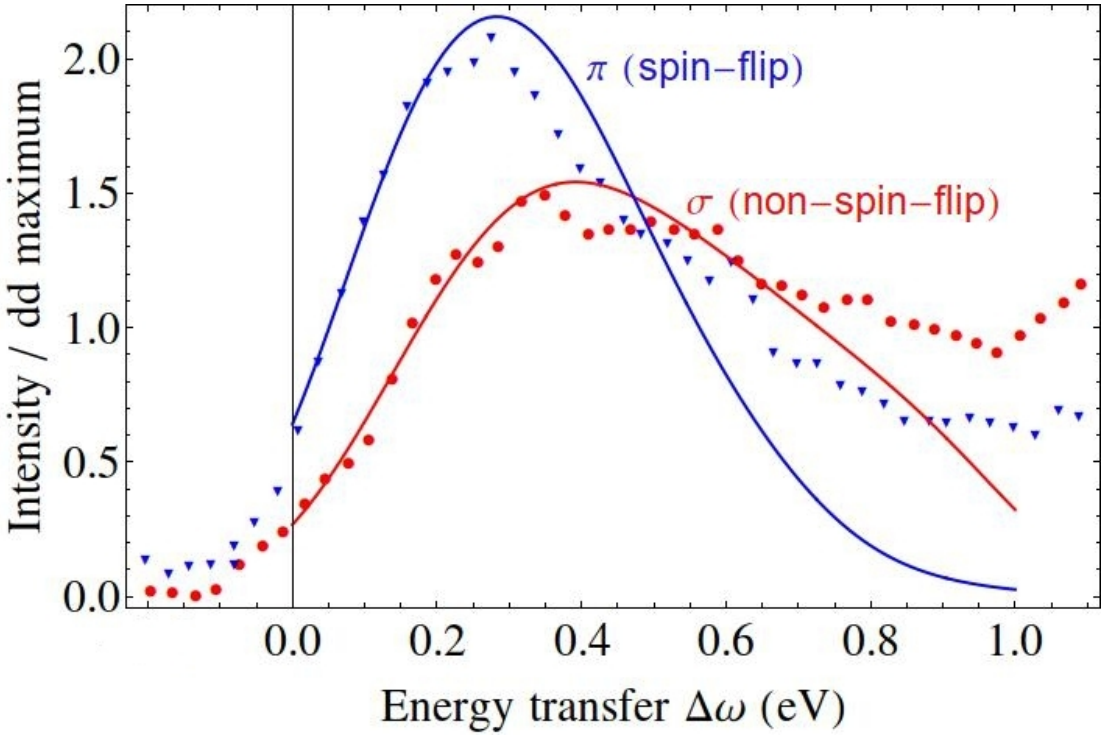

Figure 3.3: Spin-flip (π-polarized) and non-spin-flip (σ-polarized) antinodal $\mathbf{Q} = 0.80(\pi/a, 0)$ lineshapes of optimally-doped ($p = 0.15$) Bi-2212 for core hole potential $U_c = 1.0$ eV. Blue: spin-flip channel/π-polarization; red: non-spin-flip channel/σ-polarization. Solid lines: calculated results; triangles, circles: π- and σ- polarized data from Ref. [27].

in energy than SF lineshapes. These features were previously attributed to magnetic effects, but we find that band structure alone produces dispersing lineshapes, while the core hole combines with Pauli blocking to separate SF and NSF lineshapes.

3.2 Theoretical Formalism

Incident photons with momentum $\mathbf{q}$ and energy ω scatter into outgoing momentum $\mathbf{q} + \mathbf{Q}$ and energy $\omega - \Delta\omega$, where $\mathbf{Q}$ and $\Delta\omega$ are the momentum and energy transfer, with intensity[60,8,45] $I \propto \sum_f |A_f|^2 \, \delta(E_f - E_i - \Delta\omega)$, where A_f is given by the Kramers-

Heisenberg formula:

$$A_f = \sum_m e^{i\mathbf{Q}\cdot\mathbf{R}_m} \chi_{\rho\sigma} \langle f | d_{m\rho} (H_m + \omega - E_i + i\Gamma)^{-1} d^\dagger_{m\sigma} | i \rangle. \tag{3.1}$$

Here $|i, f\rangle$ and $E_{i,f}$ are the initial and final electron states and energies, $d^\dagger_{m\sigma}$ creates a valence electron of spin σ at site m, $H_m = H + V_m$ is the sum of the equilibrium Hamiltonian H and the potential V_m due to a core hole at site m, and $\chi_{\rho\sigma}$ is a polarization-dependent 2×2 spin matrix that comes from the product of two dipole matrix elements: $\langle 3d_\sigma | T_\sigma | 2p \rangle$ and $\langle 2p | T_\rho | 3d_\rho \rangle$ for absorption and emission, where T is a dipole transition operator[†]. In direct RIXS the strong ($\sim$ 20 eV) spin-orbit coupling of the Cu $2p$ core level implies that the energy eigenstates $|2p_{J,m}\rangle$ are not eigenstates of spin S_z. Thus off-diagonal elements $\rho \neq \sigma$ are permitted. One can isolate either the diagonal (NSF) or off-diagonal (SF) component of χ by varying only the incident polarization. The immobile intermediate state core hole does not appear explicitly in Eq. (3.1) but affects the valence system indirectly. It forces absorption and emission to occur on the same site m and contributes a width Γ and the potential V_m acting on valence electrons.

Due to the core hole the eigenstates of H_m have no simple relation to those of H and it is convenient to work in the time domain. This puts the intensity in the form[78]

$$I \propto \int_{-\infty}^{\infty} ds \int_0^{\infty} dt \int_0^{\infty} d\tau \, e^{i\omega(t-\tau) - is\Delta\omega - \Gamma(t+\tau)} \times \sum_{mn} e^{i\mathbf{Q}\cdot(\mathbf{R}_m - \mathbf{R}_n)} \chi_{\rho\sigma} \chi_{\mu\nu} S^{mn}_{\rho\sigma\mu\nu}, \tag{3.2}$$

$$S^{mn}_{\rho\sigma\mu\nu} = \left\langle e^{iH\tau} d_{n\rho} e^{-iH_n\tau} d^\dagger_{n\sigma} e^{iHs} \ldots d_{m\mu} e^{iH_m t} d^\dagger_{m\nu} e^{-iH(t+s)} \right\rangle. \tag{3.3}$$

[†]We explicitly derive the effects of spin-orbit coupling in the Supplemental Material. See also Refs. [8] and [45]

One obtains Eq. (3.2) via the identities $1/z = \int_0^\infty e^{-zt}dt$, $\delta(z) = \int e^{isz}ds$, replacing eigenvalues by operators, and recognizing resolutions of unity, e.g. $\sum_f |f\rangle\langle f| \ldots |i\rangle\delta(E_f - E_i - \Delta\omega) \rightarrow \int ds\, e^{-i\Delta\omega s} e^{iHs} \ldots e^{-iH_i s}|i\rangle$. However, Eq. (5.6) is best understood as a history of absorption and emission events separated by time evolution operators, that is, as the time-dependent amplitude to scatter a photon. The intensity is obtained from the square of this amplitude, hence the pair of creation and annihilation operators is followed by its Hermitian conjugate.

In the following analysis we treat the valence band as a system of non-interacting quasiparticles. This approximation is valid when the quasiparticle lifetime is long compared to the core hole lifetime $1/\Gamma$, in which case an electron is unlikely to scatter in the brief time between absorption and emission. In the cuprates, for example, typical values are $\Gamma = 300 - 500$ meV, which exceeds quasiparticle widths even quite far from the the Fermi surface. (We stress that negligible quasiparticle scattering on short time scales is conceptually distinct from a Fermi liquid ground state[29]; the former, for example, implies nothing about DC transport).

If not for the insertion of d and $d^\dagger$ operators we could easily evaluate the many-body average in Eq. (5.6) in terms of the matrices $h_{(m,n)}$, where lowercase letters denote the matrix elements of a quadratic operator: $H = d_i^\dagger h_{ij} d_j$, and the Fermi occupancy matrix $N \equiv \left(1 + e^{\beta h}\right)^{-1}$. A well-known identity[88,90] for the average of exponentiated quadratic operators $\left\langle e^Z \right\rangle = \det\left[(1 - \hat{N}) + e^z \hat{N}\right]$ extends naturally to the product of such exponentials via the Baker-Campbell-Haussdorff lemma[57]. To compute $S^{mn}_{\rho\sigma\mu\nu}$ for direct RIXS we extend a method applied to tunneling in quantum wires[2] and resonant elastic x-ray scattering[12], which involved matrix elements like those in Eq. (5.6) but with one d and one $d^\dagger$. We present the straightforward but lengthy derivation in Appendix

D. The result is

$$S^{mn}_{\rho\sigma\mu\nu} = \det(F)\left[\langle n\rho|(1-N)F^{-1}e^{-ih_n\tau}|n\sigma\rangle\ \langle m\mu|e^{-ihs}e^{ih_n\tau}(1-N)F^{-1}U_{mn}|m\nu\rangle\right.$$
$$\left. + \langle n\rho|(1-N)F^{-1}U_{mn}|m\nu\rangle\ \langle m\mu|e^{ih_mt}U_0NF^{-1}e^{-ih_n\tau}|n\sigma\rangle\right]. \tag{3.4}$$

where $U_{mn} = e^{-ih_n\tau}e^{ihs}e^{ih_mt}$, $U_0 = e^{i(\tau-t-s)h}$, and $F = 1-N+U_{mn}U_0N$. For a full band S vanishes, as it should, and for an empty band it reduces to $\langle n|e^{-ih_n\tau}|n\rangle\langle m|e^{ih_mt}|m\rangle$, a general term in the the expression $\left|\sum_m \int G^{mm}_{3d}(t)dt\right|^2$. That is, the amplitude of RIXS in an empty band is the coherent sum of electron propagators that start and end at the same core hole site. Eq. (3.4) pertains to a full spin-orbital basis, but for a spin-independent Hamiltonian easily factorizes. If H contains a singlet pairing term $d^\dagger_{m,\uparrow}B_{mn}d^\dagger_{m,\downarrow}$ it can be put into non-anomalous form suitable for matrix manipulations via a transformation $d^\dagger_{m\uparrow} \leftrightarrow d_{m\uparrow}$. This handles all spin density waves and pairing terms that occur in the cuprates. More complex spin density waves and triplet pairing require a more sophisticated formalism[58], which we present in Appendix A.

3.3 Results

We now apply this formalism to study cuprate superconductors, comparing our results to experiments on $Tl_2Ba_2CuO_{6+\delta}$ (Tl-2201) and $Bi_2Sr_2CuO_{6+x}$ (Bi-2212). An outstanding puzzle is the existence of peaks in direct RIXS not seen in neutron scattering[114] or indirect RIXS[47]. We use the single-band model $H = \sum_{\mathbf{k},\sigma}\varepsilon_{\mathbf{k}}d^\dagger_{\mathbf{k},\sigma}d_{\mathbf{k},\sigma}$, where $\varepsilon_{\mathbf{k}} = -2t_1(\cos(k_x)+\cos(k_y)) - 4t_2\cos(k_x)\cos(k_y) - 2t_3(\cos(2k_x)+\cos(2k_y)) - 4t_4(\cos(2k_x)\cos(k_y)+\cos(k_x)\cos(2k_y))$, using canonical tight-binding band structures fit to ARPES data: $(t_1,t_2,t_3,t_4) = (126,-36,15,1.5)$ meV for Bi-2212[69] and $(t_1,t_2,t_3,t_4) = (181,-75,-4,10)$ meV for Tl-2201[82]. We assume an attractive contact potential $V_m =$

$-U_c \sum_\sigma d^\dagger_{m\sigma} d_{m\sigma}$ for the core hole. We fix ω at the absorption maximum as in experiments. Fig. 3.1 shows SF intensity versus $\Delta\omega$ for antinodal momenta $\mathbf{Q} \parallel (\pi, 0)$ in optimally-doped and overdoped Tl-2201 ($p = 0.17$ and $p = 0.27$) with $U_c = 1.0$ eV along with data from Ref. [64]. We subtracted a Gaussian elastic peak at $\Delta\omega = 0$ from all experimental data and convolved calculated lineshapes with Gaussians of width equal to the instrumental resolutions of the corresponding experiments. We choose $U_c = 1.0$ eV to obtain the best fit to NSF lineshapes; SF RIXS is nearly independent of U_c. The most striking feature is an intensity peak that disperses to higher energy with increasing momentum, reaching a maximum of $250-300$ meV, as seen in experiments[63,28,26,64,27]. One possible interpretation is that these peaks are due to inelastic scattering of a collective mode. However, we see that band structure alone can produce them [‡]. Quantitatively, the calculated and experimental lineshapes agree very well, with the location of peaks and their low-energy side in nearly perfect agreement. There is a systematic discrepancy at large values of $\Delta\omega$ due to the tail of orbital dd excitations[121]. It is reassuring that this discrepancy is nearly independent of momentum, as local excitations ought to be. The calculated nodal and antinodal lineshapes also agree very well with experimental data from optimally-doped Bi-2212 [§].

In Fig. 3.3 we show that the agreement between theory and experiment extends to NSF scattering. This is important because the SF and NSF channels correspond to spin and charge degrees of freedom and a difference in their lineshapes is seen as compelling proof of magnetic physics. Indeed, the matrix elements in Eq. (3.5), below, are manifestly spin-independent, so that SF and NSF lineshapes should be identical in the absence of interactions. However, the core hole potential dramatically separates

[‡]Zeyher and Greco make a similar claim about Raman spectra in Ref. [123] and argue that RIXS behaves similarly.

[§]H. Ronnow, unpublished

SF and NSF lineshapes. As U_c increases, the NSF peak moves to higher energies and broadens while the SF peak remains relatively sharp, exactly as seen in experiments. For $U_c \sim 1.0$ eV the agreement is very good up to energies at which the *dd* tail becomes significant.

The core hole separates SF and NSF lineshapes as follows: Its attractive potential tends to keep the photoexcited electron of spin σ bound near $\mathbf{R}_m$, leading to elastic scattering. Pauli blocking prevents other electrons of spin σ from hopping onto $\mathbf{R}_m$ and filling the core hole, thereby robbing spectral weight from inelastic scattering. With sufficient energy the photoexcited electron may be dislodged, allowing inelastic scattering. Hence NSF scattering with small $\Delta\omega$ is suppressed relative to scattering with large $\Delta\omega$. This argument does not apply to SF scattering because spin-$\bar{\sigma}$ electrons are not Pauli-blocked. This explains the observed difference in SF versus NSF lineshapes as well as the insensitivity of NSF lineshapes to the core hole. Because this effect is non-perturbative an exact analysis is indispensable for detecting it. Since NSF lineshapes can be calculated reasonably well without a core hole potential a formula for the RIXS intensity in this limit may be useful. We obtain

$$I \propto \sum_{\alpha,\beta} \left| \frac{\sum_{\mathbf{k}} \chi_{\rho\sigma} \langle \alpha | \mathbf{k}+\mathbf{Q}, \rho \rangle \langle \mathbf{k}, \sigma | \beta \rangle}{\omega - \varepsilon_\beta + i\Gamma} \right|^2 n_f(\varepsilon_\alpha)(1 - n_f(\varepsilon_\beta))\delta(\varepsilon_\alpha - \varepsilon_\beta - \Delta\omega) \qquad (3.5)$$

where $|\mathbf{k}, \mathbf{k}+\mathbf{Q}\rangle$ are momentum eigenstates and $|\alpha, \beta\rangle$ are single-particle eigenstates of H in the spin-orbital basis.

Finally, we note that the overall intensity of calculated and measured lineshapes changes very little from the optimally-doped to the overdoped material. Our calculations differ from measured data by some overall multiplicative constant due to self-absorption, properties of the apparatus, and other factors. However, we used the same constant for

all lineshapes in Fig. 3.1, and thus the nearly-identical intensities at different dopings in our calculations are meaningful. If the RIXS signal came predominantly from a collective mode this would imply a spectral weight that varies little with doping. In our model, however, this happens naturally because a slight change in chemical potential does not strongly affect the band structure.

3.4 Outlook

We derived a formalism to treat band structures, pairing, and core hole potentials in direct and indirect RIXS. The lineshapes we calculated in a single-band model of mobile electrons agreed with experiments over a wide range of doping for both spin-flip and non-spin-flip scattering, and we found a mechanism by which the core hole differentiates the two channels. We concluded that dispersing peaks seen in RIXS experiments on cuprates can be attributed to band structure alone without invoking collective modes. Thus the constant intensity of peaks in RIXS as doping increases does not imply a constant spectral weight of magnetic excitations, which has important implications for the mechanism of superconductivity in these materials[89].

Our model of non-interacting quasiparticles is a priori well-supported by experimental evidence for the overdoped cuprates[76]. The agreement of our model with measured data suggests that it remains valid to doping at least as low as $p = 0.15$. We expect that it would work as far as $p = 0.08$, where a Fermi surface is found in experiments[65,31,111]. However, a non-interacting model becomes insufficient at some point in the underdoped regime. The analysis presented in this chapter can be extended to deeply-underdoped antiferromagnetic states via an RPA-like analysis, which is known to correctly reproduce spin wave excitations in the insulating state. As the insensitivity of RIXS lineshapes to

doping in the range we have considered persists to some extent to the undoped Mott antiferromagnet, a theory that bridges these two limits is very desirable.

While we showed above that a model of non-interacting quasiparticles is in excellent agreement with RIXS experiments, we have not yet presented a prediction that contrasts interpretations in terms of quasiparticles and in terms of collective modes. Such evidence, however, could easily be obtained by measuring RIXS lineshapes for incident energy ω above the absorption maximum. As shown in Fig. 3.4, as ω increases lineshapes move to larger $\Delta\omega$. The RIXS signal due to inelastic scattering of a collective mode does not behave this way because $\Delta\omega$ cannot exceed the energy of the mode. (This simple qualitative test could also prove useful in the analysis of RIXS in the Fe-based superconductors[124]. It would be interesting to apply our formalism to such systems, where an additional complicating factor is the existence of multiple bands). This exemplifies that one must calculate the RIXS signal itself, and not a proxy such as magnetic suceptibility. A susceptibility $\chi(\omega, \mathbf{k})$ depends on a single frequency ω, which corresponds to the energy of excitations. Since the energy transfer in RIXS plays a similar role the correspondence $\Delta\omega$ (RIXS) $\rightarrow \omega$ (susceptibility) is often assumed. However, this neglects the significant interplay of ω and $\Delta\omega$ in RIXS. In RIXS the phase space for final states is modified by the intermediate state resonance. For example, in Fig. 3.4 the intermediate state photoelectron's energy increases with ω, which tends to increase the energy of the final state particle-hole pair.

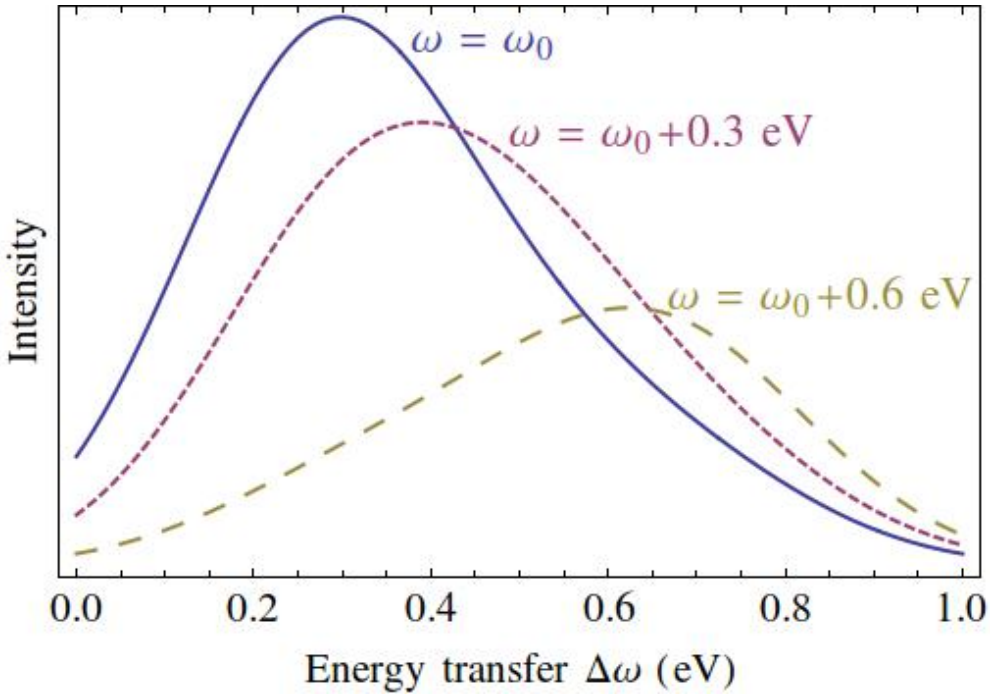

Figure 3.4: Calculated intensity vs. energy transfer for spin-flip RIXS of optimally-doped Bi-2212 (p=0.15) for antinodal momentum $\mathbf{Q} = (\pi/a, 0)$ at incident energies 0, 0.2, and 0.4 eV above the absorption maximum. The increase in $\Delta\omega$ with ω occurs when the RIXS final state belongs to the particle-hole continuum and does not occur if the final state is an excitation of a collective mode.

4

Variational Polaron Method for Bose-Bose Mixtures

4.1 Introduction

The effect on a system of interaction with a bosonic bath is an important problem in condensed matter physics, where phonons are ubiquitous and magnetic modes may

also appear. In recent years, experiments have produced degenerate Bose-Fermi[43,80,15] and Bose-Bose[20,17,37] mixtures of ultracold atoms with increasing degree of control, making possible the quantum simulation of bosonic environments. The behavior of a single impurity particle in a bosonic bath is very well-understood. Both the spin-boson problem for an immobile impurity and the polaron problem for a mobile impurity have been studied for a wide range of parameters. However, the effect of a bath on a many-body system, in which case one has overlapping interacting polarons rather than a single polaron, has not been analyzed thoroughly. It is very desirable to develop theoretical tools for this problem. Here we will examine the example of bosons in a superfluid bath and show that the variational polaron transformation is a useful, flexible, and intuitive technique.

When heavy bosons ('A') interact with a bath of light bosons ('B'), phonon-like excitations of 'B' dress particles of 'A'. Due to this dressing the 'A' bosons drag a cloud of 'B' bosons with them and see a concomitant increase in their effective mass. The dressing also induces intraspecies interactions between 'A' bosons, which see each other's associated phonon clouds. In this work we study the consequences of the 'B' phonon bath on a heavy Bose system 'A' that is near a Mott insulator-superfluid transition[34,40]. In this situation the renormalization of mass favors a Mott insulating phase. We expect instantaneous induced interactions at short distances to be attractive since two 'A' bosons near to one another will tend to distort the density of 'B' bosons in the same way. This reduction in the on-site repulsion favors the superfluid phase. At larger distances induced interactions can be attractive or repulsive due to a complicated interplay between the shape of phonon clouds and retardation effects. However, these off-site induced interactions are much weaker than the on-site one.

The canonical Lang-Firsov, or "polaron", transformation is a workhorse of condensed

matter theory that recasts a problem in terms of dressed quasiparticles. As such it encompasses the two aforementioned competing renormalizations of mass and on-site repulsion. However, there is no guarantee that it does so without bias. One can improve upon the polaron transformation by allowing parameters controlling the shape of the polaron cloud to become variational. This method was originally used to study isolated excitons interacting with phonons[118]. Here we demonstrate that this formalism is equally well-suited for analyzing multiple interacting polarons, with surprisingly little additional difficulty compared to the single polaron case. With this technique we dress each 'A' boson with a polaron cloud of Bogoliubov phonons and then obtain self-consistent ly the optimal shape of these polaron clouds. The variationally-determined polaron shape prescribes an effective renormalized 'A' Hamiltonian, the ground state of which we find to obtain the phase diagram in the presence of 'B'.

4.2 Mott-Superfluid Transition

Consider heavy bosons 'A' with filling set by chemical potential μ_a and light bosons 'B' with filling n_0 on a d-dimensional hypercubic lattice, with Hamiltonian $H = H_a + H_b + H_{ab}$, where

$$H_a = t_a \sum_{\langle ij \rangle} a_i^\dagger a_j + \sum_i \left(\frac{U_a}{2} n_i^a (n_i^a - 1) - \mu_a n_i^a \right) \tag{4.1}$$

$$H_b = t_b \sum_{\langle ij \rangle} b_i^\dagger b_j + \sum_i \frac{U_b}{2} n_i^b (n_i^b - 1) \tag{4.2}$$

$$H_{ab} = U_{ab} \sum_i n_i^a n_i^b \tag{4.3}$$

In the deep superfluid limit in which the condensate contains nearly all 'B' bosons, the Bogoliubov transformation[39], $c_{\mathbf{k}} = b_{\mathbf{0}}^\dagger (b_{\mathbf{0}}^\dagger b_{\mathbf{0}} + 1)^{-1/2} b_{\mathbf{k}}$, $\alpha_{\mathbf{k}} = u_{\mathbf{k}} c_{\mathbf{k}} + v_{\mathbf{k}} c_{-\mathbf{k}}$, diagonalizes H_b as

$$H_b = \sum_{\mathbf{k}} \omega_{\mathbf{k}} \alpha_{\mathbf{k}}^\dagger \alpha_{\mathbf{k}} \tag{4.4}$$

if $u_{\mathbf{k}}^2 = (\xi_{\mathbf{k}}/\omega_{\mathbf{k}} + 1)/2$, $v_{\mathbf{k}}^2 = (\xi_{\mathbf{k}}/\omega_{\mathbf{k}} - 1)/2$, $\xi_{\mathbf{k}} \equiv \varepsilon_{\mathbf{k}} + n_0 U_b$, $\omega_{\mathbf{k}}^2 = \varepsilon_{\mathbf{k}}(\varepsilon_{\mathbf{k}} + 2 n_0 U_b)$, $\varepsilon_{\mathbf{k}} = -2(\cos k_1 + \ldots + \cos k_d - d)$. In the same limit

$$H_{ab} = \frac{1}{\sqrt{N}} \sum_{i, \mathbf{k} \neq \mathbf{0}} n_i^{(a)} \beta_{\mathbf{k}} \Phi_{\mathbf{k}} e^{i \mathbf{k} \cdot \mathbf{R}_i}, \tag{4.5}$$

where $\beta_{\mathbf{k}} \equiv U_{ab} \sqrt{n_0} (u_{\mathbf{k}} - v_{\mathbf{k}})$ and $\Phi_{\mathbf{k}} = \alpha_{\mathbf{k}}^\dagger + \alpha_{-\mathbf{k}}$, $\Pi_{\mathbf{k}} = \alpha_{\mathbf{k}}^\dagger - \alpha_{-\mathbf{k}}$ are, up to constant factors, the 'B' density fluctuation operator at momentum $\mathbf{k}$ and its generator. We have left out a term $n_0 U_{ab} \sum n_i^a$, which shifts $\mu_a \to \mu_a - U_{ab} n_0$.

The polaron transformation[62]

$$\tilde{H} = e^S H e^{-S} = H + [S, H] + \frac{1}{2!}[S, [S, H]] \ldots, \tag{4.6}$$

$$S = \sum_{i, \mathbf{k} \neq \mathbf{0}} n_i^{(a)} \frac{f_{\mathbf{k}} \beta_{\mathbf{k}} \Pi_{\mathbf{k}}}{\sqrt{N} \omega_{\mathbf{k}}} e^{i \mathbf{k} \cdot \mathbf{R}_i} \tag{4.7}$$

cancels the interaction H_{ab} if $f_{\mathbf{k}} \equiv 1$ – this is the original Lang-Firsov transformation, which is yields an exactly-solvable Hamiltonian for a single static impurity with $t_a = 0$.

In general

$$\begin{aligned}\tilde{H} =& t_a \sum_{\langle ij \rangle} a_i^\dagger a_j \exp \sum_{\mathbf{k}\neq\mathbf{0}} \frac{f_\mathbf{k}\beta_\mathbf{k}\Pi_\mathbf{k}}{\sqrt{N}\omega_\mathbf{k}}(e^{i\mathbf{k}\cdot\mathbf{R}_i} - e^{i\mathbf{k}\cdot\mathbf{R}_j}) \\ &+ \sum_\mathbf{k} \omega_\mathbf{k}\alpha_\mathbf{k}^\dagger\alpha_\mathbf{k} + \frac{1}{2}\sum_{i,j} V_{ij} n_i n_j + \frac{U_a}{2} n_i(n_i - 1) \\ &- \mu_a n_i + \sum_{i,\mathbf{k}\neq\mathbf{0}} n_i \frac{\beta_\mathbf{k}\Phi_\mathbf{k}}{\sqrt{N}} \left(1 - f_\mathbf{k}\right) e^{i\mathbf{k}\cdot\mathbf{R}_i}, \end{aligned} \tag{4.8}$$

where for $\mathbf{R} = \mathbf{R}_i - \mathbf{R}_j$

$$V_{ij} = V_\mathbf{R} = -2\sum_{\mathbf{k}\neq\mathbf{0}} \frac{\beta_\mathbf{k}^2}{N\omega_\mathbf{k}}(2f_\mathbf{k} - f_\mathbf{k}^2)e^{i\mathbf{k}\cdot\mathbf{R}}. \tag{4.9}$$

We note that the series Eq. (4.6) ends after one or two successive commutators for all terms in $\tilde{H}$ except the renormalized hopping term. However, this term in Eq. (4.8) is also exact as we recognize the infinite series as the Taylor series of the exponential function. We shall later use the fact that

$$\begin{aligned}\sum_\mathbf{R} V_\mathbf{R} &= -2\sum_{\mathbf{k}\neq\mathbf{0}} \frac{\beta_\mathbf{k}^2}{N\omega_\mathbf{k}}(2f_\mathbf{k} - f_\mathbf{k}^2)\sum_\mathbf{R} e^{i\mathbf{k}\cdot\mathbf{R}} \\ &= -2N\sum_{\mathbf{k}\neq\mathbf{0}} \frac{\beta_\mathbf{k}^2}{N\omega_\mathbf{k}}(2f_\mathbf{k} - f_\mathbf{k}^2)\delta_{\mathbf{k},\mathbf{0}} = 0. \end{aligned} \tag{4.10}$$

This identity is a statement of charge conservation – the change in potentials seen by 'A' bosons due to a polaron cloud is simply U_{ab} times the redistributed 'B' density of the cloud, which must sum to zero.

The polaron transformation, which we presented above as a transformation on the Hamiltonian is, equivalently, a transformation on wavefunctions $\Psi \to e^S\Psi$. In S, a factor proportional to $f_\mathbf{k}$ and the density $\sum_i n_i e^{i\mathbf{k}\cdot\mathbf{R}_i}$ of'A' multiply the generator $\Pi_\mathbf{k}$.

Thus the polaron transformation aligns the density fluctuations of the two species, dressing 'A' bosons with coherent states of 'B' phonons, with the amount of alignment set by $f_{\mathbf{k}}$. This reduces potential energy at the cost of exciting phonons. Alternatively, considering the transformation on operators, the 'B' density transforms as

$$\tilde{b}_i^\dagger \tilde{b}_i = b_i^\dagger b_i + \sum_{\mathbf{R},\mathbf{k}\neq\mathbf{0}} n_{\mathbf{R}_i+\mathbf{R}} e^{i\mathbf{k}\cdot\mathbf{R}} \frac{f_{\mathbf{k}}\beta_{\mathbf{k}}}{\sqrt{N}\omega_{\mathbf{k}}}(u_{\mathbf{k}} - v_{\mathbf{k}}), \tag{4.11}$$

from which it is clear that $f_{\mathbf{k}}$ determines the shape of the phonon cloud attached to each 'A' boson. The induced interactions $V_{\mathbf{R}}$ are the self-interactions of 'A' mediated by 'B'. Furthermore, it is evident that by adjusting $\{f_{\mathbf{k}}\}$ we can obtain an arbitrary (Fourier-transformed) phonon cloud density, thus highlighting the generality of the variational polaron approach.

We take as a variational ansatz a polaron-transformed product wavefunction $\Psi = e^S|\Psi_a\rangle \otimes |0_b\rangle$, where $|0_b\rangle$ is the 'B' phonon vacuum. The variational energy is

$$E[f] = \langle\Psi_a|\langle 0_b|e^{-S}He^S|\Psi_a\rangle|0_b\rangle = \langle\Psi_a|\langle 0_b|\tilde{H}|0_b\rangle|\Psi_a\rangle. \tag{4.12}$$

Averaging with respect to the phonon vacuum simplifies the terms of $\tilde{H}$ in Eq. 4.8 greatly. The residual interaction is proportional to $\Phi_{\mathbf{k}} = \alpha_{\mathbf{k}}^\dagger + \alpha_{-\mathbf{k}}$ and vanishes upon averaging with respect to $|0_b\rangle$, as does the phonon energy. The dressed hopping term becomes $\tilde{t}\sum_{\langle ij\rangle} a_i^\dagger a_j$, with a renormalized hopping

$$\tilde{t} = t_a \exp\left[-\frac{2}{z}\sum_{\mathbf{k},\mathbf{a}} \frac{f_{\mathbf{k}}^2\beta_{\mathbf{k}}^2}{N\omega_{\mathbf{k}}^2}\sin^2(\mathbf{k}\cdot\mathbf{a}/2)\right] \tag{4.13}$$

where $\mathbf{a}$ are nearest-neighbor displacements and $z = 2d$. Species B has dropped out

of the variational energy completely and the variational energy functional $E[f]$ is the ground state energy of an effective Hamiltonian

$$H_{\text{eff}} = H_a(t_a \to \tilde{t}) + \frac{1}{2}\sum_{i,j} V_{ij} n_i n_j. \tag{4.14}$$

This readily generalizes to finite temperature by use of the Gibbs-Bogoliubov inequality[118,96], an upper bound on the free energy that one minimizes with respect to the parameters of the variational Hamiltonian, in contrast to the Rayleigh-Ritz inequality, which is an upper bound on the ground state energy.

We find empirically that the onsite induced interaction $V_{\mathbf{0}}$ is dominant, with the nearest-neighbor interaction $V_{nn} \equiv V_{\mathbf{a}}$ significantly smaller and all other interactions miniscule. Therefore we partition H_{eff} as

$$H_{\text{eff}} = H_a(t_a, U_a, \mu_a \to \tilde{t}, \tilde{U}, \tilde{\mu}) + \sum_{\langle ij \rangle} V_{\mathbf{a}} n_i n_j + V' \tag{4.15}$$

where $\tilde{U} = U_a + V_{\mathbf{0}}$, $\tilde{\mu} = \mu_a - V_{\mathbf{0}}/2$, and $V' = \frac{1}{2}\sum_{i \neq j, j+\mathbf{a}} V_{ij} n_i n_j$.

Iskin and Freericks[52] have calculated the phase diagram of a Bose-Hubbard model with nearest neighbor interaction using a third-order strong coupling expansion. They calculated the energy of particle and hole defects in the Mott insulating phase. Phase boundaries occur when the energy of either defect vanishes. However, we cannot simply discard the longer-range interactions V' and use Ref. [52] directly. Although each term in V' is small, the first order contribution from their sum is non-negligible. This is due to the fact that $\sum V_{\mathbf{R}} = 0$, which implies $\sum_{|\mathbf{R}|>1} V_{\mathbf{R}} = -V_{\mathbf{0}} - zV_{\mathbf{a}}$. The corrections to

first order in V' for the nth Mott lobe are

$$\langle V' \rangle_{\text{Mott}} = -\, n^2(V_{\mathbf{0}} + zV_{\mathbf{a}})/2 \tag{4.16}$$

$$\langle V' \rangle_{\text{part}} = -\, (n^2/2 + n)(V_{\mathbf{0}} + zV_{\mathbf{a}}) \tag{4.17}$$

$$\langle V' \rangle_{\text{hole}} = -\, (n^2/2 - n)(V_{\mathbf{0}} + zV_{\mathbf{a}}). \tag{4.18}$$

The hopping amplitude $\tilde{t}$ does not appear in the corrections due to V', so, except for zeroth order terms in $\tilde{t}$, Eqs. (14-15) of Ref [52] for the particle and hole gaps apply provided that we use $t, U, \mu, V_{nn} \to \tilde{t}, \tilde{U}, \tilde{\mu}, V_{\mathbf{a}}$. Adding the corrections from Eqs. (4.16 - 4.18) to the strong-coupling expansions derived by Iskin and Freericks we have, to third order

$$\begin{aligned}
\Delta_p =& U_a n - \mu_a + V_{\mathbf{0}}/2 - (n+1)z\tilde{t} + n\left\{(n+1)\left[\frac{1-z}{\tilde{U}} + \frac{2-2z}{\tilde{U}-2V_{\mathbf{a}}} + \frac{2z}{\tilde{U}-V_{\mathbf{a}}}\right]\right. \\
&\left. - \frac{n+2}{2\tilde{U}-2V_{\mathbf{a}}}\right\} z\tilde{t}^2 - n(n+1)\left\{n\left[\frac{z-2}{\tilde{U}^2} + \frac{z^2-3z+3}{(\tilde{U}-V_{\mathbf{a}})^2}\right] + (n+1)\left[\frac{2z^2-6z+6}{\tilde{U}(\tilde{U}-V_{\mathbf{a}})}\right.\right. \\
&\left.\left. + \frac{z-z^2}{\tilde{U}^2} + \frac{2z-2z^2}{(\tilde{U}-2V_{\mathbf{a}})^2} - \frac{2z^2-6z+6}{(\tilde{U}-V_{\mathbf{a}})^2} + \frac{4z-8}{\tilde{U}(\tilde{U}-2V_{\mathbf{a}})} + \frac{4z^2-12z+12}{(\tilde{U}-V_{\mathbf{a}})(\tilde{U}-2V_{\mathbf{a}})}\right]\right. \\
&\left. + (n+2)\left[\frac{z-1}{\tilde{U}(\tilde{U}-V_{\mathbf{a}})} - \frac{z}{4(\tilde{U}-V_{\mathbf{a}})^2}\right]\right\} z\tilde{t}^3
\end{aligned} \tag{4.19}$$

$$\begin{aligned}
\Delta_h =& -\, U_a(n-1) + \mu_a + V_{\mathbf{0}}/2 - nz\tilde{t} + (n+1)\left\{n\left[\frac{1-z}{\tilde{U}} + \frac{2-2z}{\tilde{U}-2V_{\mathbf{a}}} + \frac{2z}{\tilde{U}-V_{\mathbf{a}}}\right]\right. \\
&\left. - \frac{n-1}{2\tilde{U}-2V_{\mathbf{a}}}\right\} z\tilde{t}^2 - n(n+1)\left\{(n+1)\left[\frac{z-2}{\tilde{U}^2} + \frac{z^2-3z+3}{(\tilde{U}-V_{\mathbf{a}})^2}\right] + n\left[\frac{2z^2-6z+6}{\tilde{U}(\tilde{U}-V_{\mathbf{a}})}\right.\right. \\
&\left.\left. + \frac{z-z^2}{\tilde{U}^2} + \frac{2z-2z^2}{(\tilde{U}-2V_{\mathbf{a}})^2} - \frac{2z^2-6z+6}{(\tilde{U}-V_{\mathbf{a}})^2} + \frac{4z-8}{\tilde{U}(\tilde{U}-2V_{\mathbf{a}})} + \frac{4z^2-12z+12}{(\tilde{U}-V_{\mathbf{a}})(\tilde{U}-2V_{\mathbf{a}})}\right]\right. \\
&\left. + (n-1)\left[\frac{z-1}{\tilde{U}(\tilde{U}-V_{\mathbf{a}})} - \frac{z}{4(\tilde{U}-V_{\mathbf{a}})^2}\right]\right\} z\tilde{t}^3
\end{aligned} \tag{4.20}$$

To third order the Mott energy is

$$E_{\mathrm{Mott}} = \frac{U_a}{2} n(n-1) - \mu_a n - n(n+1)\frac{z\tilde{t}^2}{\tilde{U} - V_{\mathbf{a}}}. \tag{4.21}$$

The Mott energy to zeroth order in $\tilde{t}$, that is, the first two terms of Eq. (4.21), depends on *unrenormalized* U_a and μ_a. This reflects the fact that a homogeneous system cannot be dressed by density fluctuations. Likewise, the particle and hole excitations are homogeneous except for one particle or hole with self-energy $V_{\mathbf{0}}$. Higher-order contributions, in contrast, involve renormalized parameters because the Mott phase contains quantum fluctuations that can be dressed. In other words, the Mott phase contains a sea of virtual polarons.

We must determine the variational parameters $f_{\mathbf{k}}$ in order to obtain the phase diagram. Minimizing the $f_{\mathbf{k}}$-dependent part $\tilde{t}^2/(\tilde{U} - V_{\mathbf{a}})$ of E_{Mott} yields the analytic expression

$$f_{\mathbf{k}} = \left(1 + \frac{U_a}{2z\omega_{\mathbf{k}}} - \frac{4}{z^2\omega_{\mathbf{k}}}\lambda\right)^{-1}, \tag{4.22}$$

$$\lambda = \frac{1}{N}\sum_{\mathbf{q}\neq\mathbf{0},\mathbf{a}} \frac{\beta_{\mathbf{q}}^2}{\omega_{\mathbf{q}}} \sin^2(\mathbf{q}\cdot\mathbf{a}/2)(2f_{\mathbf{q}} - f_{\mathbf{q}}^2) \tag{4.23}$$

This equation can be solved iteratively, converging to a solution for λ in several iterations even near the critical point. From $f_{\mathbf{k}}$ we then have $V_{\mathbf{R}}$ and $\tilde{t}_a$ and can solve $\Delta_{p(h)} = 0$ using the strong-coupling expressions with modified zeroth-order terms to find μ_a at the upper and lower boundaries of the Mott lobe in the $t_a - \mu_a$ plane. As $f_{\mathbf{k}}$ and the renormalizations are independent of μ_a, the equations for the phase boundaries are linear in μ_a, hence trivially solved.

It is well-known that strong-coupling perturbation theory overestimates the size of

the Mott lobe. To mitigate its deficiencies near the critical point, we use the chemical potential extrapolation method[36]. Let $\mu_\pm$ denote the upper and lower edges of the Mott lobes and let $\mu_\pm^{\rm SC}$ denote the upper and lower edges as obtained from our strong coupling approximation. The idea is to fit the phase boundary to the scaling form

$$\mu_\pm = A(t_a) \pm \frac{1}{2} B(t_a)(t_a^c - t_a)^{z\nu}, \tag{4.24}$$

where $A(x)$ and $B(x)$ are smooth functions of $x = t_a$. We will use the constrained extrapolation method in which we use the known critical exponent $z\nu = 2/3$ (species 'B' does not undergo a phase transition and so does not modify critical exponents, and the Mott-superfluid transition of the single species 'A' belongs to the universality class of the $(d+1)$-dimensional XY model, the renormalization group treatment of which is well-known). The best fit for $A(t)$ is clearly

$$A(t_a) = (\mu_+^{\rm SC}(t_a) + \mu_-^{\rm SC}(t_a))/2. \tag{4.25}$$

We extrapolate t_a^c to infinite order by least-squares fitting of the critical point $t_a^c(m)$,where m is the order of perturbation theory, to a function linear in $1/m$. Finally, we expand $B(t_a) \approx \alpha + \beta t_a + \gamma t_a^2 + \delta t_a^3$ and use least-squares fitting of

$$\mu_+^{\rm SC}(t_a) - \mu_-^{\rm SC}(t_a) = B(t_a)(t_a^c - t_a)^{z\nu} \tag{4.26}$$

to obtain α, β, γ, δ and t_a^c.

In Fig. 4.1 we compare our results for the $n = 1$ Mott lobe in two dimensions to numerically exact quantum Monte Carlo simulations[42]. Parameters are $U_{ab} = U_b = 10$, $t_a = t_b = 1$, with U_a varying, for $n_b = 0, 0.1, 0.5, 0.75$. The agreement is very good,

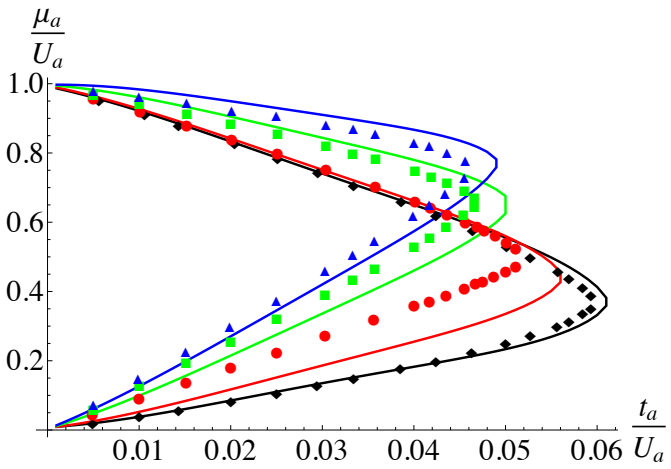

Figure 4.1: Analytic (solid lines) and quantum Monte Carlo (shapes) from Ref. [42] Mott insulator-superfluid phase diagrams for $t_a = t_b = 1$, $U_b = U_{ab} = 10$. n_b=0.0 (black, diamond); 0.1 (red, circle); 0.5 (blue, square); 0.75 (green, triangle).

although for for $t_b/U_b = 10$ the light bosons are not sufficiently deep in the superfluid phase for a perfect comparison. The most noticeable difference is the greater instability to hole formation for $n_b = 0.1$. We attribute this to the formation of localized bound states of 'B' particles with 'A' holes, which cannot be described in terms of phonons. This does not occur on the upper side of the Mott lobe due to the greater kinetic energy of particles, which have a hopping amplitude $\propto \sqrt{n+1}$ as opposed to $\sqrt{n}$ for holes.

4.3 Strong Coupling versus Gutzwiller Approach

The formalism presented above required a rather baroque third-order perturbative expression for the ground state energy of Eq. (4.14). For situations where such an expression may be excessively complicated or tedious to derive we would like to combine the variational polaron method with a simpler way of dealing with the effective Hamiltonian of 'A'. It is also useful exercise to give an explicit example that logically decouples

solving H_{eff} from performing the variational polaron transformation. The simplest approach to the Mott-superfluid transition in a Bose-Hubbard model, one which becomes increasingly accurate for high dimensions, is the Gutzwiller ansatz, where we take the uncorrelated state of 'A' in Eq. (4.12) to be $|\Psi_a\rangle = \otimes_i |\psi_i\rangle$, where the Gutzwiller state on site i is

$$|\psi_i\rangle = \sin\theta\cos\phi|n-1\rangle_i + \cos\theta|n\rangle_i + \sin\theta\sin\phi|n+1\rangle_i. \tag{4.27}$$

Equivalently, we use the ansatz Eq. (4.27) to estimate the ground state energy of the effective Hamiltonian Eq. (4.14). In both this approach and the strong-coupling treatment above all inter-species correlations are generated by the transformation e^S. However, in the present Gutzwiller approach this operator acts on states with no *intra*-species correlations of 'A', while in the strong-coupling approach we had correlations in the form of virtual particle-hole excitations in the Mott state even prior to the variational polaron transformation. The expectation of the induced interactions term in Eq. (4.14) is

$$\begin{aligned}
\frac{1}{2}\sum_{ij} V_{ij}\langle n_i n_j\rangle =& \frac{1}{2}\left[\sum_{i\neq j} V_{ij}\langle n_i\rangle\langle n_j\rangle + \sum_{i=j}\langle n_i^2\rangle\right] \\
=& \frac{1}{2}\left[\langle n\rangle^2\sum_{ij} V_{ij} + (\langle n^2\rangle - \langle n\rangle^2)\sum_i V_{\mathbf{0}}\right] \\
=& \frac{N}{2}V_{\mathbf{0}}(\langle n^2\rangle - \langle n\rangle^2),
\end{aligned} \tag{4.28}$$

where we have used the fact that $\sum_{ij} V_{ij} = N\sum_{\mathbf{R}} V_{\mathbf{R}} = 0$. That this result depends only on the same-site induced interaction $V_{\mathbf{0}}$ makes sense because the Gutzwiller state

only has same-site density correlations. The expectation of $H_a(t_a \to \tilde{t}_a)$ is

$$\left\langle H_a(\tilde{t}_a)\right\rangle = -z\tilde{t}_a \left\langle b\right\rangle^2 - \mu_a \left\langle n\right\rangle + \frac{U_a}{2}\left(\left\langle n^2\right\rangle - \left\langle n\right\rangle\right). \tag{4.29}$$

The Gutzwiller averages in Eqs. (4.28 - 4.29) are

$$\left\langle b\right\rangle = \sin\theta\cos\theta\left(\sqrt{n}\cos\phi + \sqrt{n+1}\sin\phi\right) \tag{4.30}$$

$$\left\langle n\right\rangle = n - \sin^2\theta\cos^2 2\phi \tag{4.31}$$

$$\left\langle n^2\right\rangle = n^2 + \sin^2\theta\left(1 - 2n\cos 2\phi\right). \tag{4.32}$$

Minimizing the energy with respect to $\{f\mathbf{k}\}$ again gives a self-consistent set of equations that can be solved iteratively:

$$f_{\mathbf{k}}(\theta,\phi) = \left(1 + \frac{2\tilde{t}_a}{\omega_{\mathbf{k}}}\frac{\left\langle b\right\rangle^2}{\left\langle n^2\right\rangle - \left\langle n\right\rangle^2}\sum_{\mathbf{a}}\sin^2(\mathbf{k}\cdot\mathbf{a}/2)\right)^{-1}. \tag{4.33}$$

Reinserting the result of iterating Eq. (4.33) into Eqs. (4.28 - 4.29) with the renormalizations Eqs. (4.9) and (4.13) gives an energy functional $E(\theta,\phi)$, which we minimize numerically. The system is in the Mott phase when $\theta = 0$ minimizes the energy; otherwise it is in a superfluid phase. In Fig. 4.2 we compare results of strong coupling perturbation theory to those of the Gutzwiller approximation, for a three-dimensional Bose-Bose mixture. In the case of strong coupling perturbation theory we employ the same critical extrapolation scheme as above. The Gutzwiller approximation, like any mean-field theory, overestimates the extent of the ordered superfluid phase. In three dimensions it predicts Mott lobes that are about 20% too small. For the single-species case it predicts $(t/U)_c = 0.0286$ in three dimensions, compared to the quantum Monte

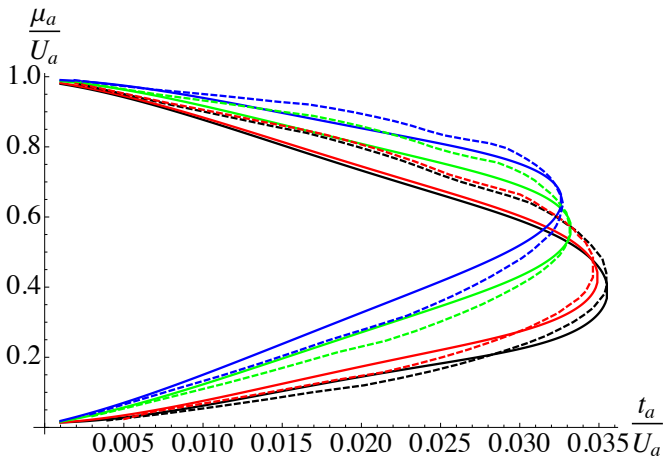

Figure 4.2: Calculated phase diagrams in three dimensions using strong coupling perturbation theory (solid) and Gutzwiller approximation (dashed) for parameters $t_a = t_b = 1$, $U_b = U_{ab} = 10$. n_b=0.0 (black); 0.1 (red); 0.5 (blue); 0.75 (green).

Carlo result $(t/U)_c = 0.03408$[19]. We therefore scale the Gutzwiller results via $t_a \to \lambda t_a$, where empirically $\lambda = 1.24$, to obtain agreement with the critically-extrapolated strong coupling phase diagram. Importantly, we use the same λ to rescale all four curves in Fig. 4.2. Having scaled the Gutzwiller ansatz result in this manner the Mott lobes predicted by the two methods appear virtually identical. In particular, the shift of the critical value of t_a/U_a as the density n_b of the superfluid increase is the same. Thus we conclude that the Gutzwiller approximation fits into the variational polaron scheme as well as strong coupling perturbation theory. The only limitation, that of underestimating the critical t_a/U_a is inherent to the Gutzwiller approximation itself and is not related to the interplay of the Gutzwiller ansatz with the variational polaron transformation. That is, the variational polaron transformation gives *quantitative* information about the effect of mixing even when the state $|\Psi_A\rangle$ underlying the ansatz $\Psi = e^S|\Psi_A\rangle \otimes |0_b\rangle$ is only qualitatively accurate.

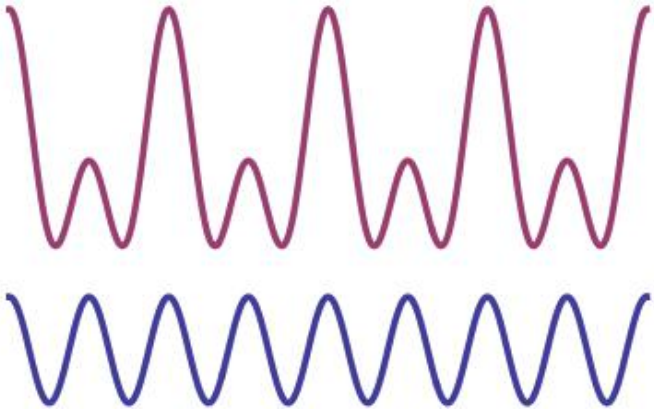

Figure 4.3: Top: double-well superlattice potential seen by heavy species 'A'. Bottom: potential seen by light species 'B'.

4.4 Half-Filled Superlattice

We now consider a 1-D mixture in which hard-core species 'B' has filling $0 \leq n_b \leq 1$ and species 'A' is at half-filling. 'A' bosons see a superlattice of double wells (see Fig. 4.3) and can only hop within double wells. The Hamiltonian $H = H_a + H_b + H_{ab}$ is

$$\begin{aligned} H = &- t_a \sum_m \left(a^\dagger_{2m+1} a_{2m} + \text{h.c.} \right) - t_b \sum_n \left(b^\dagger_n b_{n+1} + \text{h.c.} \right) \\ &- \mu_b \sum_n b^\dagger_n b_n + U_{ab} \sum_n a^\dagger_n a_n b^\dagger_n b_n \end{aligned} \tag{4.34}$$

When interactions are not so strong as to destabilize the superfluidity of 'B' there are three phases of 'A' (see Fig 4.4): a "ferromagnetic" (FM) phase with period-2 CDW, an "antiferromagnetic" (AF) phase with period-4 CDW, and a "paramagnetic" (PM) phase with no translational symmetry breaking.

Let $|L(R)\rangle$ be orbitals centered on the left (right) site of a double well and define $\psi^{L(R)} = \cos\theta_A |L(R)\rangle + \sin\theta_A |R(L)\rangle$ as double well states with density skewed to the

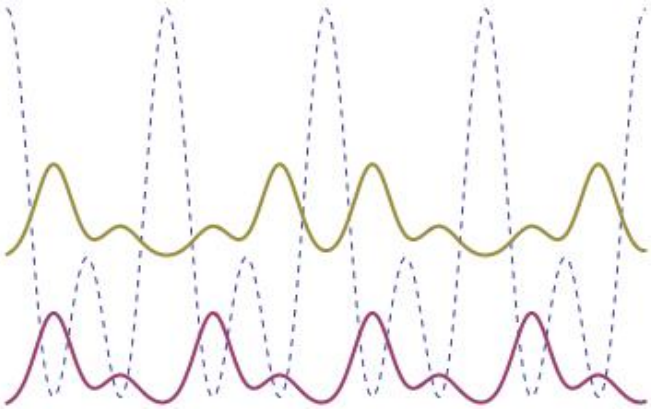

Figure 4.4: Top: antiferromagnetic phase of heavy species 'A'. Bottom: ferromagnetic phase of heavy species 'A'.

left (right). The FM and AF states of 'A' are $\psi^L \otimes \psi^L \otimes \psi^L \ldots$ and $\psi^L \otimes \psi^R \otimes \psi^L \ldots$, respectively. We write the 'B' FM and AF mean field states $\psi^1 \otimes \psi^2 \otimes \psi^1 \otimes \psi^2 \ldots$ and $\psi^1 \otimes \psi^2 \otimes \psi^2 \otimes \psi^1 \ldots$ in terms of single-site Gutzwiller states $\psi^{1(2)} = \cos\phi_{1(2)}|0\rangle + \sin\phi_{1(2)}|1\rangle$. Parametrizing $\sin^2\phi_1 = 2n_b\cos^2\theta_B$, $\sin^2\phi_2 = 2n_b\sin^2\theta_B$ gives the correct density n_b.

The mean-field kinetic energy of 'A' per site is

$$\langle H_a \rangle / N = -t_a \sin\theta_A \cos\theta_A \tag{4.35}$$

for both phases, while the kinetic energies from 'B' are

$$\mathrm{E}^B_{\mathrm{FM}} = -2t_b \cos\phi_1 \sin\phi_1 \cos\phi_2 \sin\phi_2 \tag{4.36}$$

$$\mathrm{E}^B_{\mathrm{AF}} = -\frac{1}{2} t_b \left(\cos\phi_1 \sin\phi_1 + \cos\phi_2 \sin\phi_2\right)^2 \tag{4.37}$$

and the interaction energy is, for both phases,

$$\mathrm{E}^{AB} = \frac{1}{4} U_{ab} \left(\cos^2\theta_A - \sin^2\theta_A\right) \left(\sin^2\phi_1 - \sin^2\phi_2\right). \tag{4.38}$$

The difference $E_{\mathrm{FM}} - E_{\mathrm{AF}}$ is $-t_b\left(\sqrt{x_1 x_2} - \frac{1}{2}(x_1 + x_2)\right)$ for $x_i = \cos^2\phi_i \sin^2\phi_i$. It follows from the AM-GM inequality that the $E_{\mathrm{AF}} \leq E_{\mathrm{FM}}$, with equality when $n_b = 1/2$. However, near $n_b = 1/2$, quantum fluctuations favor the FM phase, which gives 'B' bosons more space since density maxima are not on adjacent sites. To analyze this competition, we include fluctuations of 'B' about the mean field and perform a variational polaron transformation.

To include fluctuations of 'B' define operators $t^\dagger_{0(1),n}|\mathrm{vac}\rangle_{\mathrm{n}} = |0(1)\rangle_{\mathrm{n}}$ so that $b_n = t^\dagger_{0n} t_{1n}$ and the 'B' Hamiltonian, including the mean-field potential from 'A'

$$\begin{aligned} H_b = &- t_b \sum_{\langle ij\rangle} t^\dagger_{1i} t_{0i} t^\dagger_{0j} t_{1i} - \mu_b \sum_i t^\dagger_{1i} t_{1i} \\ &+ \frac{U_{ab}\left(\cos^2\theta_A - \sin^2\theta_A\right)}{2} \sum_n \sigma_n t^\dagger_{1n} t_{1n}, \end{aligned} \tag{4.39}$$

where $\sigma_n = 1, -1, 1, -1 \ldots$ (FM) or $1, -1, -1, 1 \ldots$ (AF). We define operators $c_i = \cos\phi_i t_{0i} + \sin\phi_i t_{1i}$ and $d_i = \sin\phi_i t_{0i} - \cos\phi_i t_{1j}$ corresponding to the mean field and excitations. To quadratic order we take $c_i, c_i^\dagger \to 1$ and $c_i^\dagger c_i \to 1 - d_i^\dagger d_i$ and obtain the k-space Hamiltonian

$$\begin{aligned} H_b = &\sum_k{}' \left[\left(\chi^{\dagger\intercal}_k, \chi^{\dagger\intercal}_{-k}\right) \begin{pmatrix} \mathbf{A}_k & 0 \\ 0 & \mathbf{A}_{-k} \end{pmatrix} \begin{pmatrix} \chi_k \\ \chi_{-k} \end{pmatrix} \right. \\ &\left. + \left[\left(\chi^{\dagger\intercal}_k, \chi^{\dagger\intercal}_{-k}\right) \begin{pmatrix} 0 & \mathbf{B}_k \\ \mathbf{B}^\intercal_k & 0 \end{pmatrix} \begin{pmatrix} \chi^\dagger_k \\ \chi^\dagger_{-k} \end{pmatrix} + \mathrm{hc.} \right] \right], \end{aligned} \tag{4.40}$$

where $\chi_k^\intercal = (d_k, d_{k+\pi})$ and $\mathbf{A}_k$, $\mathbf{B}_k$ are 2×2 matrices in the FM phase and $\chi_k^\intercal = (d_k, d_{k+\pi/2}, d_{k+\pi}, d_{k-\pi/2})$ and $\mathbf{A}_k$, $\mathbf{B}_k$ are 4×4 matrices in the AF phase. The k-space sums are over reduced Brillouin zones $[0, \pi)$ and $[0, \pi/2)$. We perform the operator algebra to find terms of the matrices $\mathbf{A}_k$ and $\mathbf{B}_k$ using the "SNEG" *Mathematica* package[113].

The Bogoliubov transformation $\xi_k = \mathbf{U}_k^\dagger \chi_k - \mathbf{V}_k^\intercal \chi_{-k}^\dagger$, $\chi_k = \mathbf{U}_k \xi_k - \mathbf{V}_k^* \xi_{-k}^\dagger$ diagonalizes the Hamiltonian as

$$H_b = \sum_k{}' \left(\xi_k^{\dagger\intercal} \mathbf{\Omega}_k \xi_k - \mathrm{Tr} \mathbf{V}_k^\dagger \mathbf{\Omega}_k \mathbf{V}_k \right), \tag{4.41}$$

where $\mathbf{\Omega}_k$ is a diagonal matrix, and the τ-th columns of $\mathbf{U}_k$, $\mathbf{V}_k$ and the τ-th diagonal element of $\mathbf{\Omega}_k$ corresponding to the τ-th *positive* eigenvalue[16] $\omega(k, \tau)$ of the equation

$$\begin{pmatrix} \mathbf{A}_k & \mathbf{B}_k \\ -\mathbf{B}_k^\dagger & -\mathbf{A}_{-k}^* \end{pmatrix} \begin{pmatrix} \mathbf{U}_k \\ \mathbf{V}_k \end{pmatrix}_\tau = \omega(k, \tau) \begin{pmatrix} \mathbf{U}_k \\ \mathbf{V}_k \end{pmatrix}_\tau . \tag{4.42}$$

The polaron transformation requires that we write H_{ab} in terms of Bogoliubov modes. The density fluctuations $\delta\rho_n^B \equiv t_{1,n}^\dagger t_{1,n} - \left\langle t_{1,n}^\dagger t_{1,n} \right\rangle$ can be written as

$$\delta\rho_n^B = \frac{1}{\sqrt{N}} \sum_{k,\tau}{}' e^{-ikn} \left(\beta_{k\tau}^n \xi_{k,\tau} + \beta_{k\tau}^{n*} \xi_{k,\tau}^\dagger \right), \tag{4.43}$$

$$\beta_{k\tau}^n = \frac{-\sin 2\phi_n}{2} \left(c_{nm}^* \left(\mathbf{U}_k \right)_{m\tau} + c_{nm} \left(\mathbf{V}_k \right)_{m\tau} \right). \tag{4.44}$$

Here $m, n, \tau = 1, 2$, $Q = \pi$ (FM) and $m, \tau, n = 1 \ldots 4$, $Q = \pi/2$ (AF), where τ is the phonon branch index and n is a sublattice index, and $c_{nm} = e^{imQn}$.

The polaron transformation $\tilde{H} = e^{-S} H e^S$ for multiple phonon modes and inequiva-

lent sites is

$$S = \frac{1}{\sqrt{N}} \sum_{k,\tau,n}{}' \frac{\beta^n_{k\tau} f^n_{k\tau}}{\omega_{k\tau}} e^{ikn} n^A_n (\xi^\dagger_{k,\tau} - \xi_{-k,\tau}). \tag{4.45}$$

The sum in Eq. (4.45) is over all sites n, but $f_{nk\tau}$, like $\beta_{nk\tau}$, depends only on the sublattice n. As before $f_{nk\tau} = 1$ completely removes the interaction. The partial polaron transformation leaves the terms of H_B (phonon and zero-point energies) in Eq. (4.41) unchanged, dresses the hopping of 'A' bosons, and generates an interaction $\hat{V} = \sum_{rs} V_{rs} n^A_r n^A_s$, where

$$V_{rs} = \frac{U^2_{ab}}{N} \sum_{k,\tau}{}' e^{-ik(r-s)} \frac{\mathrm{Re}[\beta^r_{k\tau} \beta^{s*}_{k\tau}][f^r_{k\tau} f^s_{k\tau} - f^r_{k\tau} - f^s_{k\tau}]}{\omega_{k\tau}} \tag{4.46}$$

Averaging the dressed hopping over an ansatz $|\Psi\rangle = e^S |\Psi^A\rangle \otimes |0_B\rangle$, where $|\Psi^A\rangle$ is an FM or AF mean-field wavefunction and $|0_B\rangle$ is the 'B' phonon vacuum, gives

$$\tilde{t}_a = t_a \exp\left[-\frac{U^2_{ab}}{2N} \sum_{k,\tau}{}' \frac{\left| \beta^1_{k\tau} f^1_{k,\tau} + e^{ik} \beta^2_{k\tau} f^2_{k,\tau} \right|^2}{\omega^2_{k\tau}} \right] \tag{4.47}$$

The total variational energy is the sum of induced interactions Eq. (4.46), zero-point energy$-\mathrm{Tr}\mathbf{V}^\dagger_k \mathbf{\Omega}_k \mathbf{V}_k$, and mean-field energy Eqs. (4.35-4.38), with $\tilde{t}_a$ replacing t_a. The variational energy of induced interactions is

$$\left\langle \hat{V} \right\rangle^{FM} = 2 \left\langle \hat{V} \right\rangle^{AF} = \frac{\sin^2(2\theta_A)}{4} \left(V_{11} + V_{22} - 2V_{12} \right). \tag{4.48}$$

Eq. 4.48 can be understood as follows: an atom in sublattice 1 experiences an average potential with wavevector $Q = \pi$ from all other sublattice 1 sites. Since $Q = \pi$ is excluded from the sum $\sum'_k$, the expectation of this interaction should vanish. How-

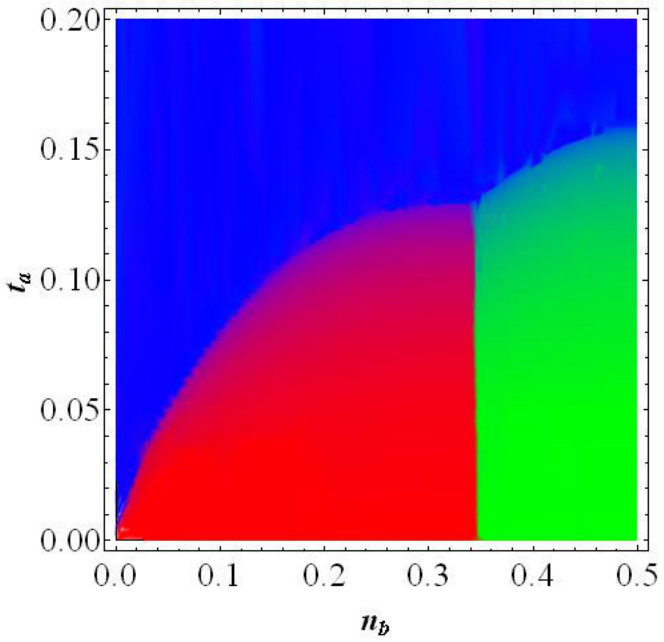

Figure 4.5: Superlattice phase diagram for $U_a b = 1.0$ as a sunction of 'B' filling n_b and 'A' hopping t_a in units $t_b = 1$. Green: FM order parameter; Red: AF order parameter; Blue: PM phase.

ever, there is self-interaction correction because $\langle n_i n_i \rangle = \langle n_i \rangle = \cos^2 \theta_A$, in contrast to $\langle n_i n_j \rangle = \langle n_i \rangle \langle n_j \rangle = \cos^4 \theta_A$ when sites i and j belong to different double wells. Hence the sum vanishes except for a correction $V_{11} \left(\cos^2 \theta_A - \cos^4 \theta_A \right) = V_{11} \sin^2(2\theta_A)/4$. The V_{22} and V_{12} contributions are similar.

In one dimension it is not too computationally expensive to minimize the energy with respect to θ_A, θ_B, and $\{f^n_{k\tau}\}$. Minimizing for both AF and FM phases and comparing their minima gives the phase diagram. In Figs. 4.5 and 4.6 we plot the order parameter $\cos^2 \theta_a - \sin^2 \theta_A$ as a function of n_b and t_a/t_b for different couplings U_{ab}/t_b. There are second-order FM-PM and AF-PM transitions and a first-order FM-AF transition. The FM region is centered around $n_b = 1/2$.

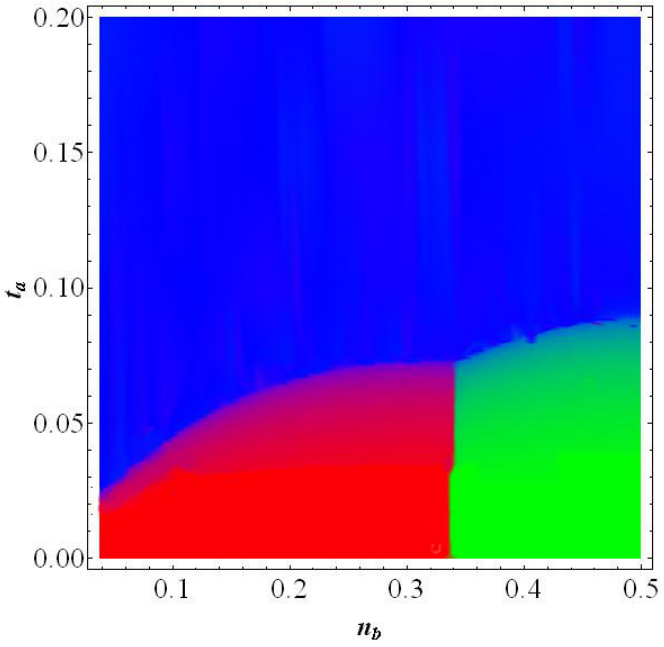

Figure 4.6: Superlattice phase diagram for $U_a b = 0.5$ as a sunction of 'B' filling n_b and 'A' hopping t_a in units $t_b = 1$. Green: FM order parameter; Red: AF order parameter; Blue: PM phase.

4.5 Summary and Conclusion

We showed that the polaron transformation, which has traditionally been used to study a single impurity in a phonon bath, can be extended to handle a many-body system interacting with a bath, and that its variational extension is a powerful method giving quantitatively accurate results. Using Bose-Bose mixtures as a test case we showed that it is possible to efficiently determine the self-consistent variational polaron transformation that minimizes energy. In two dimensions our calculations using strong coupling perturbation theory to find the ground state energy of the variational polaron-transformed effective Hamiltonian of the heavy boson species compared very well with numerically exact quantum Monte Carlo calculations. Having justified the variational polaron method in this way, we proceeded to couple the variational polaron transformation to a Gutzwiller ansatz for the effective Hamiltonian, showing that in three dimensions it yielded very similar results to the strong coupling approach. Thus we established the Gutzwiller approximation as a reliable tool to use with the variational polaron transformation in cases where perturbation theory is too cumbersome. This makes the variational polaron method a viable tool for studying more complicated systems, such as those withwith broken symmetries.

5

RF Absorption of a Mobile Impurity

5.1 Introduction

Radiative transitions in which the final state interacts with an otherwise-noninteracting Fermi gas are one of the few solvable many-body non-equilibrium problems. They have practical importance in that x-ray absorption experiments in condensed matter systems involve a positively-charged hole left behind when a core electron jumps to

a higher band[60]. Modern resonant x-ray scattering techniques contain a core hole in their intermediate state and also require a treatment of the core hole in the analysis of lineshapes. Furthermore, the so-called "orthogonality catastrophe"[10,79] is relatively easy to implement in ultracold atomic gases as an RF hyperfine transition of an impurity for which only one internal state interacts with a Fermi gas[59].

What these problems have in common that makes them tractable is that the core hole or impurity are essentially immobile and effectively yield a static potential for the Fermi gas that is switched on at time $t = 0$. In the case of a free gas with spherical symmetry this feature leads to a solution in terms of the phase shifts of different angular momentum components. For arbitrary dispersion, such an in lattice systems, a numerically exact solution to essentially arbitrary accuracy is still available via a determinantal formula[23,59]. Essentially, this idea works because the problem is only a many-body one by virtue of the antisymmetrization requirement, which is encoded as a determinant of a single-particle matrix.

We are interested in extending the physics of the orthogonality catastrophe to that of a mobile core hole or impurity. This is inherently interesting as a more-complicated non-equilibrium problem that can be measured with cold atoms. It would also be useful in describing certain resonant x-ray probes, such as indirect RIXS, that contain mobile electrons above the valence band in their intermediate state.

To tackle the problem of a mobile impurity, we first make contact with previous work with a transformation to a frame where the impurity is a static potential[61]. This effectively removes the impurity from the system but comes at the cost of a strange momentum-dependent interaction in the fermion Hamiltonian. We decouple this anomalous interaction term via a Hubbard-Stratonovich transformation and expand the effective action of the Hubbard-Stratonovich field to quadratic order. Using the method of

fermion functional determinants we obtain the form of this effective field theory in a numerically exact way. Finally, we integrate this effective quadratic theory exactly. The method of functional determinants that we use to integrate out the Fermi sea and obtain an effective theory of the Hubbard-Stratonovich field also underlies the technique of determinantal Monte Carlo[88,90]. However, in contrast to our approach, determinantal Monte Carlo samples configurations of the Hubbard-Stratonovich field stochastically. Although determinants treat fermion antisymmetry exactly and avert a fermion sign problem, the integral over the auxiliary field may be highly oscillatory, which limits the application of determinantal Monte Carlo. In contrast, we numerically determine the effective action of the Hubbard-Stratonovich field but integrate analytically over all field configurations in an aymptotic expansion. This method is generalizable to other nonequilibrium problems with a single Hubbard-Stratonovich field, such as those involving the Kondo effect and quantum dots.

5.2 Formalism

Consider spinless, noninteracting lattice fermions and an impurity particle with position $\mathbf{R}$ and momentum $\mathbf{P}$. Suppose the impurity has two hyperfine states, $|\downarrow\rangle$ and $|\uparrow\rangle$, separated by energy Δ and that the $|\uparrow\rangle$ state of the impurity interacts with the Fermi gas via a potential $\hat{V}(\mathbf{R}) = \sum_{\mathbf{r}} V(\mathbf{r}-\mathbf{R}) f_{\mathbf{r}}^\dagger f_{\mathbf{r}}$. This system is described by

$$\hat{H} = \hat{H}_0 + E(\mathbf{P}) + \Delta|\uparrow\rangle\langle\uparrow| + |\uparrow\rangle\langle\uparrow| \otimes \hat{V}(\mathbf{R}), \tag{5.1}$$

where $\hat{H}_0 = \sum_{\mathbf{k}} \varepsilon_{\mathbf{k}} f_{\mathbf{k}}^\dagger f_{\mathbf{k}}$. Here we will use $\varepsilon(\mathbf{k}) = -2t_f \cos k$ and $E(\mathbf{P}) = -2t_i \cos k$. We consider the effect of interaction on RF absorption $|\downarrow\rangle \to |\uparrow\rangle$ from an initial state $|\Omega; \mathbf{P}, \downarrow\rangle$, where Ω is the equilibrium Fermi sea. That is, we are interested in the orthogo-

nality catastrophe of a mobile impurity. For our analysis it is convenient to work in a co-moving frame[100,85,61] via the transformation $U = \exp\left(i|\uparrow\rangle\langle\uparrow|\mathbf{R}\cdot\mathbf{P}_f\right)$, $\mathbf{P}_c \equiv \sum_{\mathbf{k}} \mathbf{k} f_{\mathbf{k}}^\dagger f_{\mathbf{k}}$. As $\mathbf{R}$ generates momentum boosts of the impurity and $\mathbf{P}_f$ generates translations of the Fermi sea, it is easy to see that $\hat{H} \to U^\dagger \hat{H} U = \hat{H}'$ transforms as

$$\hat{H}' = \hat{H}_0 + E(\mathbf{P} - |\uparrow\rangle\langle\uparrow|\mathbf{P}_f) + \Delta|\uparrow\rangle\langle\uparrow| + |\uparrow\rangle\langle\uparrow| \otimes \hat{V}(\mathbf{0}). \tag{5.2}$$

This describes a Fermi sea and a *stationary* impurity at $\mathbf{R} = \mathbf{0}$ at the cost of a $\cos(\mathbf{P} - \mathbf{P}_f)$ term. Since $\mathbf{R}$ is absent from $\hat{H}'$, $\mathbf{P}$ is a constant of motion and the only dynamics are those of the Fermi sea. The transformation does not affect the initial state because $\mathbf{P}_c|\Omega\rangle = 0$.

The absorption rate from an RF perturbation $\hat{H}_{\mathrm{RF}} = e^{-i\omega t}|\uparrow\rangle\langle\downarrow|$ is[59,94]

$$\begin{aligned} R(\omega) =& \mathrm{Re}\int_0^\infty dt\, \langle\Omega;\mathbf{P},\uparrow|e^{i\hat{H}'t}\hat{H}_{\mathrm{RF}}e^{-i\hat{H}'t}|\Omega;\mathbf{P},\downarrow\rangle & (5.3)\\ =& \mathrm{Re}\int_0^\infty dt\, e^{i(\Delta-\omega-E(\mathbf{P}))t}S(t), & (5.4)\end{aligned}$$

where

$$\begin{aligned} S(t) =& \langle\Omega|e^{i\left(\hat{H}_0+\hat{V}(\mathbf{0})+E(\mathbf{P}-\mathbf{P}_c)\right)t}e^{-i\hat{H}_0 t}|\Omega\rangle & (5.5)\\ =& \langle\Omega|e^{i(H_1+E(\mathbf{P}-\mathbf{P}_c))t}e^{-i\hat{H}_0 t}|\Omega\rangle & (5.6)\end{aligned}$$

where $H_1 = \hat{H}_0 + \hat{V}(\mathbf{0})$.

For $M = \infty$ the problematic $E(\mathbf{P} - \mathbf{P}_c)$ term drops out and we could compute $S(T)$ with the formula[74,57,1,58]

$$\langle\Omega|e^{\hat{X}_N}\dots e^{\hat{X}_1}|\Omega\rangle = \det\left[(1-N) + e^{X_N}\dots e^{X_1}N\right], \tag{5.7}$$

where $N = 1/(1+e^{\beta H_0})$, which applies for quadratic operators $\hat{X}_{1\ldots N}$. (For the remainder of this chapter, we denote a many-body Fock space operator by $\hat{X}$ and its corresponding single-particle matrix by X: $\hat{X} = c^\dagger_{\mathbf{k}} X_{\mathbf{k},\mathbf{k}'} c_{\mathbf{k}'}$). In order to exploit Eq. (5.7), we must relate the non-bilinear term $E(\mathbf{P}-\mathbf{P}_c)$ to an exponentiated quadratic operator.

If the thermal energy is less than the recoil energy of the impurity one can ignore umklapp processes and safely assume that its momentum does not leave the first Brillouin zone. In such a case we may expand its kinetic energy to quadratic order:

$$E(\mathbf{P}) = -2t_i \cos \mathbf{k} \approx t_i P^2 = \frac{P^2}{2M}, \tag{5.8}$$

where $M \equiv 1/(2t_i)$. We then have

$$S(t) = \langle \Omega | e^{i\left(H_1 + (\mathbf{P}-\mathbf{P}_c)^2/2M\right)t} e^{-i\hat{H}_0 t} | \Omega \rangle. \tag{5.9}$$

In order to exploit Eq. (5.7), we divide the time interval T into N segments of length $\Delta t = T/N$ and decouple the $(\mathbf{P}-\mathbf{P}_c)$ term via a Hubbard-Stratonovich transformation as follows:

$$S(T) = \int D[\phi] e^{S_0[\phi]} \langle \Omega | T \left(e^{i\int_0^t H_1 - \phi(t')\cdot \mathbf{P}_c \, dt'} \right) e^{-iH_0 t} | \Omega \rangle, \tag{5.10}$$

where $S_0[\phi] \equiv i\int_0^t \left(-\frac{M}{2}\phi^2(t') + \phi(t')\cdot\mathbf{P}\right) dt'$, T is the time-ordering operator, and the functional integral is normalized as

$$\int D[\phi] \equiv \prod_m \int_{-\infty}^{\infty} \left(\frac{iM\Delta t}{2\pi}\right)^{d/2} d^d\phi_m, \tag{5.11}$$

where $\phi_m = \phi(t'_m)$ is discretized on $t'_m = m\Delta t$.

The exponentiated operators in Eq. (5.10) are quadratic and we may use Eq. (5.7), along with $\ln\det M = \operatorname{tr}\ln M$, to obtain $S(t) = \int D[\phi] e^{S_0[\phi]+S_1[\phi]}$, where $S_1[\phi] = \ln\det B[\phi] = \operatorname{tr}\ln B[\phi]$ for

$$B[\phi] = (1-N) + T\left(e^{i\int_0^t H_1 - \phi(t')\cdot\mathbf{P}_c\,dt'}\right)e^{-iH_0 t}N \tag{5.12}$$

For a heavy impurity, oscillations in $S_0[\phi]$ cause cancellation except at $\phi \equiv 0$, so that in effect only $S_1[0]$ contributes. Therefore we may obtain an asymptotic correction to the $M \to \infty$ limit by expanding $S_1[\phi]$ to second order about $\phi = 0$, which is straightforward but cumbersome. The zeroth order term is

$$S_1[0] = \ln\det\left[(1-N) + e^{iH(0)t}e^{-iH_0 t}N\right], \tag{5.13}$$

which gives the absorption of an immobile impurity[59]. By symmetry, the first order term vanishes. We expand $S_1[\phi]$ to second order as follows:

$$\begin{aligned} B[\phi] =& (1-N) + \left(e^{iH_1 t} + i\int_0^t \phi^\alpha(t_1)\cdot e^{iH_1(t-t_1)}\mathbf{P}_c^\alpha e^{iH_1 t_1}\,dt_1\right. \\ &\left. - \int_{t_1<t_2}\phi^\alpha(t_1)\phi^\beta(t_2)e^{iH_1(t-t_2)}\mathbf{P}_c^\alpha e^{iH_1(t_2-t_1)}\mathbf{P}_c^\beta e^{iH_1 t_1}\,dt_1\,dt_2\right)e^{-iH_0 t}N \qquad (5.14) \\ =& B[0] + e^{iH_1 t}\left(i\int_0^t \phi^\alpha(t_1)\Gamma^\alpha(t_1)\,dt_1\right. \\ &\left. - \int_{t_1<t_2}\phi^\alpha(t_1)\phi^\beta(t_2)\Gamma^\beta(t_2)\Gamma^\alpha(t_1)\,dt_1\,dt_2\right)e^{-iH_0 t}N, \qquad (5.15) \end{aligned}$$

where we define $\Gamma(\tau) \equiv e^{-iH_1\tau}\mathbf{P}_c e^{iH_1\tau}$. Then to second order in ϕ

$$\begin{aligned} S_1[\phi] - S_1[0] =& \ln\det\left[1 + \left(i\int_0^t \phi^\alpha(t_1)\Gamma^\alpha(t_1)\,dt_1 \right.\right. \\ & \left.\left. - \int_{t_1<t_2} \phi^\alpha(t_1)\phi^\beta(t_2)\Gamma^\beta(t_2)\Gamma^\alpha(t_1)\,dt_1\,dt_2\right) D\right], \end{aligned} \tag{5.16}$$

where $D = e^{-iH_0 t}NB[0]^{-1}e^{iH_1 t}$. Here we have exploited the fact that $\det(1+AB) = \det(A^{-1}(1+AB)A) = \det(1+BA)$ to bring the factor $e^{iH_1 t}$ to the right. Writing $\ln\det M = \mathrm{tr}\ln M$ and expanding the logarithm to second order we obtain

$$\begin{aligned} S_1[\phi] - S_1[0] =& \mathrm{tr}\left[-\left(\int_{t_1<t_2} \phi^\alpha(t_1)\phi^\beta(t_2)\Gamma^\beta(t_2)\Gamma^\alpha(t_1)\,dt_1\,dt_2\right) D \right. \\ & \left. + \frac{1}{2}\left(\int_0^t \phi^\alpha(t_1)\Gamma^\alpha(t_1)\,dt_1\right) D \left(\int_0^t \phi^\beta(t_2)\Gamma^\beta(t_2)\,dt_2\right) D\right], \end{aligned} \tag{5.17}$$

The first order term $i\mathrm{tr}\left[\left(\int_0^t \phi^\alpha(t_1)\Gamma^\alpha(t_1)\,dt_1\right) D\right]$ vanishes because Γ is odd under reflection $\mathbf{k} \leftrightarrow -\mathbf{k}$, while H_0, H_1, N, and $B[0]$ are invariant; hence traces of odd-order terms in Γ vanish. Similarly, the only non-vanishing contribution to Eq. (5.17) occurs for matched components $\alpha = \beta$. Thus we have the second order expansions

$$S_1[\phi] = S_1[0] + \frac{1}{2}\sum_\alpha \int_0^t\int_0^t \phi^\alpha(t_1)\phi^\alpha(t_2)\mathrm{tr}\left[\Gamma^\alpha(t_1)D\Gamma^\alpha(t_2)(D-1)\right]\,dt_1\,dt_2 \tag{5.18}$$

$$= S_1[0] + \frac{1}{2}\sum_\alpha \int_0^t\int_0^t \phi^\alpha(t_1)\phi^\alpha(t_2)K(t_1,t_2,t)\,dt_1\,dt_2, \tag{5.19}$$

where we have defined the kernel

$$K(t_1,t_2,t) \equiv \mathrm{tr}\left[\Gamma^x(t_1)D\Gamma^x(t_2)(D-1)\right]. \tag{5.20}$$

The form of Eq. (5.20) is very useful for computations. Suppose we discretize time into

N chunks: $\Delta t = T/N$. The kernel has N^2 elements, but after computing the N elements of lists $\{\Gamma^x(t_m)D\}$ and $\{\Gamma^x(t_m)(D-1)\}$, which involve expensive matrix multiplication, the elements of the kernel are traces of products, a computationally cheap operation. Discretizing time in this way, the second order expansion of $S_1[\phi]$ makes Eq. (5.10) a Gaussian integral that we can readily evaluate:

$$S(t) = e^{S_1[0]} \left(\frac{iM\Delta t}{2}\right)^{\frac{dt}{2\Delta t}} \det(\mathbf{A}_1)^{-d/2} \prod_\alpha e^{\frac{1}{4}\mathbf{A}_2^\alpha \mathbf{A}_1^{-1} \mathbf{A}_2^\alpha} \tag{5.21}$$

where $\phi^\alpha = (\phi_1^\alpha \dots \phi_{t/\Delta t}^\alpha)$, $\mathbf{A}_2^\alpha = i\Delta t P^\alpha(1 \dots 1)$ and

$$(\mathbf{A}_1)_{jk} = i\frac{M}{2}\Delta t \delta_{jk} - \frac{\Delta t^2}{2} K(t_j, t_k, t). \tag{5.22}$$

5.3 Error Analysis

If truncating $S_1[\phi]$ to second order in ϕ is to be a controlled approximation, we must have some way of estimating the size of the next term in the expansion, which by symmetry comes in at fourth order. By methods very similar to those that led up to Eqs. (5.19) and (5.20) – we expand $B[\phi]$ to fourth order and also go to fourth order in the series expansion of $\ln(1+x)$ – we obtain the fourth-order contribution of $S_1[\phi]$:

$$S_1^{(4)}[\phi] = \sum_{\alpha,\beta,\gamma,\delta} \int \phi^\alpha(t_1)\phi^\beta(t_2)\phi^\gamma(t_3)\phi^\delta(t_4) \\ K_{\alpha,\beta,\gamma,\delta}(t_1, t_2, t_3, t_4, t)\, dt_1\, dt_2,\, dt_3,\, dt_4, \tag{5.23}$$

where, using the shorthand Γ_1, Γ_2 for $\Gamma^\alpha(t_1)$, $\Gamma^\beta(t_2)$ etc. we have

$$K_{\alpha,\beta,\gamma,\delta}(t_1,t_2,t_3,t_4,t) = \mathrm{tr}\left[\frac{1}{24}T\left(\Gamma_1\Gamma_2\Gamma_3\Gamma_4\right)D - \frac{1}{6}\Gamma_1 DT\left(\Gamma_2\Gamma_3\Gamma_4\right)\right.$$
$$\left. - \frac{1}{8}T\left(\Gamma_1\Gamma_2\right)DT\left(\Gamma_3\Gamma_4\right)D + \frac{1}{2}\Gamma_1 D\Gamma_2 DT\left(\Gamma_3\Gamma_4\right)D - \frac{1}{4}\Gamma_1 D\Gamma_2 D\Gamma_3 D\Gamma_4 D\right]. \quad (5.24)$$

If we were interested in evaluating the correction due to the fourth order term $S_1^{(4)}$ we could expand $\exp S_1^{(4)}$ and obtain perturbative corrections via Wick's theorem. Letting $S(t)$ be as calculated above – using the second-order approximation for $S_1[\phi]$ – and $\Delta S(t)$ be the fourth-order correction, we have

$$\frac{\Delta S(t)}{S(t)} = \frac{\int D[\phi] e^{S_0[\phi]+S_1^{(2)}[\phi]} S_1^{(4)}[\phi]}{\int D[\phi] e^{S_0[\phi]+S_1^{(2)}[\phi]}} \quad (5.25)$$

$$= (\Delta t)^4 \sum_{r,s,u,v} K(t_r,t_s,t_u,t_v,t)\left(A^{-1}_{rs}A^{-1}_{uv} + A^{-1}_{ru}A^{-1}_{sv} + A^{-1}_{rv}A^{-1}_{us}\right), \quad (5.26)$$

where the indices r,s,u,v label discretized times in the interval $[0,t]$. If, however, we need only an estimate of the validity of truncating $S_1[\phi]$ at second order, we may calculate the ratio of expectations $\left\langle S_1^{(2)}\right\rangle$ and $\left\langle S_1^{(4)}\right\rangle$, with averages taken with respect to the action $S_0[\phi]$. We may again use Wick's theorem, but now with the simpler diagonal Green function

$$\left(A^{-1}\right)_{mn} \to -\frac{2i}{M\Delta t}\delta_{mn} \quad (5.27)$$

We therefore have

$$\frac{\left\langle S_1^{(4)}\right\rangle_0}{\left\langle S_1^{(2)}\right\rangle_0} = -2i\frac{t}{M}\left(\langle K(r,r,s,s,t)\rangle + \langle K(r,s,r,s,t)\rangle + \langle K(r,s,s,r,t)\rangle\right) / \langle K(s,s,t)\rangle \quad (5.28)$$

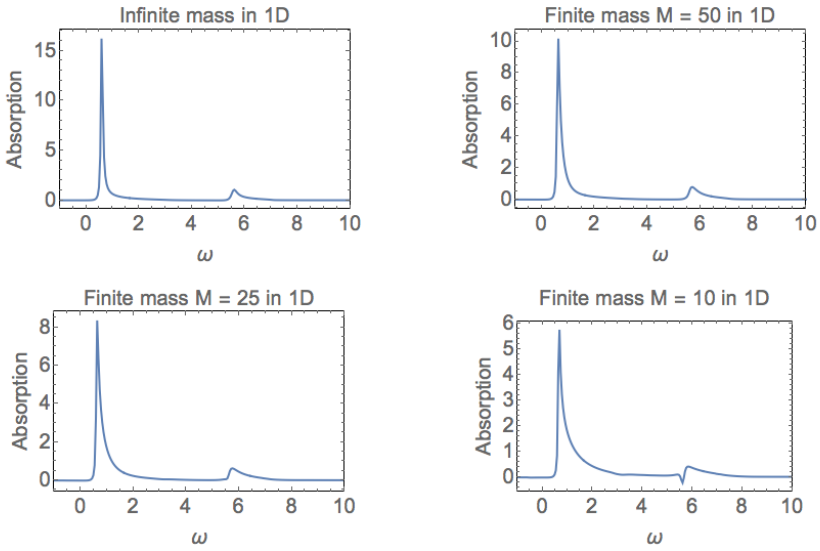

Figure 5.1: RF absorption in one dimension.

where the averages are Monte Carlo averages over r, s in the interval $[0, t]$.

5.4 Results

First of all, our results so far are asymptotic in impurity mass but not in time. Eq. (5.28) indicates an increasing error at large times, and we must know something about the decay of $S(t)$, which will hopefully occur quickly enough that the error introduced by a second order expansion is not too severe. This decay is inherent to the infinite-mass case and is not dramatically affected by the finite-mass correction. In addition to an algebraic decay due to the orthogonality catastrophe, the time-domain consequence of vanishing overlap between the ground states of H_0 and H_1, the decay of $S(t)$ is further accelerated by finite temperature. This is relevant to experiments with ultracold atoms, where temperatures of trapped fermion systems generally exceed $0.2t_f$. In Fig. 5.3 we plot this decay for one- and two-dimensional systems at T=0.1, 0.2 t_f, the former of

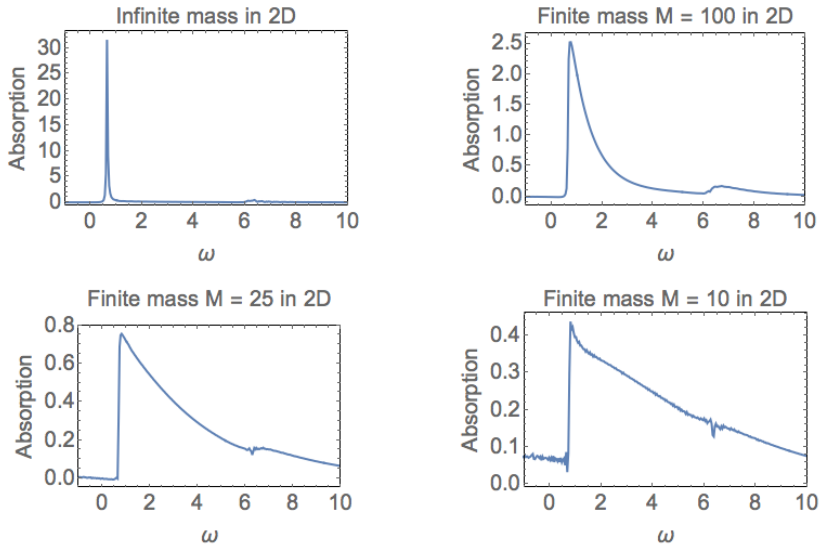

Figure 5.2: RF absorption in two dimensions.

which is somewhat beyond current technology. These will inform the error analysis below by determining which values of t contribute to the integral for $R(\omega)$.

In Fig. 5.1 we apply our formalism to a length-$L = 500$ 1D system at chemical potential $\mu = -0.5t_f$ and temperature $T = 0.1t_f$ with a repulsive contact interaction of strength $V = 4t_f$ and zero initial impurity momentum. We obtain for $M = \infty$ a power-law singularity of $R(\omega)$ in both cases, as is well known. For finite masses $M = 100,\ 25\,10\,t_f$ this behavior persists, with renormalization of the singular exponent.

In addition to the dominant absorption threshold singularity there is an addition peak. We attribute this to the formation of a repulsively-bound state, which we may easily justify in the infinite-mass case as follows. For an N-particle system the first peak occurs at the many-body ground state energy of H_1, which is the sum of the N lowest eigenenergies. For $M = \infty$ H_1 is simply a single-particle matrix and is easily diagonalized. When $V > 0$ is repulsive, all energies but one lie in a continuum band;

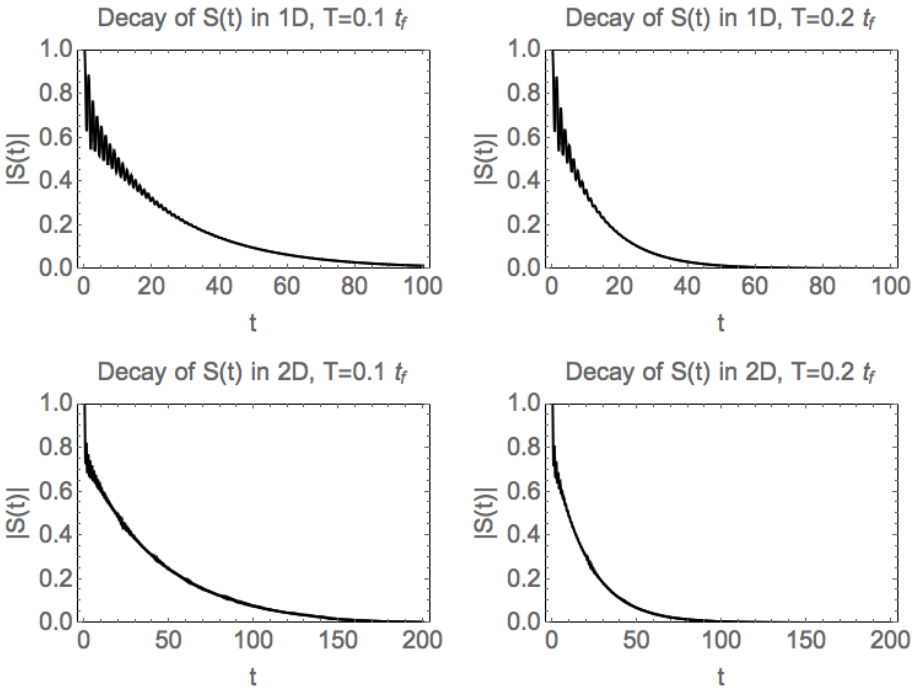

Figure 5.3: Decay of $|S(t)|$ in 40×40 2D systems and $L = 500$ 1D systems at temperatures of $0.2t_f$ and $0.1t_f$. Parameters are $\mu = -0.5t_f$, $V = 4t_f$, and $M = \infty$.

the last, which is above the continuum, belongs to the repulsively-bound state. Thus the second absorption threshold energy is the sum of the $N-1$ lowest eigenenergies and the highest eigenenergy of H_1. The separation between the two peaks is the difference between the highest and the Nth lowest of eigenenergies of H_1. For the parameters given above we obtain a separation of 4.97 t_f, which agrees exactly with the plotted values.

The physics of repulsively-bound states is unfamiliar to many but very simple. Basically, particles obeying a bounded dispersion cannot convert an arbitrary amount of potential energy due to being placed near a repulsive impurity into kinetic energy, and thus remain in a bound state. As an additional check, we have verified that our formalism does not produce this second peak in a continuum system, where the lack of Bloch bands circumvents this argument. To our knowledge, this work is the first theoretical work to analyze a repulsively-bound state in a many-body medium. We have shown here that it exists and is experimentally detectable.

In Fig. 5.2 we repeat this analysis for a $L \times L = 40 \times 40$ 2D system at chemical potential $\mu = -0.5t_f$ and temperature $T = 0.1t_f$ with a repulsive contact interaction of strength $V = 4t_f$ and zero initial impurity momentum. We again find singular behavior for an infinite mass impurity, but find that this behavior is dramatically influenced by arbitrary finite mass, unlike the 1D case. We again see evidence of a repulsively-bound state.

To justify the second order approximation to $S_1[\phi]$ we can use Eq. (5.28) to determine the values of t/M for which this approximation is valid, that is, for which the fourth-order correction is small. In Fig. 5.4 we show the ratio $\left\langle S_1^{(4)} \right\rangle_0 / \left\langle S_1^{(2)} \right\rangle_0$ in units of t/M for relevant times (in both the 1D and 2D cases, $S(t)$ decays by 4 orders of magnitude by time $t = 100$. Due to the smallness of this ratio, we can see that for the smallest

mass and longest time considered the error ratio reaches about 1/3. Thus $M = 10$ is roughly the smallest mass that can be studied at this temperature. However, $S(t)$ decays much more rapidly with increasing temperature, allowing one to study smaller masses. For example, in the 1D system above at temperature $T = 0.2t_f$ (which again, is at the extreme limit of current capabilities for non-lattice systems and remains beyond the limit for lattice systems), $S(t)$ decays almost completely by time $t = 50(t_f)^{-1}$. From Fig. 5.4 we see that the relative size of the fourth-order correction at this time is around $0.015 \times t/M$, which is only about 1/6 even for a fairly light mass $M = 5$. Thus it is safe to conclude that our results are will be quantitatively valid in real experiments. Finally, we note that if advances in technology lead to fermion trapping at temperatures lower than those considered here, the same analysis that led to the fourth-order error can also be used, with minor modifications, to actually calculate the correction to $S(t)$ from the fourth order term.

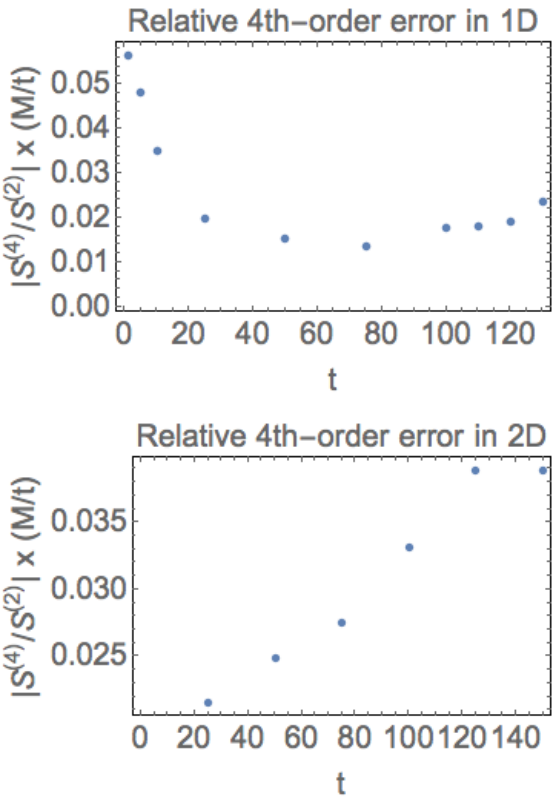

Figure 5.4: Relative contribution of fourth order correction in one and two dimensions.

A

Functional Determinants for General Bilinear Hamiltonians

We saw in chapters 1-3 how to compute exact Green functions of the form $\langle c^\dagger \dots c e^Z \rangle$, where Z is many-body operator of the form $Z = c_i^\dagger z_{ij} c_j$. (Recall that the indices i and j combine spin and orbital degrees of freedom). This sufficed to handle all the examples

considered in this thesis. Furthermore a Hamiltonian with a singlet pairing term:

$$H = \sum_{i,j,\sigma} H_{ij}^{\sigma} c_{i,\sigma}^{\dagger} c_{j,\sigma} + \sum_{i,j} \left(H'_{ij} c_{i,\uparrow}^{\dagger} c_{j,\downarrow}^{\dagger} + \text{h.c.} \right) \tag{A.1}$$

can be recast via the unitary particle-hole transformation $c_{i,\downarrow}^{\dagger} \leftrightarrow c^{i,\downarrow}$, yielding

$$H = \sum_{i,j} H_{ij}^{\uparrow} c_{i,\uparrow}^{\dagger} c_{j,\uparrow} - \sum_{i,j} H_{ij}^{\downarrow} c_{j,\downarrow}^{\dagger} ci,\downarrow + \sum_{i,j} \left(H'_{ij} c_{i,\uparrow}^{\dagger} c_{j,\downarrow} + \text{h.c.} \right) + \text{tr} H^{\downarrow}, \tag{A.2}$$

which is a non-anomalous quadratic Hamiltonian plus a c-number.

However more exotic spin order than the simple antiferromagetism we considered above, or triplet superconductivity with pairing terms $c_{i,\uparrow}^{\dagger} c_{j,\uparrow}^{\dagger}$ require a more significant addition to the formalism. Israel Klich has devised an ingenious method wherein creation and annihilation operators are treated on equal footing in a redundant basis of Majorana fermions. Consider a general bilinear Hamiltonian on an n-dimensional basis $i = 1, 2, \ldots n$.

$$\mathcal{H} = H_{ij} f_i^{\dagger} f_j + \frac{1}{2} \left(\Delta_{ij} f_i f_j + \text{h.c.} \right), \tag{A.3}$$

where Δ_{ij} is antisymmetric and H is Hermitian. We can rewrite $\mathcal{H}$ in terms of the $2n$ Majorana fermions

$$c_i = f_i^{\dagger} + f_i \qquad i = 1, 2, \ldots n \tag{A.4}$$

$$c_i = i(f_i^{\dagger} - f_i) \qquad i = n+1, n+2, \ldots 2n, \tag{A.5}$$

which obey $c_i = c_i^{\dagger}$ and $c_i c_j + c_j c_i = 2\delta_{ij}$, as

$$\mathcal{H} = A_{ij} c_i c_j, \tag{A.6}$$

where

$$A = i \begin{pmatrix} \mathrm{Im}(\Delta + H) & \mathrm{Re}(\Delta + H) \\ -\mathrm{Re}(\Delta - H) & \mathrm{Im}(\Delta - H) \end{pmatrix} \tag{A.7}$$

Therefore, we are interested in traces of the form

$$Z(A) \equiv \mathrm{tr} e^{A_{ij} c_i c_j} \tag{A.8}$$

with respect to 2^n-dimensional Fock space, where A_{ij} is an antisymmetric $2n \times 2n$ matrix. Some thought about how the calculation for the simple case $\Delta = 0$ was carried out will indicate how to proceed with the general case. There, we appealed to the existence of a basis in which H is diagonal to reduce the Fock-space trace to a product of traces over two-dimensional Fock spaces $n_\alpha = 0, 1$ for individual eigenstates. The success of this procedure ultimately relied on the invariance of the trace under unitary transformations. Therefore, the first step is to determine what group of transformations takes the place of $U(n)$. To preserve the defining anticommutator $\{c_i, c_j\} = 2\delta_{ij}$ of the Clifford algebra under some transformation $c'_i = M_{ij} c_j$ we require

$$M_{ik} M_{jl} (c_k c_l + c_l c_k) = 2\delta_{ij} \tag{A.9}$$

$$M_{ik} M_{jl} 2\delta_k l = 2\delta_{ij} \tag{A.10}$$

$$M_{ik} M_{jk} = \delta_i j \tag{A.11}$$

$$M M^\intercal = I \tag{A.12}$$

Thus we are concerned with complex orthogonal transformations, not unitary transformations. That is, we have so far seen that if any sort of transformation is to leave $Z(A)$ invariant, it is the orthogonal transformations. We will see below that this condition is

sufficient.

As before, our goal is to cast the trace purely in terms on manipulations on the matrix A. To that end, we note that under transformations $c_i' = O_{ij}c_j$ the bilinear operator transforms as

$$A_{ij}c_ic_j \to A_{ij}O_{ik}c_kO_{jl}c_l = (O^\intercal AO)_{kl}\, c_kc_l \tag{A.13}$$

so that in effect $A \to O^\intercal AO$. A natural conjecture is therefore that $Z(A) = Z(O^\intercal AO)$, which would allow us to transform A into a convenient canonical form in which the Fock space trace decomposes as the product of simple factors. A sufficient condition for this is as follows: suppose that for complex orthogonal O there existed $U(O)$ such that the action of O on the set of Majorana fermions is identical to a similarity transformation:

$$O_{ij}c_j = U(O)c_iU(O)^{-1} \tag{A.14}$$

If such a U exists we then have, using the cyclicity of the trace

$$Z(A) = \mathrm{tr}e^{A_{ij}c_ic_j} = \mathrm{tr}\left[U(O)e^{A_{ij}c_ic_j}U(O)^{-1}\right] = \mathrm{tr}\left[e^{U(O)A_{ij}c_ic_jU(O)^{-1}}\right] \tag{A.15}$$

$$= \mathrm{tr}\left[e^{A_{ij}U(O)c_iU(O)^{-1}U(O)c_jU(O)^{-1}}\right] \tag{A.16}$$

$$= \mathrm{tr}\left[e^{(O^\intercal AO)_{ij}c_ic_j}\right] = Z(O^\intercal AO), \tag{A.17}$$

which is the desired result.

To establish the existence of $U(O)$ we note that any matrix in the connected component of $O(2n, \mathbb{C})$ containing the identity can be written as e^{iK} where K is (complex) antisymmetric (The latter is the Lie algebra of the former). For orthogonal matrices of

this form we can then write

$$\left(e^{iK}\right)_{ml} c_l = e^{-\frac{i}{4}K_{ij}c_ic_j} c_m e^{\frac{i}{4}K_{mn}c_mc_n}, \tag{A.18}$$

which explicitly gives $U(O) = e^{-\frac{i}{4}K_{mn}c_mc_n}$. We may verify this via a form of the Baker-Campbell-Haussdorff lemma:

$$e^X Y e^{-X} = Y + [X, Y] + \frac{1}{2!}[X, [X, Y]] \dots \tag{A.19}$$

with $X = -\frac{i}{4}K_{ij}c_ic_j$ and $Y = c_m$. We require the commutator

$$\begin{aligned}
[c_ic_j, c_m] =& c_ic_jc_m - c_mc_ic_j && \text{(A.20)}\\
=& c_i(-c_mc_j + 2\delta_{mj}) - c_mc_ic_j && \text{(A.21)}\\
=& -(-c_mc_i + 2\delta_{im})c_j + 2\delta_{mj}c_i - c_mc_ic_j && \text{(A.22)}\\
=& 2\delta_{mj}c_i - 2\delta_{mi}c_j && \text{(A.23)}
\end{aligned}$$

Then, using the antisymmetry of K, we have

$$[X, Y] = -\frac{i}{2}K_{im}c_i - K_{mj}c_j = iK_{mi}c_i. \tag{A.24}$$

Treating c as a column vector of the operators c_m, we have

$$[X, c_m] = i(Kc)_m,\ [X, [X, c_m]] = i^2K_{mi}(Kc)_i = i^2(K^2c)_m, \dots, \tag{A.25}$$

so that

$$e^X c_m e^{-X} = \left(\sum_{n=0}^{\infty} \frac{i^n}{n!} K^n c \right)_m \tag{A.26}$$

$$= \left(e^{iK} \right)_{ml} c_l \tag{A.27}$$

Finally, to get the whole complex orthogonal group and not just one connected component, we need a similarity transformation that acts like a matrix with negative determinant. This is provided by

$$c_m \to c_j c_m c_j^{-1} = c_j c_m c_j = -c_m + 2\delta_{mj} c_j = \begin{cases} -c_m & (m = j) \\ c_m & (m \neq j) \end{cases} \tag{A.28}$$

This is equivalent to the action of an orthogonal matrix equal to the identity but with a single diagonal element equal to minus-one, which clearly provides the necessary link to the connected component of the orthogonal group with negative determinant.

Now that we have established the invariance of the trace with respect to arbitrary orthogonal transformations in the Majorana basis, we need to find the orthogonal transformation that simplifies the trace. Importantly, we need only know the *existence* of some transformation. For antisymmetric $2n \times 2n$ matrix A with non-degenerate eigenvalues, it is proven in the book by Gantmacher that A is orthogonally similar to a block-diagonal matrix containing n blocks of the form

$$B_i = \begin{pmatrix} 0 & \varepsilon_i \\ -\varepsilon_i & 0 \end{pmatrix}, \tag{A.29}$$

where $\pm i\varepsilon_i$, $i = 1, \ldots n$ are the eigenvalues of A. That is, there exists orthogonal O such

that $OAO^\intercal = \oplus B_i$. Thus

$$Z(A) = \mathrm{tr} e^{\sum \varepsilon_i (c_{2i}c_{2i+1} - c_{2i+1}c_{2i})} = \mathrm{tr} e^{\sum 2\varepsilon_i c_{2i}c_{2i+1}} \tag{A.30}$$

Due to the invariance under orthogonal similarity transformations, we may perform an arbitrary permutation change-of-basis of the Majorana fermions such that $c_{2i} = f_j^\dagger + f_j$ and $c_{2i+1} = i(f_j^\dagger - f_j)$ for some fermion state j. The trace then decomposes as a product:

$$Z = \prod_i \mathrm{tr} e^{2i\varepsilon_i (f_j^\dagger f_j - f_j f_j^\dagger)} = \prod_i \sum_{n_j = 0,1} e^{2i\varepsilon_i (2n_j - 1)} = \prod_i \left(e^{2i\varepsilon_i} + e^{-2i\varepsilon_i} \right) \tag{A.31}$$

$$= \prod_i 2\cos(2\varepsilon_i) = \prod_i \frac{\sin(4\varepsilon_i)}{\sin(2\varepsilon_i)} \tag{A.32}$$

At this point, we can't quite relate Z to a determinant involving e^A because of the ambiguity in the sign of ε_i. Instead of a determinant involving n values ε_i, that is, a determinant of an $n \times n$ matrix, we can relate Z to the *Pfaffian* of a $2n \times 2n$ matrix involving the $2n$ values $\pm\varepsilon_i$. As the Pfaffian, like the determinant, factorizes over block diagonal matrices, we need to relate the factors $\sin(m\varepsilon_i)$ to a Pfaffian involving the block B_i. Such a relation can be obtained via

$$\mathrm{Pf}\left(e^{mB_i} - e^{-mB_i} \right) = \mathrm{Pf} \begin{pmatrix} 0 & 2\sin(m\varepsilon_i) \\ -2\sin(m\varepsilon_i) & 0 \end{pmatrix} = 2\sin(m\varepsilon_i) \tag{A.33}$$

By the block-factorizability of the Pfaffian, we have

$$Z(A) = \prod_i \frac{\mathrm{Pf}\left(e^{4B_i} - e^{-4B_i} \right)}{\mathrm{Pf}\left(e^{2B_i} - e^{-2B_i} \right)} = \frac{\mathrm{Pf}\left(e^{4A} - e^{-4A} \right)}{\mathrm{Pf}\left(e^{2A} - e^{-2A} \right)} \tag{A.34}$$

Finally, we must extend the argument to the degenerate case. Since the definition of

$Z(A)$ is analytic, and since both the numerator and denominator of Eq. (A.34) are analytic, the only potential problem would be if the denominator has zero of higher order than the numerator. Using the identity $\mathrm{Pf}^2(M) = \det(M)$ we have

$$Z^2(A) = \frac{\det(e^{4A} - e^{-4A})}{\det(e^{2A} - e^{-2A})} = \det(e^{2A} + e^{-2A}), \tag{A.35}$$

which is manifestly analytic. Thus by analytic continuing the case with an arbitrarily small degeneracy-breaking perturbation, we establish the result Eq. (A.34) also for the degenerate case. For the same reason as for Hamiltonians without pairing, the trace formula extends

B

Additional REXS calculations

B.1 Effect of Core Hole in REXS Spectra

In Figure (B.1) we show the effect of varying core hole strengths on the REXS spectrum. The essential features to note are (i) flattening of the high energy peak and growth of the low energy peak, and (ii) slight increase in peak separation, as core hole strength is increased. By $U_0 = -0.75$ eV, the upper peak is almost invisible.

The peak energies themselves depend on U_0 in that an attractive potential tends to lower all energies. However, the separation between peaks depends only weakly on U_0. Zero energy, i.e. the Fermi energy E_f, is not at the first maximum. The location of this maximum is determined by dynamic nesting, which occurs at some energy above E_f, and the excitonic effect, which lowers energies of transient states. Thus in principle the first peak could be at positive or negative energy.

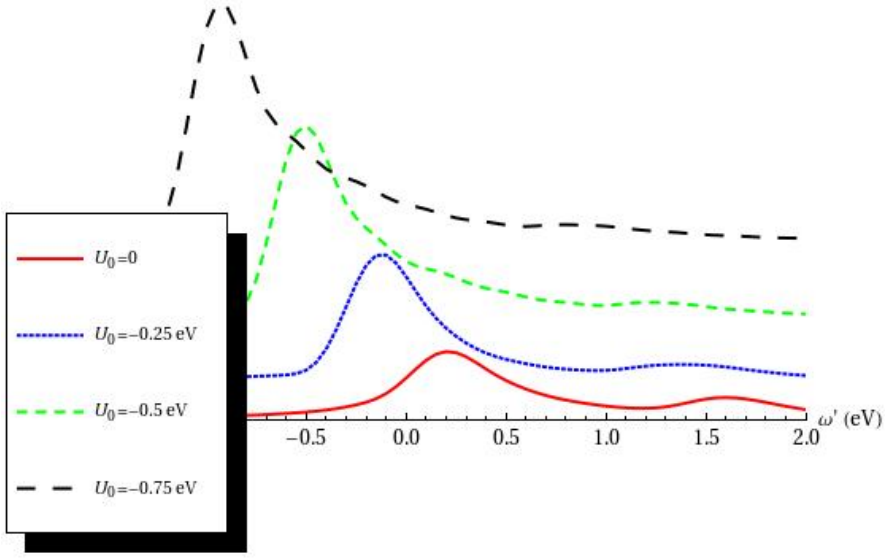

Figure B.1: REXS spectra of LBCO at different core hole strengths. ω' is defined as in Figure (1) of the main text.

B.2 Core Hole Yukawa Potentials

Figure (B.2) shows the calculated REXS spectra for parameters identical to those in the main text but Yukawa core hole potentials of the form

$$U(\mathbf{r}) = U_0 \begin{cases} 1 & (\mathbf{r} = \mathbf{0}) \\ \frac{e^{-r/r_0}}{r} & (\mathbf{r} \neq \mathbf{0} \end{cases}, \tag{B.1}$$

where r_0 is the range of the potential. The effect is quite similar to that obtained by increasing U_0 in the case of a contact potential, which is sensible – a potential well can become bigger by growing deeper or wider. The high energy peak becomes less pronounced and both peaks move to lower energies. For the Yukawa case, unlike for contact potentials, the separation between peaks decreases slightly as the range increases. This is not profound – it merely reflects the fact that different potentials yield different excitonic effects. Incidentally, we note that it is possible that LDA-derived tight-binding parameters are quite accurate and that excitonic effects of a Yukawa potential reduce the separation of peaks to the experimentally-observed value.

B.3 LDA- vs. ARPES-derived Band Structure

Figure (B.3) shows REXS spectra using the same parameters as in the main text except for replacing hopping strengths with those obtained from LDA and ARPES. The spectra are qualitatively the same but with different peak separations. The experimentally-observed peak separation is less than that of LDA and more than that of ARPES.

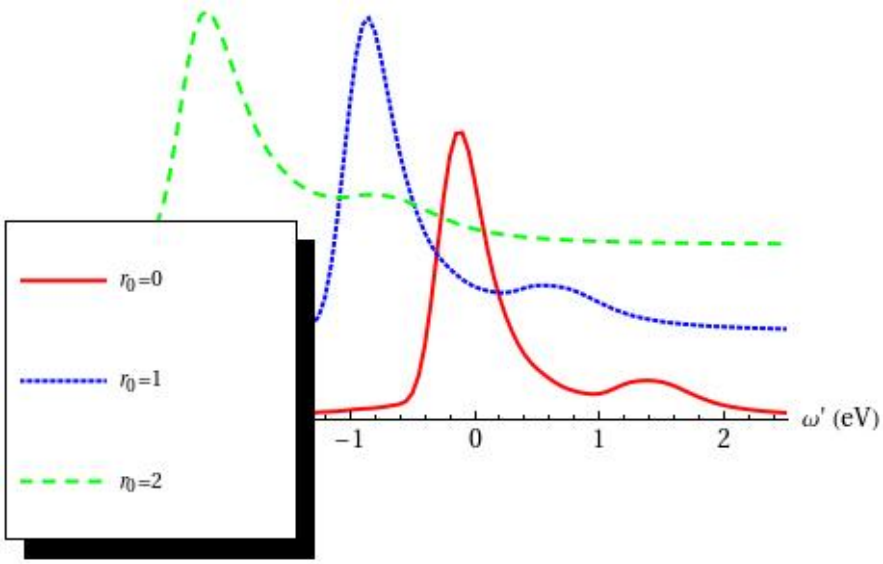

Figure B.2: REXS spectra of LBCO at different Yukawa potential ranges for fixed core hole potential depth $U_0 = -0.25$ eV. ω' is defined as in Figure (1) of the main text.

B.4 Slightly-Inelastic Scattering

We assumed purely elastic scattering in which $|f\rangle = |i\rangle$. However, resolutions of both energy and momentum are finite and, assuming $T = 0$ for simplicity, a final state containing electron-hole pairs of very small total energy and momenta could correspond to apparently-elastic scattering. We can give two simple reasons why this does not affect the validity of setting $|f\rangle = |i\rangle$. Firstly, the rate of producing any given electron-hole pair, for example by scattering of Fermi sea electrons by the core hole potential, is independent of the transient state of the photoelectron. Thus the creation of low-energy and low-momentum excitations in the final state will increase the measured elastic intensity uniformly by an $|n\rangle$-independent factor. Secondly, matrix elements to produce a particle of momentum $\mathbf{q}$ vary slowly as a function of $\mathbf{q}$, hence slightly-

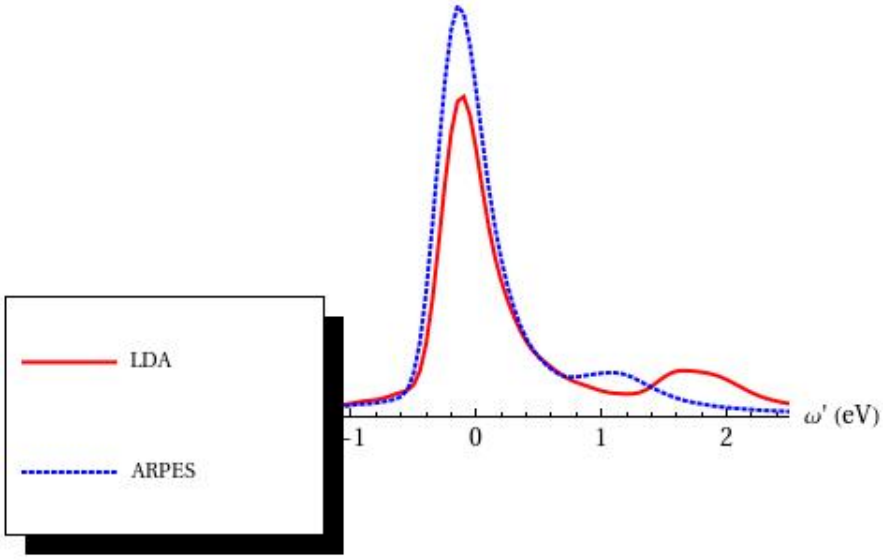

Figure B.3: REXS spectra of LBCO at different for LDA and ARPES tight-binding parameters. ω' is defined as in Figure (1) of the main text.

inelastic processes do not exhibit a peak in momentum transfer. They contribute a constant incoherent background which is easily isolated from the diffraction peak. In practice, this is done by measuring REXS spectra over a range of momentum transfer that crosses the ordering wavevector $\mathbf{Q}$.

C

Derivation of REXS Formula

Here we use the method of Klich to compute expressions of the form

$$A = \frac{\mathrm{tr}_F \left[d_{j,\sigma} e^{-i\mathcal{H}_1 t} d^\dagger_{j,\sigma} e^{-\beta \mathcal{H}_0} \right]}{\mathrm{tr}_F \left[e^{-\beta \mathcal{H}_0} \right]}, \tag{C.1}$$

where $\mathcal{H}_{0,1}$ are quadratic Hamiltonians and d_j annihilates the single-particle Wannier orbital $|j\rangle$. We write tr_F and tr_H for traces with respect to many-particle Fock space

and single-particle Hilbert space, respectively.We split them into commuting parts that act on electrons of spins σ and $\bar{\sigma}$: $\mathcal{H}_{0(1)} = \mathcal{H}_{0(1),\sigma} + \mathcal{H}_{0(1),\bar{\sigma}}$. Then the traces factorize into different spin sectors:

$$A = \frac{\mathrm{tr}_F\left[d_{j,\sigma} e^{-i\mathcal{H}_{1,\sigma}t} d^\dagger_{j,\sigma} e^{-\beta\mathcal{H}_{0,\sigma}}\right]}{\mathrm{tr}_F\left[e^{-\beta\mathcal{H}_{0,\sigma}}\right]} \frac{\mathrm{tr}_F\left[e^{-i\mathcal{H}_{1,\bar{\sigma}}t} e^{-\beta\mathcal{H}_{0,\bar{\sigma}}}\right]}{\mathrm{tr}_F\left[e^{-\beta\mathcal{H}_{0,\bar{\sigma}}}\right]}, \tag{C.2}$$

Each trace is spin-independent, so let us introduce

$$X_0 = -\beta\mathcal{H}_{0,\sigma} = -\beta\mathcal{H}_{0,\bar{\sigma}} \tag{C.3}$$

$$X_1 = -it\mathcal{H}_{1,\sigma} = -it\mathcal{H}_{1,\bar{\sigma}}, \tag{C.4}$$

where equality is up to isomorphism of spin-σ and spin-$\bar{\sigma}$ subspaces. That is, $X_{0,1}$ act on the Fock space of a spinless conduction band. Equation (C.2) then reads

$$A = \frac{\mathrm{tr}_F\left[d_j e^{X_1} d^\dagger_j e^{X_0}\right]}{\mathrm{tr}_F\left[e^{X_0}\right]} \frac{\mathrm{tr}_F\left[e^{X_1} e^{X_0}\right]}{\mathrm{tr}_F\left[e^{X_0}\right]}, \tag{C.5}$$

Define X_2 such that $\exp(X_1)\exp(X_0) \equiv \exp(X_2)$. By the Baker-Campbell-Haussdorff Lemma, X_2 is quadratic. Label the eigenstates of X_i as follows:

$$X_i|\alpha, i\rangle = \omega_{\alpha,i}|\alpha, i\rangle,\ X_i = \sum \omega_{\alpha,i} d^\dagger_{\alpha,i} d_{\alpha,i} = \sum \omega_{\alpha,i} n_{\alpha,i} \tag{C.6}$$

Change of basis is done with $d_j = \sum_\alpha \langle j|\alpha, i\rangle d_{\alpha,i}$ etc, and the useful corollary

$$\sum_\alpha |\alpha, i\rangle d_{\alpha,i} = \sum_\alpha |\alpha, i\rangle\langle\alpha, i| \left(\sum_\beta |\beta, j\rangle d_{\beta,j}\right) = \sum_\beta |\beta, j\rangle d_{\beta,j}. \tag{C.7}$$

The denominator traces in Equation C.5 are the simplest to evaluate and are a useful

warm-up for the numerator traces. The first step in the basis $\{|\alpha, 0\rangle\}$ in which X_0 is diagonal and the many-body trace factorizes in terms of traces over the occupation numbers $n_{\alpha,0} = 0, 1$ of eigenstates:

$$\mathrm{tr}_F\left[e^{X_0}\right] = \mathrm{tr}_F\left[e^{\sum_\alpha \omega_{\alpha,0} n_{\alpha,0}}\right] = \prod_\alpha \sum_{n_{\alpha,0}=0,1} e^{\sum_\alpha \omega_{\alpha,0} n_{\alpha,0}} = \prod_\alpha (1 + e^{\omega_{\alpha,0}}). \tag{C.8}$$

Next we use the fact that $(1 + e^{\omega_\alpha,0})$ are the eigenvalues of the *single-particle* operator $1 + \exp(X_{0,\mathrm{sp}})$, where $X_{0,\mathrm{sp}}$ is the projection of X_0 into Hilbert space. (We define $X_{1,\mathrm{sp}}$ and $X_{2,\mathrm{sp}}$ analogously). Furthermore, the product of an operator's eigenvalues is its determinant, so we have

$$\mathrm{tr}_F\left[e^{X_0}\right] = \prod_\alpha (1 + e^{\omega_{\alpha,0}}) = \det\left(1 + e^{X_{0,\mathrm{sp}}}\right). \tag{C.9}$$

Of the two distinct numerators in Equation (C.5) the simpler one, which has no injected electron, follows almost immediately fromEquation (C.9):

$$\mathrm{tr}_F\left[e^{X_1} e^{X_0}\right] = \mathrm{tr}_F\left[e^{X_2}\right] = \det\left(1 + e^{X_{2,\mathrm{sp}}}\right) = \det\left(1 + e^{X_{1,\mathrm{sp}}} e^{X_{0,\mathrm{sp}}}\right) \tag{C.10}$$

Note that we never have to go through the exercise in commutator algebra to obtain X_2 explicitly. All we needed was that it is quadratic.

To calculate the last and most difficult trace, we again want to write it as a product of traces over occupation numbers 0 and 1. This means that we wish to put the d and $d^\dagger$ next to one another to form a number operator n. We use the cyclic property of the

trace to put d_j to the right of $d_j^\dagger$ and switch to a basis in which X_0 is diagonal: :

$$\mathrm{tr}_F\left[d_j e^{X_1} d_j^\dagger e^{X_0}\right] = \mathrm{tr}_F\left[e^{X_1} d_j^\dagger e^{X_0} d_j\right] = \sum_{\alpha,\alpha'} \langle j|\alpha,0\rangle \mathrm{tr}_F\left[e^{X_1} d_{\alpha',0}^\dagger e^{X_0} d_{\alpha,0}\right] \langle \alpha',0|j\rangle. \tag{C.11}$$

In this basis we may exploit the commutator $d_{\alpha,0}^\dagger e^{X_0} = e^{X_0} d_{\alpha,0}^\dagger e^{-\omega_{\alpha,0}}$ to get

$$\mathrm{tr}_F\left[d_j e^{X_1} d_j^\dagger e^{X_0}\right] = \sum_{\alpha,\alpha'} \langle j|\alpha,0\rangle \mathrm{tr}_F\left[e^{X_1} e^{X_0} d_{\alpha',0}^\dagger d_{\alpha,0}\right] e^{-\omega_{\alpha',0}} \langle \alpha',0|j\rangle \tag{C.12}$$

Next we wish to combine e^{X_1} and e^{X_0} as e^{X_2} and use Equation (C.7) with $i = 0$, $j = 2$ to switch to the eigenbasis of X_2. We first need to remove the factor $e^{-\omega_{\alpha',0}}$ via

$$e^{-\omega_{\alpha',0}} \langle \alpha',0| = \langle \alpha',0|e^{-X_{0,\mathrm{sp}}}. \tag{C.13}$$

By Equations (C.7) and (C.13), Equation (C.12) becomes

$$\begin{aligned}\mathrm{tr}_F\left[d_j e^{X_1} d_j^\dagger e^{X_0}\right] &= \sum_{\beta,\beta'} \langle j|\beta,2\rangle \mathrm{tr}_F\left[e^{X_2} d_{\beta',2}^\dagger d_{\beta,2}\right] \langle \beta',2|e^{-X_{0,\mathrm{sp}}}|j\rangle \\ &= \sum_{\beta} \langle j|\beta,2\rangle \mathrm{tr}_F\left[e^{\sum \omega_{\gamma,2} n_{\gamma,2}} n_{\beta,2}\right] \langle \beta,2|e^{-X_{0,\mathrm{sp}}}|j\rangle. \end{aligned} \tag{C.14}$$

We used the fact that $\beta \neq \beta'$ is purely off-diagonal and has vanishing trace. We evaluate the trace in Equation (C.14) the same way as Equation (C.8), with the slight

complication that we must distinguish the case $\gamma = \beta$ and $\gamma \neq \beta$:

$$\begin{aligned}\mathrm{tr}_F\left[e^{\sum \omega_{\gamma,2} n_{\gamma,2}} n_{\beta,2}\right] =& \sum_{n_{\beta,2}=0,1} e^{\omega_{\beta,2} n_{\beta,2}} n_{\beta,2} \prod_{\gamma\neq\beta} \sum_{n_{\gamma,2}=0,1} e^{\omega_{\gamma,2} n_{\gamma,2}} \\ =& e^{\omega_{\beta,2}} \prod_{\gamma\neq\beta} (1 + e^{\omega_{\gamma,2}}) = \frac{e^{\omega_{\beta,2}}}{1 + e^{\omega_{\beta,2}}} \prod_{\gamma} (1 + e^{\omega_{\gamma,2}}) \\ =& \frac{e^{\omega_{\beta,2}}}{1 + e^{\omega_{\beta,2}}} \det\left(1 + e^{X_{2,\mathrm{sp}}}\right). \end{aligned} \tag{C.15}$$

When we substitute Equation (C.15) back into Equation (C.14), we again use the trick of replacing a scalar by an operator,

$$\frac{e^{\omega_{\beta,2}}}{1 + e^{\omega_{\beta,2}}} \langle \beta, 2| = \langle \beta, 2| \frac{e^{X_{2,\mathrm{sp}}}}{1 + e^{X_{2,\mathrm{sp}}}}, \tag{C.16}$$

to obtain

$$\begin{aligned}\mathrm{tr}_F\left[d_j e^{X_1} d_j^\dagger e^{X_0}\right] =& \det\left(1 + e^{X_{2,\mathrm{sp}}}\right) \sum_{\beta} \langle j|\beta, 2\rangle\langle \beta, 2| \frac{e^{X_{2,\mathrm{sp}}}}{1 + e^{X_{2,\mathrm{sp}}}} e^{-X_{0,\mathrm{sp}}} |j\rangle \\ =& \det\left(1 + e^{X_{2,\mathrm{sp}}}\right) \langle j| \frac{e^{X_{2,\mathrm{sp}}}}{1 + e^{X_{2,\mathrm{sp}}}} e^{-X_{0,\mathrm{sp}}} |j\rangle \end{aligned} \tag{C.17}$$

Combining Equations (C.9), (C.10), and (C.17), we have

$$\begin{aligned} A =& \frac{\det^2\left(1 + e^{X_{1,\mathrm{sp}}} e^{X_{0,\mathrm{sp}}}\right)}{\det^2\left(1 + e^{X_{0,\mathrm{sp}}}\right)} \langle j| \frac{e^{X_{1,\mathrm{sp}}} e^{X_{0,\mathrm{sp}}} e^{-X_{0,\mathrm{sp}}}}{1 + e^{X_{1,\mathrm{sp}}} e^{X_{0,\mathrm{sp}}}} |j\rangle \\ =& \det\left(\frac{1 + e^{X_{1,\mathrm{sp}}} e^{X_{0,\mathrm{sp}}}}{1 + e^{X_{0,\mathrm{sp}}}}\right)^2 \langle j| \frac{e^{X_{1,\mathrm{sp}}}}{1 + e^{X_{1,\mathrm{sp}}} e^{X_{0,\mathrm{sp}}}} |j\rangle \end{aligned} \tag{C.18}$$

Now define $N \equiv e^{X_{0,\mathrm{sp}}}/(1 + e^{X_{0,\mathrm{sp}}}), e^{X_{0,\mathrm{sp}}} = N/(1 - N)$, the meaning of which is clear

when $X_0 = -\beta H_0$. Substituting N for $e^{X_{0,\mathrm{sp}}}$, we obtain

$$\begin{aligned} A &= \det\left((1-N) + e^{X_{1,\mathrm{sp}}} N\right)^2 \left(\frac{N}{1-N} + e^{-X_{1,\mathrm{sp}}}\right)^{-1}_{jj} \\ &= \det\left((1-N) + e^{-itH_{1,\mathrm{sp}}} N\right)^2 \left(\frac{N}{1-N} + e^{itH_{1,\mathrm{sp}}}\right)^{-1}_{jj}. \end{aligned} \tag{C.19}$$

We have reduced the expression to one involving operations on matrices in single-particle Hilbert space.

D

Derivation of Direct RIXS Formula

Here we derive in full detail Eq. (6) of the paper, extending a method used in Refs. [2] and [12].

The averages S_{mn} at finite temperatures have the form

$$S^{mn}_{\rho\sigma\mu\nu} = \mathrm{tr}\left[e^{iH\tau} d_p e^{-iH_n\tau} d_q^\dagger e^{iHs} d_r \ldots\ldots e^{iH_m t} d_s^\dagger e^{-iH(t+s)-\beta H}\right] / \mathrm{tr}\left[e^{-\beta H}\right], \quad \text{(D.1)}$$

where p, q, r, s are combined site and spin indices in a spin-Wannier basis, eg. $|r\rangle = |m, \mu\rangle$ in Eq. 5.6. From the identity $\mathrm{tr}\, e^X = \det(1 + e^x)$, the denominator of Eq. (D.1) is $\det(1 + e^{-\beta h})$. We define $X_1 = (i(\tau - t - s) - \beta)\, H_0$, $X_2 = iH_m t$, $X_3 = iH_0 s$, $X_4 = -iH_n \tau$ and use the cyclicity property to express the numerator N as $N = \mathrm{tr}\left[d_p e^{X_4} d_q^\dagger e^{X_3} d_r e^{X_2} d_s^\dagger e^{X_1}\right]$. Switching to an arbitrary basis of spin-orbitals, with implicit summation over Greek indices, gives

$$N = \langle p|\alpha\rangle\langle\beta|q\rangle\langle r|\gamma\rangle\langle\delta|s\rangle \mathrm{tr}\left[d_\alpha e^{X_4} d_\beta^\dagger e^{X_3} d_\gamma e^{X_2} d_\delta^\dagger e^{X_1}\right]. \tag{D.2}$$

We move all $d/d^\dagger$ to the left as follows. Choose β to be eigenstates of X_4 with eigenvalues ω_β. Then $\langle\beta|..e^{X_4} d_\beta^\dagger = \langle\beta|..e^{\omega_\beta} d_\beta^\dagger e^{X_4} = \langle\beta|e^{X_4}..d_\beta^\dagger e^{X_4}$. After absorbing the c-number e^{ω_β} as $\langle\beta|e^{X_4}$, the basis β is again arbitrary. The general pattern is to commute $d_\delta^\dagger$ with e^X via $\langle\delta| \to \langle\delta|e^X$ and commute d_γ with e^X via $|\gamma\rangle \to e^{-X}|\gamma\rangle$. Successive applications yield

$$N = \langle p|\alpha\rangle\langle\beta|e^{X_4}|q\rangle\langle r|e^{-X_3}e^{-X_4}|\gamma\rangle\langle\delta|e^{X_4}e^{X_3}e^{X_2}|s\rangle \mathrm{tr}\left[d_\alpha d_\beta^\dagger d_\gamma d_\delta^\dagger e^Z\right], \tag{D.3}$$

where Z is a quadratic operator such that $e^Z = e^{X_4}e^{X_3}e^{X_2}e^{X_1}$ whose existence is guaranteed by the Baker-Campbell-Haussdorff lemma. If there were no $d/d^\dagger$ insertions we would evaluate the trace in an eigenbasis $Z|\phi\rangle = \omega_\phi|\phi\rangle$, in which it factorizes as $\mathrm{tr}\, e^Z = \prod_\phi \sum_{n_\phi=0,1} e^{n_\phi\omega_\phi} = \prod_\phi (1 + e^{\omega_\phi}) = \det(1 + e^z)$. Now choose $\alpha, \beta, \gamma, \delta$ to be eigenstates of Z with eigenvalues ω_α etc. The trace vanishes unless the $d/d^\dagger$ match pairwise. For example, if $\alpha = \beta \neq \gamma = \delta$ we have $\mathrm{tr}\left[(1 - n_\alpha)(1 - n_\gamma)e^Z\right]$. This is identical to $\mathrm{tr}\, e^Z$ except the factor $(1 + e^{\omega_\alpha})$ is replaced by $\sum_{n_\alpha=0,1}(1 - n_\alpha)e^{n_\alpha\omega_\alpha} = 1$, and similarly for γ giving $(1 + e^{\omega_\alpha})^{-1}(1 + e^{\omega_\gamma})^{-1} \det(1 + e^z)$. Including the other cases

$\alpha = \delta \neq \beta = \gamma$ and $\alpha = \beta = \gamma = \delta$ we get

$$\begin{aligned}\text{tr}\left[d_\alpha d_\beta^\dagger d_\gamma d_\delta^\dagger e^Z\right] &= \left[\delta_{\alpha\beta}\delta_{\gamma\delta}\delta_{\beta\gamma}(1+e^{\omega_\alpha})^{-1} + \delta_{\alpha\delta}\delta_{\beta\gamma}(1-\delta_{\alpha\beta})(1+e^{\omega_\alpha})^{-1}e^{\omega_\beta}(1+e^{\omega_\beta})^{-1}\right. \\ &\left. + \delta_{\alpha\beta}\delta_{\gamma\delta}(1-\delta_{\alpha\gamma})(1+e^{\omega_\alpha})^{-1}(1+e^{\omega_\gamma})^{-1}\right]\det(1+e^Z) \\ &= \det(1+e^Z)\left[\delta_{\alpha\delta}\delta_{\beta\gamma}(1+e^{\omega_\alpha})^{-1}e^{\omega_\beta}(1+e^{\omega_\beta})^{-1} + \delta_{\alpha\beta}\delta_{\gamma\delta}(1+e^{\omega_\alpha})^{-1}(1+e^{\omega_\gamma})^{-1}\right].\end{aligned} \tag{D.4}$$

Next, we absorb the c-numbers in Eq. D.4 as operators via $|\alpha\rangle..(1+e^{\omega_\alpha})^{-1} = (1+e^Z)^{-1}|\alpha\rangle$ and apply the Kronecker δ's via eg. $\langle p|..|\alpha\rangle\langle\beta|..|q\rangle\delta_{\alpha\beta} = \langle p|..|q\rangle$, obtaining

$$\begin{aligned}S_{pqrs} =& \frac{\det(1+e^Z)}{\det(1+e^{-\beta H_0})} \times \left[\langle p|(1+e^{x_5})^{-1}e^{x_4}|q\rangle\ \langle r|e^{-x_3}e^{-x_4}(1+e^{x_5})^{-1}e^{x_4}e^{x_3}e^{x_2}|s\rangle\right. \\ &\left. + \langle p|(1+e^{x_5})^{-1}e^{x_4}e^{x_3}e^{x_2}|s\rangle\ \langle r|e^{-x_3}e^{-x_4}e^{x_6}(1+e^{x_5})^{-1}e^{x_4}|q\rangle\right]\end{aligned} \tag{D.5}$$

Eq. (D.5) becomes more physical upon introducing $U_{mn} = e^{x_4}e^{x_3}e^{x_2} = e^{-ih_n\tau}e^{ihs}e^{ih_m t}$ and $U_0 = e^{i(\tau-t-s)h}$, which are Keldysh propagators with and without core holes. Additionally, we rewrite $e^{-\beta h_0} = N/(1-N)$ in terms of occupation operators. Then we have $(1+e^{x_5})^{-1} = (1-N)(1-N+U_{mn}U_0N)^{-1} = (1-N)F^{-1}$, where $F = 1-N+U_{mn}U_0N$ gives the overlap of core-hole and core-hole-less propagation of initially occupied states. The ratio of determinants comes out to $\det(1+e^z)/\det(1+e^{-\beta h}) = \det(F)$ and we obtain, after restoring $p = n,\rho; q = n,\sigma; r = m,\mu; s = m,\nu$,

$$\begin{aligned}S^{mn}_{\rho\sigma\mu\nu} = \det(F)&\left[\langle n\rho|(1-N)F^{-1}e^{-ih_n\tau}|n\sigma\rangle\ \langle m\mu|e^{-ihs}e^{ih_n\tau}(1-N)F^{-1}U_{mn}|m\nu\rangle\right. \\ &\left. + \langle n\rho|(1-N)F^{-1}U_{mn}|m\nu\rangle\ \langle m\mu|e^{ih_m t}U_0NF^{-1}e^{-ih_n\tau}|n\sigma\rangle\right].\end{aligned} \tag{D.6}$$

So far this all pertains to the full Hilbert space of spin-orbitals. If H contains no spin-

flip terms $S^{mn}_{\rho\sigma\mu\nu}$ simplifies. The Fermi sea term $\det F$ factorizes as $\det F_\uparrow \det F_\downarrow$. Spin flip processes have $\sigma = \bar{\rho}$ and $\mu = \bar{\nu}$, whence the term $\langle n\rho| \ldots |n\sigma\rangle$ vanishes. Thus all matrices need pertain only to spinless Hilbert space, not the spin-doubled Hilbert space.

$$S^{\text{cons}}_{mn} = \det(F_\uparrow F_\downarrow) \sum_\sigma \langle n|(1 - N_{\bar{\sigma}}) F^{-1}_{\bar{\sigma}} U^{\bar{\sigma}}_{mn}|m\rangle \langle m|e^{iH^\sigma_m t} U^\sigma_0 N_\sigma F^{-1}_\sigma e^{-iH^\sigma_n \tau}|n\rangle \qquad \text{(D.7)}$$

for the non-spin-flip intensity and

$$\begin{aligned} S^{\text{flip}}_{mn} = \det(F_\uparrow F_\downarrow) \Bigg\{ & \sum_\sigma \langle n|(1 - N_\sigma) F^{-1}_\sigma U^\sigma_{mn}|m\rangle \ \langle m|e^{iH^\sigma_m t} U^\sigma_0 N_\sigma F^{-1}_\sigma e^{-iH^\sigma_n \tau}|n\rangle \\ & + \sum_{\sigma,\sigma'} \langle n|(1 - N_{\sigma'}) F^{-1}_{\sigma'} e^{-iH^{\sigma'}_n \tau}|n\rangle \ \langle m|e^{iH^\sigma_m t} U^\sigma_0 N_\sigma F^{-1}_\sigma e^{-iH^\sigma_n \tau}|m\rangle \Bigg\} \end{aligned} \qquad \text{(D.8)}$$

for the spin-conserving intensity. These formula suffice to handle Hamiltonians with no spin-flip interactions but in which there is a spin-dependent external potential. If H_0 is entirely spin-independent the sums $\sum_\sigma$ and $\sum_{\sigma,\sigma'}$ reduce to factors of 2 and 4.

E

Explicit Derivation of Spin-Orbit Effects

Here we provide an explicit derivation of the separation of RIXS scattered intensity into spin-flip and spin-conserving channels due to spin-orbit coupling a the $2p$ core hole. For earlier discussions see Refs. [7], [8], and [45]. We calculate the polarization dependence of the two channels and verify that experiments with grazing-exit geometry afford a very clean separation. In doing so, we justify the form of dipole transition operators $T/T^{\dagger}$ discussed in the text.

In the electric dipole approximation, matrix elements for light of polarization $\hat{\varepsilon}$ to cause an electronic transition from state $|\psi_i, \sigma_i\rangle$ to $|\psi_f, \sigma_f\rangle$ is

$$\hat{\varepsilon} \cdot \langle \psi_f | \mathbf{r} | \psi_i \rangle \delta_{\sigma_i, \sigma_f}. \tag{E.1}$$

At the cuprate $L3$ edge we are interested in $|\psi_i\rangle = |2p; m = -1, 0, 1\rangle$ and $|\psi_f\rangle = |3d_{x^2-y^2}\rangle$. Dipole matrix elements are most easily evaluated in the $\{p_x, p_y, p_z\}$ basis, where by basic parity considerations we can easily see that the only non-zero matrix elements are

$$\langle 3d_{x^2-y^2} | x | 2p_x \rangle = -\langle 3d_{x^2-y^2} | y | 2p_y \rangle. \tag{E.2}$$

We switch from the $|2p_{x,y,z}\rangle$ basis to the $|m_\ell = -1, 0, 1\rangle$ basis via

$$|m_\ell = 0\rangle = |2p_z\rangle,\ |m_\ell = \pm 1\rangle = \frac{1}{\sqrt{2}} \left(|2p_x\rangle \pm i |2p_y\rangle \right) \tag{E.3}$$

to obtain the dipole matrix elements (up to an overall multiplicative constant)

$$\hat{\eta}_m \equiv \langle 3d_{x^2-y^2} | \mathbf{r} | 2p_m \rangle = \begin{cases} 0 & (m = 0) \\ \frac{1}{\sqrt{2}} \left(\hat{x} \mp i\hat{y} \right) & (m = \pm 1) \end{cases} \tag{E.4}$$

To include the spin-orbit effect, we must be able to translate between the basis $|m_\ell = -1, 0, 1; \sigma = \uparrow, \downarrow\rangle$, which is most convenient for expressing dipole matrix elements, to the basis $|j, m_j\rangle$ of total angular momentum and energy eigenstates. From a Clebsch-

Gordan table we find

$$|3/2, 3/2\rangle = |1, \uparrow\rangle \tag{E.5}$$

$$|3/2, 1/2\rangle = \sqrt{1/3}|1, \downarrow\rangle + \sqrt{2/3}|0, \uparrow\rangle \tag{E.6}$$

$$|3/2, -1/2\rangle = \sqrt{2/3}|0, \downarrow\rangle + \sqrt{1/3}|-1, \uparrow\rangle \tag{E.7}$$

$$|3/2, -3/2\rangle = |-1, \downarrow\rangle. \tag{E.8}$$

We invert this and drop terms from the $|j = 1/2\rangle$ subspace, which are off resonance by ~ 20 eV at the $L3$ edge. This omission of $|j = 1/2\rangle$ terms breaks spin rotational symmetry and allows for spin-flip RIXS. We find for the $|m_\ell = \pm 1\rangle$ states (as seen above, $|m_\ell = 0\rangle$ has vanishing matrix elements)

$$|1, \uparrow\rangle = |3/2, 3/2\rangle \tag{E.9}$$

$$|1, \downarrow\rangle = \sqrt{1/3}|3/2, 1/2\rangle \tag{E.10}$$

$$|-1, \uparrow\rangle = \sqrt{1/3}|3/2, -1/2\rangle \tag{E.11}$$

$$|-1, \downarrow\rangle = |3/2, -3/2\rangle \tag{E.12}$$

The Kramers-Heisenberg amplitude for initial state $|i\rangle$ and final state $|f\rangle$ is

$$A_{i\to f} = \sum_n \frac{\langle f|T_f|n\rangle\langle n|T_i^\dagger|n\rangle}{\omega - E_n + i\Gamma} = \langle f|T_f G T_i^\dagger|i\rangle, \tag{E.13}$$

where $T_i^\dagger$ and T_f are absorption and emission dipole transition operators and $G \equiv (\omega - H + i\Gamma)^{-1}$ is the intermediate state Green function. The transition operators are obtained by adding dipole absorption/emission events for all possible σ, m_ℓ, and core

hole sites $\mathbf{R}$:

$$T_i^\dagger = \sum_{\mathbf{R},m,\sigma} e^{-i\mathbf{q}_i\cdot\mathbf{R}}\hat{\varepsilon}_i \cdot \hat{\eta}_m d^\dagger_{\mathbf{R},\sigma} p_{\mathbf{R},\sigma,m} \tag{E.14}$$

$$T_f = \sum_{\mathbf{R},m,\sigma} e^{i\mathbf{q}_f\cdot\mathbf{R}}\hat{\varepsilon}^*_f \cdot \hat{\eta}^*_m p^\dagger_{\mathbf{R},\sigma,m} d_{\mathbf{R},\sigma}, \tag{E.15}$$

where $\hat{\varepsilon}_{i(f)}$ and $\mathbf{q}_{i(f)}$ are incident (final) polarizations and photon momenta. Writing this in terms of spin-orbit eigenstates and dropping off-resonance $|j = 1/2\rangle$ terms as shown above gives

$$\begin{aligned} T_i^\dagger =& \sum_{\mathbf{R}} e^{-i\mathbf{q}_i\cdot\mathbf{R}}\hat{\varepsilon}_i \left[\hat{\eta}_1 \left(d^\dagger_{\mathbf{R},\uparrow} p_{\mathbf{R},m_j=3/2} + \sqrt{1/3} d^\dagger_{\mathbf{R},\downarrow} p_{\mathbf{R},m_j=1/2}\right)\right. \\ &\left. + \hat{\eta}_{-1} \left(d^\dagger_{\mathbf{R},\downarrow} p_{\mathbf{R},m_j=-3/2} + \sqrt{1/3} d^\dagger_{\mathbf{R},\uparrow} p_{\mathbf{R},m_j=-1/2}\right)\right] \end{aligned} \tag{E.16}$$

$$\begin{aligned} T_f =& \sum_{\mathbf{R}} e^{i\mathbf{q}_f\cdot\mathbf{R}}\hat{\varepsilon}^*_f \left[\hat{\eta}^*_1 \left(d^\dagger_{\mathbf{R},\uparrow} p_{\mathbf{R},m_j=3/2} + \sqrt{1/3} d^\dagger_{\mathbf{R},\downarrow} p_{\mathbf{R},m_j=1/2}\right)\right. \\ &\left. + \hat{\eta}^*_{-1} \left(d^\dagger_{\mathbf{R},\downarrow} p_{\mathbf{R},m_j=-3/2} + \sqrt{1/3} d^\dagger_{\mathbf{R},\uparrow} p_{\mathbf{R},m_j=-1/2}\right)\right]. \end{aligned} \tag{E.17}$$

Finally, since the spin orbit states labelled by $\{\mathbf{R}, j, m_j\}$ are eigenstates of H, each term in $T_i^\dagger$ must be matched with the corresponding term in T_f. That is, the only terms in $T_f G T_i^\dagger$ that give a non-vanishing contribution to the Kramers-Heisenberg matrix element are those in which T_f and $T_i^\dagger$ carry the same quantum numbers $\mathbf{R}$, j (which we have already enforced by projecting into a single resonant subspace), and m_j. Thus we obtain

$$A_{i\to f} = \sum_{\mathbf{R}} e^{i\Delta\mathbf{q}\cdot\mathbf{R}} \chi_{\alpha,\beta} \langle f | d_{\mathbf{R},\alpha} G d^\dagger_{\mathbf{R},\beta} | i\rangle, \tag{E.18}$$

where

$$\chi_{\uparrow,\uparrow} = \chi^*_{\downarrow,\downarrow} = (\hat{\varepsilon_f} \cdot \hat{\eta}_1)^* (\hat{\varepsilon_i} \cdot \hat{\eta}_1) + (1/3)(\hat{\varepsilon_f} \cdot \hat{\eta}_{-1})^* (\hat{\varepsilon_i} \cdot \hat{\eta}_{-1}) \tag{E.19}$$

$$\chi_{\uparrow,\downarrow} = \chi_{\downarrow,\uparrow} = 0. \tag{E.20}$$

That $\chi_{\uparrow,\uparrow} = \chi^*_{\downarrow,\downarrow}$ follows from $\hat{\eta}_1 = \hat{\eta}^*_{-1}$.

To separate the spin and charge channels, we decompose χ into symmetric and antisymmetric parts: $\chi = \chi_S + \chi_A$, where

$$\chi_S = (\chi + \chi^*)/2 \tag{E.21}$$

$$\chi_A = (\chi - \chi^*)/2. \tag{E.22}$$

Then, in the basis of $\hat{S}_z$ eigenstates $|\uparrow,\downarrow\rangle$, where $\hat{z}$ is perpendicular to the copper-oxide plane, we have

$$(\chi_S)_{\uparrow,\uparrow} = (\chi_S)_{\downarrow,\downarrow} = (2/3)\left(\hat{\varepsilon}^*_f \cdot \hat{\varepsilon}_i - \varepsilon^*_{f,z}\varepsilon_{i,z}\right) \qquad \equiv \chi_S \tag{E.23}$$

$$(\chi_A)_{\uparrow,\uparrow} = -(\chi_A)_{\downarrow,\downarrow} = -(i/3)\hat{\varepsilon}^*_f \cdot (\hat{z} \times \hat{\varepsilon}_i) \qquad \equiv \chi_A \tag{E.24}$$

With respect to the basis of eigenstates of $\hat{S}_x$, obtained via the transformations $|\uparrow\rangle \rightarrow (1/\sqrt{2})(|\uparrow\rangle + |\downarrow\rangle)$ and $|\downarrow\rangle \rightarrow (1/\sqrt{2})(|\uparrow\rangle - |\downarrow\rangle)$, the symmetric amplitude transforms trivially:

$$\chi_S d_\uparrow G d^\dagger_\uparrow + \chi_S d_\downarrow G d^\dagger_\downarrow \rightarrow \chi_S \left(d_\uparrow G d^\dagger_\uparrow + d_\downarrow G d^\dagger_\downarrow\right). \tag{E.25}$$

An isotropic contribution can't represent a spin flip in any basis. The antisymmetric

contribution, however, transforms as

$$\chi_A d_\uparrow G d_\uparrow^\dagger - \chi_A d_\downarrow G d_\downarrow^\dagger \to \chi_A \left(d_\uparrow G d_\downarrow^\dagger + d_\downarrow G d_\uparrow^\dagger \right), \tag{E.26}$$

a pure spin flip in the basis oriented parallel to the copper-oxide planes. Now we need to compare the prefactors $|\chi_{S(A)}|^2$ to obtain the relative intensities of spin-flip and non-spin-flip scattering processes.

For experimental geometry where incident and scattered radiation make angles ϕ_1 and ϕ_2 with $\hat{z}$ polarization vectors are $\hat{\varepsilon}_i = \hat{\varepsilon}_f = \hat{y}$ for σ polarization (WLOG) and $\hat{\varepsilon}_i = \cos\phi_1 \hat{x} + \sin\phi_1 \hat{z}$, $\hat{\varepsilon}_f = \cos\phi_2 \hat{x} + \sin\phi_2 \hat{z}$ for π polarization. Then we can calculate χ_S and χ_A for all pairs of incident and emitted polarizations:

$\hat{\varepsilon}_i$	$\hat{\varepsilon}_f$	χ_S	χ_A
σ	σ	$2/3$	0
σ	π	0	$(i/3)\cos\phi_2$
π	π	$(2/3)\cos\phi_1\cos\phi_2$	0
π	σ	0	$-(i/3)\cos\phi_1$

(E.27)

For unpolarized scattered radiation we average intensity over scattered polarizations:

$\hat{\varepsilon}_i$	$\langle\lvert\chi_S\rvert^2\rangle$	$\langle\lvert\chi_A\rvert^2\rangle$
σ	$2/9$	$(1/18)\cos^2\phi_2$
π	$(2/9)\cos^2\phi_1\cos^2\phi_2$	$(1/18)\cos^2\phi_1$

(E.28)

Fortunately, the prefactors $|\chi_S(\hat{\varepsilon}_i, \hat{\varepsilon}_f)|^2$ and $|\chi_A(\hat{\varepsilon}_i, \hat{\varepsilon}_f)|^2$ depend only on the polarizations and as such do not affect the lineshape of intensity vs. momentum transfer and energy transfer. The only effect of the experimental geometry is to adjust an overall

ratio between spin-flip and non-spin-flip intensities. This means that we can write

$$I_{\sigma}^{\text{total}} = |\chi_{S,\sigma}|^2 I^{\text{NSF}} + |\chi_{A,\sigma}|^2 I^{\text{SF}} \tag{E.29}$$

$$I_{\pi}^{\text{total}} = |\chi_{S,\pi}|^2 I^{\text{NSF}} + |\chi_{A,\pi}|^2 I^{\text{SF}}. \tag{E.30}$$

Even without resolving the polarization of scattered radiation, the charge and spin channels can, in principle, be separated by solving a 2×2 linear equation. Ideally, however, one could simply choose geometries where $\langle |\chi_S|^2 \rangle$ is much larger than $\langle |\chi_A|^2 \rangle$ and vice versa.

We consider the experiments of Refs. [26] and [64], with grazing exit geometry. For concreteness we use values from Ref.[26]: $\phi_i = -25.6°$ and $\phi_f = 76.6°$ (the minus sign denotes that incident and scattered radiation are on the same side of the normal in the scattering plane). For this geometry, averaging over final states we get

$$\begin{array}{ccc} \hat{\varepsilon}_i & \langle |\chi_S|^2 \rangle & \langle |\chi_A|^2 \rangle \\ \sigma & 0.22 & 0.003 \\ \pi & 0.010 & 0.045 \end{array} . \tag{E.31}$$

Thus the two polarizations of incident radiation in an experiment with grazing exit geometry offer a fairly clean separation between spin-flip and spin-conserving cross sections.

References

[1] Abanin, D. & Levitov, L. (2004). Tunable Fermi-Edge Resonance in an Open Quantum Dot. *Physical Review Letters*, 93(12), 126802.

[2] Abanin, D. & Levitov, L. (2005). Fermi-Edge Resonance and Tunneling in Nonequilibrium Electron Gas. *Physical Review Letters*, 94(18), 186803.

[3] Abbamonte, P., Blumberg, G., Rusydi, A., Gozar, A., Evans, P. G., Siegrist, T., Venema, L., Eisaki, H., Isaacs, E. D., & Sawatzky, G. A. (2004). Crystallization of charge holes in the spin ladder of $Sr_{14}Cu_{24}O_{41}$. *Nature*, 431(7012), 1078–81.

[4] Abbamonte, P., Demler, E., Davis, J. C. S., Campuzano, J.-C., & Séamus Davis, J. (2011). Resonant soft X-ray scattering, stripe order, and the electron spectral function in cuprates. *Physica C: Superconductivity*, 481(5), 15–22.

[5] Abbamonte, P., Rusydi, A., Smadici, S., Gu, G. D., Sawatzky, G. A., & Feng, D. L. (2005). Spatially modulated 'Mottness' in $La_{2-x}Ba_xCuO_4$. *Nature Physics*, 1(3), 155–158.

[6] Abbamonte, P., Venema, L., Rusydi, A., Sawatzky, G. A., Logvenov, G., & Bozovic, I. (2002). A structural probe of the doped holes in cuprate superconductors. *Science (New York, N.Y.)*, 297(5581), 581–4.

[7] Ament, L., Ghiringhelli, G., Sala, M., Braicovich, L., & van den Brink, J. (2009). Theoretical Demonstration of How the Dispersion of Magnetic Excitations in Cuprate Compounds can be Determined Using Resonant Inelastic X-Ray Scattering. *Physical Review Letters*, 103(11), 117003.

[8] Ament, L., van Veenendaal, M., Devereaux, T., Hill, J., & van den Brink, J. (2011). Resonant inelastic x-ray scattering studies of elementary excitations. *Reviews of Modern Physics*, 83(2), 705–767.

[9] Andersen, O., Liechtenstein, A., Rodriguez, O., Mazin, I., Jepsen, O., Antropov, V., Gunnarsson, O., & Gopalan, S. (1991). Electrons, phonons, and their interaction in $YBa_2Cu_3O_7$. *Physica C: Superconductivity*, 185-189(null), 147–155.

[10] Anderson, P. (1967). Infrared Catastrophe in Fermi Gases with Local Scattering Potentials. *Physical Review Letters*, 18(24), 1049–1051.

[11] Baeriswyl, D., Eichenberger, D., & Menteshashvili, M. (2009). Variational ground states of the two-dimensional Hubbard model. *New Journal of Physics*, 11(7), 075010.

[12] Benjamin, D., Abanin, D., Abbamonte, P., & Demler, E. (2013). Microscopic Theory of Resonant Soft-X-Ray Scattering in Materials with Charge Order: The Example of Charge Stripes in High-Temperature Cuprate Superconductors. *Physical Review Letters*, 110(13), 137002.

[13] Benjamin, D., Klich, I., & Demler, E. (2014). Single-Band Model of Resonant Inelastic X-Ray Scattering by Quasiparticles in High-T_c Cuprates. *Physical Review Letters*, 112(24), 247002.

[14] Berg, E., Fradkin, E., Kivelson, S. A., & Tranquada, J. M. (2009). Striped superconductors: how spin, charge and superconducting orders intertwine in the cuprates. *New Journal of Physics*, 11(11), 115004.

[15] Best, T., Will, S., Schneider, U., Hackermüller, L., van Oosten, D., Bloch, I., & Lühmann, D.-S. (2009). Role of Interactions in ^{87}Rb-^{40}K Bose-Fermi Mixtures in a 3D Optical Lattice. *Phys. Rev. Lett.*, 102(3), 30408.

[16] Bogolubov, N. N. & Jr, N. N. B. (2009). *Introduction to Quantum Statistical Mechanics*. World Scientific Publishing Company.

[17] Buonsante, P., Giampaolo, S. M., Illuminati, F., Penna, V., & Vezzani, A. (2008). Mixtures of Strongly Interacting Bosons in Optical Lattices. *Phys. Rev. Lett.*, 100(24), 240402.

[18] Campuzano, J. C., Norman, M. R., & Randeria, M. (2004). *Physics of Superconductors Vol. II*. Springer.

[19] Capogrosso-Sansone, B., Prokof'ev, N., & Svistunov, B. (2007). Phase diagram and thermodynamics of the three-dimensional Bose-Hubbard model. *Physical Review B*, 75(13), 134302.

[20] Catani, J., De Sarlo, L., Barontini, G., Minardi, F., & Inguscio, M. (2008). Degenerate Bose-Bose mixture in a three-dimensional optical lattice. *Phys. Rev. A*, 77(1), 11603.

[21] Chakravarty, S., Laughlin, R., Morr, D., & Nayak, C. (2001). Hidden order in the cuprates. *Physical Review B*, 63(9).

[22] Chen, C.-C., Moritz, B., Vernay, F., Hancock, J. N., Johnston, S., Jia, C. J., Chabot-Couture, G., Greven, M., Elfimov, I., Sawatzky, G. A., & Devereaux, T. P. (2010). Unraveling the Nature of Charge Excitations in La_2CuO_4 with Momentum-Resolved Cu K-Edge Resonant Inelastic X-Ray Scattering. *Physical Review Letters*, 105(17), 177401.

[23] Combescot, M. & Nozières, P. (1971). Infrared catastrophy and excitons in the X-ray spectra of metals. *Journal de Physique*, 32, 913–929.

[24] Damascelli, A. & Shen, Z.-X. (2003). Angle-resolved photoemission studies of the cuprate superconductors. *Reviews of Modern Physics*, 75(2), 473–541.

[25] Davis, J. C. S. & Lee, D.-H. (2013). Concepts relating magnetic interactions, intertwined electronic orders, and strongly correlated superconductivity. *Proceedings of the National Academy of Sciences of the United States of America*, 110(44), 17623–30.

[26] Dean, M. & Dellea, G. (2013). Persistence of magnetic excitations in La2-xSrxCuO4 from the undoped insulator to the heavily overdoped non-superconducting metal. *Nature Materials*, 12, 1019.

[27] Dean, M. P. M., James, A. J. A., Springell, R. S., Liu, X., Monney, C., Zhou, K. J., Konik, R. M., Wen, J. S., Xu, Z. J., Gu, G. D., Strocov, V. N., Schmitt, T., & Hill, J. P. (2013). High-Energy Magnetic Excitations in the Cuprate Superconductor $Bi_2Sr_2CaCu_2O_{8+\delta}$: Towards a Unified Description of Its Electronic and Magnetic Degrees of Freedom. *Physical Review Letters*, 110(14), 147001.

[28] Dean, M. P. M., Springell, R. S., Monney, C., Zhou, K. J., Pereiro, J., Božović, I., Dalla Piazza, B., Rønnow, H. M., Morenzoni, E., van den Brink, J., Schmitt, T., & Hill, J. P. (2012). Spin excitations in a single La_2CuO_4 layer. *Nature materials*, 11(10), 850–4.

[29] Deng, X., Mravlje, J., Žitko, R., Ferrero, M., Kotliar, G., & Georges, A. (2013). How Bad Metals Turn Good: Spectroscopic Signatures of Resilient Quasiparticles. *Physical Review Letters*, 110(8), 086401.

[30] Dhesi, S., Mirone, A., De Nadaï, C., Ohresser, P., Bencok, P., Brookes, N., Reutler, P., Revcolevschi, A., Tagliaferri, A., Toulemonde, O., & van der Laan, G. (2004). Unraveling Orbital Ordering in $La_0.5Sr_1.5MnO_4$. *Physical Review Letters*, 92(5), 056403.

[31] Doiron-Leyraud, N., Proust, C., LeBoeuf, D., Levallois, J., Bonnemaison, J.-B., Liang, R., Bonn, D. A., Hardy, W. N., & Taillefer, L. (2007). Quantum oscillations and the Fermi surface in an underdoped high-Tc superconductor. *Nature*, 447(7144), 565–8.

[32] Fink, J., Schierle, E., Weschke, E., Geck, J., Hawthorn, D., Soltwisch, V., Wadati, H., Wu, H.-H., Dürr, H., Wizent, N., Büchner, B., & Sawatzky, G. (2009). Charge ordering in $La_{1.8x}Eu_0.2Sr_xCuO_4$ studied by resonant soft x-ray diffraction. *Physical Review B*, 79(10), 100502.

[33] Fischer, O., Kugler, M., Maggio-Aprile, I., Berthod, C., & Renner, C. (2007). Scanning tunneling spectroscopy of high-temperature superconductors. *Reviews of Modern Physics*, 79(1), 353–419.

[34] Fisher, M. P. A., Weichman, P. B., Grinstein, G., & Fisher, D. S. (1989). Boson localization and the superfluid-insulator transition. *Phys. Rev. B*, 40(1), 546–570.

[35] Fradkin, E., Kivelson, S. A., & Tranquada, J. M. (2014). Theory of Intertwined Orders in High Temperature Superconductors. cond-mat.supr-con/1407.4480.

[36] Freericks, J. & Monien, H. (1996). Strong-coupling expansions for the pure and disordered Bose-Hubbard model. *Physical Review B*, 53(5), 2691–2700.

[37] Gadway, B., Pertot, D., Reimann, R., & Schneble, D. (2010). Superfluidity of Interacting Bosonic Mixtures in Optical Lattices. *Phys. Rev. Lett.*, 105(4), 45303.

[38] Ghiringhelli, G., Tacon, M. L., Minola, M., Blanco-Canosa, S., Mazzoli, C., Brookes, N. B., De Luca, G. M., Frano, A., Hawthorn, D. G., He, F., Loew, T., Sala, M. M., Peets, D. C., Salluzzo, M., Schierle, E., Sutarto, R., Sawatzky, G. A., Weschke, E., Keimer, B., & Braicovich, L. (2012). Long-range incommensurate charge fluctuations in $(Y,Nd)Ba_2Cu_3O_{6+x}$.

[39] Girardeau, M. & Arnowitt, R. (1959). Theory of Many-Boson Systems: Pair Theory. *Physical Review*, 113(3), 755–761.

[40] Greiner, M., Mandel, O., Esslinger, T., Hansch, T. W., & Bloch, I. (2002). Quantum phase transition from a superfluid to a mott insulator in a gas of ultracold atoms. *Nature*, 415(6867), 39–44.

[41] Grenier, S., Hill, J., Gibbs, D., Thomas, K., Zimmermann, M., Nelson, C., Kiryukhin, V., Tokura, Y., Tomioka, Y., Casa, D., Gog, T., & Venkataraman, C. (2004). Resonant x-ray diffraction of the magnetoresistant perovskite $Pr_{0.6}Ca_{0.4}MnO_3$. *Physical Review B*, 69(13), 134419.

[42] Guglielmino, M., Penna, V., & Capogrosso-Sansone, B. (2010). Mott insulator-superfluid transition in Bose-Bose mixtures in a two-dimensional lattice. *Phys. Rev. A*, 82(2), 21601.

[43] Günter, K., Stöferle, T., Moritz, H., Köhl, M., & Esslinger, T. (2006). Bose-Fermi Mixtures in a Three-Dimensional Optical Lattice. *Phys. Rev. Lett.*, 96(18), 180402.

[44] Hackl, A., Vojta, M., & Sachdev, S. (2010). Quasiparticle Nernst effect in stripe-ordered cuprates. *Physical Review B*, 81(4), 045102.

[45] Haverkort, M. (2010). Theory of Resonant Inelastic X-Ray Scattering by Collective Magnetic Excitations. *Physical Review Letters*, 105(16), 167404.

[46] Herrero-Martín, J., García, J., Subías, G., Blasco, J., Sánchez, M., & Stanescu, S. (2006). Double stripe ordering in $Nd_{0.5}Sr_{0.5}MnO_3$ determined by resonant soft x-ray scattering. *Physical Review B*, 73(22), 224407.

[47] Hill, J., Blumberg, G., Kim, Y.-J., Ellis, D., Wakimoto, S., Birgeneau, R., Komiya, S., Ando, Y., Liang, B., Greene, R., Casa, D., & Gog, T. (2008). Observation of a 500 meV Collective Mode in $La_{2-x}Sr_xCuO_4$ and Nd_2CuO_4 Using Resonant Inelastic X-Ray Scattering. *Physical Review Letters*, 100(9), 097001.

[48] Hoffman, J. E., Hudson, E. W., Lang, K. M., Madhavan, V., Eisaki, H., Uchida, S., & Davis, J. C. (2002). A four unit cell periodic pattern of quasi-particle states surrounding vortex cores in $Bi_2Sr_2CaCu_2O_{8+\delta}$. *Science (New York, N.Y.)*, 295(5554), 466–9.

[49] Howald, C., Eisaki, H., Kaneko, N., Greven, M., & Kapitulnik, A. (2003). Periodic density-of-states modulations in superconducting $Bi_2Sr_2CaCu_2O_{8+\delta}$. *Phys. Rev. B*, 67(1), 14533.

[50] Hüfner, S. (2003). *Photoelectron Spectroscopy: Principles and Applications*. Springer.

[51] Ino, A., Kim, C., Nakamura, M., Yoshida, T., Mizokawa, T., Fujimori, A., Shen, Z.-X., Kakeshita, T., Eisaki, H., & Uchida, S. (2002). Doping-dependent evolution of the electronic structure of $La_{2-x}Sr_xCuO_4$ in the superconducting and metallic phases. *Physical Review B*, 65(9), 094504.

[52] Iskin, M. & Freericks, J. (2009). Strong-coupling perturbation theory for the extended Bose-Hubbard model. *Physical Review A*, 79(5), 053634.

[53] J. Birgeneau, R., Stock, C., M. Tranquada, J., & Yamada, K. (2006). Magnetic Neutron Scattering in Hole-Doped Cuprate Superconductors. *Journal of the Physical Society of Japan*, 75(11), 111003.

[54] Jia, C. J., Nowadnick, E. A., Wohlfeld, K., Chen, C. C., Johnston, S., Tohyama, T., Moritz, B., & Devereaux, T. P. (2013). Persistent spin excitations in doped antiferromagnets revealed by resonant inelastic light scattering.

[55] Kivelson, S. A., Bindloss, I. P., Oganesyan, V., Tranquada, J. M., Kapitulnik, A., & Howald, C. (2003). How to detect fluctuating stripes in the high-temperature superconductors. *Reviews of Modern Physics*, 75(4), 1201–1241.

[56] Kivelson, S. A., Fradkin, E., & Emery, V. J. (1998). Electronic liquid-crystal phases of a doped Mott insulator. 393(6685), 550–553.

[57] Klich, I. (2003). Quantum Noise in Mesoscopic Physics. In Y. Nazarov (Ed.), *Quantum Noise in Mesoscopic Physics*. Springer.

[58] Klich, I. (2014). A note on the Full Counting Statistics of paired fermions. cond-mat.mes-hall/1403.7824.

[59] Knap, M., Shashi, A., Nishida, Y., Imambekov, A., Abanin, D. A., & Demler, E. (2012). Time-Dependent Impurity in Ultracold Fermions: Orthogonality Catastrophe and Beyond. *Physical Review X*, 2(4), 041020.

[60] Kotani, A. & Shin, S. (2001). Resonant inelastic x-ray scattering spectra for electrons in solids. *Reviews of Modern Physics*, 73(1), 203–246.

[61] Lamacraft, A. (2009). Dispersion relation and spectral function of an impurity in a one-dimensional quantum liquid. *Physical Review B*, 79(24), 241105.

[62] Lang, I. G. & Firsov, Y. A. (1962). Kinetic theory of semiconductors with low mobility. *Zh. Eksp. Teor. Fiz.*, 43, 1843.

[63] Le Tacon, M., Ghiringhelli, G., Chaloupka, J., Sala, M. M., Hinkov, V., Haverkort, M. W., Minola, M., Bakr, M., Zhou, K. J., Blanco-Canosa, S., Monney, C., Song, Y. T., Sun, G. L., Lin, C. T., De Luca, G. M., Salluzzo, M., Khaliullin, G., Schmitt, T., Braicovich, L., & Keimer, B. (2011). Intense paramagnon excitations in a large family of high-temperature superconductors. *Nature Physics*, 7(9), 725–730.

[64] Le Tacon, M., Minola, M., Peets, D. C., Moretti Sala, M., Blanco-Canosa, S., Hinkov, V., Liang, R., Bonn, D. A., Hardy, W. N., Lin, C. T., Schmitt, T., Braicovich, L., Ghiringhelli, G., & Keimer, B. (2013). Dispersive spin excitations in highly overdoped cuprates revealed by resonant inelastic x-ray scattering. *Physical Review B*, 88(2), 020501.

[65] LeBoeuf, D., Doiron-Leyraud, N., Levallois, J., Daou, R., Bonnemaison, J.-B., Hussey, N. E., Balicas, L., Ramshaw, B. J., Liang, R., Bonn, D. A., Hardy, W. N., Adachi, S., Proust, C., & Taillefer, L. (2007). Electron pockets in the Fermi surface of hole-doped high-Tc superconductors. *Nature*, 450(7169), 533–6.

[66] Li, J.-X., Wu, C.-Q., & Lee, D.-H. (2006). Checkerboard charge density wave and pseudogap of high-Tc cuprate. *Physical Review B*, 74(18), 184515.

[67] Lu, D., Vishik, I. M., Yi, M., Chen, Y., Moore, R. G., & Shen, Z.-X. (2012). Angle-Resolved Photoemission Studies of Quantum Materials. *Annual Review of Condensed Matter Physics*, 3(1), 129–167.

[68] Mahan, G. (1967). Excitons in Metals: Infinite Hole Mass. *Physical Review*, 163(3), 612–617.

[69] Markiewicz, R. S., Sahrakorpi, S., Lindroos, M., Lin, H., & Bansil, A. (2005). One-band tight-binding model parametrization of the high- T_c cuprates including the effect of k_z dispersion. *Physical Review B*, 72(5), 054519.

[70] Marra, P., Sykora, S., Wohlfeld, K., & van den Brink, J. (2013). Resonant Inelastic X-Ray Scattering as a Probe of the Phase and Excitations of the Order Parameter of Superconductors. *Physical Review Letters*, 110(11), 117005.

[71] Martin, I., Ortiz, G., Balatsky, A. V., & Bishop, A. R. (2000). Competing quantum orderings in cuprate superconductors: a minimal model. *International Journal of Modern Physics B*, 14(29), 3567–3576.

[72] McElroy, K., Lee, D.-H., Hoffman, J. E., Lang, K. M., Lee, J., Hudson, E. W., Eisaki, H., Uchida, S., & Davis, J. C. (2005). Coincidence of Checkerboard Charge Order and Antinodal State Decoherence in Strongly Underdoped Superconducting $Bi_2Sr_2CaCu_2O_{8+\delta}$. *Phys. Rev. Lett.*, 94(19), 197005.

[73] Millis, A. & Norman, M. (2007). Antiphase stripe order as the origin of electron pockets observed in 1/8-hole-doped cuprates. *Physical Review B*, 76(22), 220503.

[74] Muzykantskii, B., D'Ambrumenil, N., & Braunecker, B. (2003). Fermi-Edge Singularity in a Nonequilibrium System. *Physical Review Letters*, 91(26), 266602.

[75] Nazarenko, E., Lorenzo, J. E., Joly, Y., Hodeau, J. L., Mannix, D., & Marin, C. (2006). Resonant X-Ray Diffraction Studies on the Charge Ordering in Magnetite. *Physical Review Letters*, 97(5), 056403.

[76] Norman, M. R., Ding, H., Randeria, M., Campuzano, J. C., Yokoya, T., Takeuchi, T., Takahashi, T., Mochiku, T., Kadowaki, K., Guptasarma, P., & Hinks, D. G. (1998). Destruction of the Fermi surface in underdoped high-Tc superconductors. *Nature*, 392(6672), 157–160.

[77] Norman, M. R., Pines, D., & Kallin, C. (2005). The pseudogap: friend or foe of high Tc? *Advances in Physics*, 54(8), 715–733.

[78] Nozières, P. & Abrahams, E. (1974). Threshold singularities of the x-ray Raman scattering in metals. *Physical Review B*, 10(8), 3099–3112.

[79] Nozières, P. & de Dominicis, C. (1969). Singularities in the X-Ray Absorption and Emission of Metals. III. One-Body Theory Exact Solution. *Physical Review*, 178(3), 1097–1107.

[80] Ospelkaus, C., Ospelkaus, S., Sengstock, K., & Bongs, K. (2006). Interaction-Driven Dynamics of ^{40}K-^{87}Rb Fermion-Boson Gas Mixtures in the Large-Particle-Number Limit. *Phys. Rev. Lett.*, 96(2), 20401.

[81] Peets, D. C., Hawthorn, D. G., Shen, K. M., Kim, Y.-J., Ellis, D. S., Zhang, H., Komiya, S., Ando, Y., Sawatzky, G. A., Liang, R., Bonn, D. A., & Hardy, W. N. (2009). X-Ray Absorption Spectra Reveal the Inapplicability of the Single-Band Hubbard Model to Overdoped Cuprate Superconductors. *Physical Review Letters*, 103(8), 087402.

[82] Peets, D. C., Mottershead, J. D. F., Wu, B., Elfimov, I. S., Liang, R., Hardy, W. N., Bonn, D. A., Raudsepp, M., Ingle, N. J. C., & Damascelli, A. (2007). $Tl_2Ba_2CuO_{6+\delta}$ brings spectroscopic probes deep into the overdoped regime of the high- Tc cuprates. *New Journal of Physics*, 9(2), 28–28.

[83] Podolsky, D., Demler, E., Damle, K., & Halperin, B. (2003). Translational symmetry breaking in the superconducting state of the cuprates: Analysis of the quasiparticle density of states. *Physical Review B*, 67(9), 094514.

[84] Rohlfing, M. & Louie, S. (1998). Excitonic Effects and the Optical Absorption Spectrum of Hydrogenated Si Clusters. *Physical Review Letters*, 80(15), 3320–3323.

[85] Rosch, A. (1999). Quantum-coherent transport of a heavy particle in a fermionic bath. *Advances in Physics*, 48(3), 295–394.

[86] Sachdev, S. (2000). Quantum Criticality: Competing Ground States in Low Dimensions. *Science*, 288(5465), 475–480.

[87] Sachdev, S. (2003). Colloquium: Order and quantum phase transitions in the cuprate superconductors. *Reviews of Modern Physics*, 75(3), 913–932.

[88] Scalapino, D. & Sugar, R. (1981). Method for Performing Monte Carlo Calculations for Systems with Fermions. *Physical Review Letters*, 46(8), 519–521.

[89] Scalapino, D. J. (2012). A common thread: The pairing interaction for unconventional superconductors. *Reviews of Modern Physics*, 84(4), 1383–1417.

[90] Scalettar, R., Scalapino, D., & Sugar, R. (1986). New algorithm for the numerical simulation of fermions. *Physical Review B*, 34(11), 7911–7917.

[91] Schulz, H. (1990). Incommensurate antiferromagnetism in the two-dimensional Hubbard model. *Physical Review Letters*, 64(12), 1445–1448.

[92] Schüßler-Langeheine, C., Schlappa, J., Tanaka, A., Hu, Z., Chang, C., Schierle, E., Benomar, M., Ott, H., Weschke, E., Kaindl, G., Friedt, O., Sawatzky, G., Lin, H.-J., Chen, C., Braden, M., & Tjeng, L. (2005). Spectroscopy of Stripe Order in $La_{1.8}Sr_{0.2}NiO_4$ Using Resonant Soft X-Ray Diffraction. *Physical Review Letters*, 95(15), 156402.

[93] Sedrakyan, T. A. & Chubukov, A. V. (2010). Pseudogap in underdoped cuprates and spin-density-wave fluctuations. *Physical Review B*, 81(17), 174536.

[94] Shashi, A., Grusdt, F., Abanin, D. A., & Demler, E. (2014). Radio-frequency spectroscopy of polarons in ultracold Bose gases. *Physical Review A*, 89(5), 053617.

[95] Shen, K. M., Ronning, F., Lu, D. H., Baumberger, F., Ingle, N. J. C., Lee, W. S., Meevasana, W., Kohsaka, Y., Azuma, M., Takano, M., Takagi, H., & Shen, Z.-X. (2005). Nodal quasiparticles and antinodal charge ordering in $Ca_{2-x}Na_xCuO_2Cl_2$. *Science (New York, N.Y.)*, 307(5711), 901–4.

[96] Silbey, R. & Harris, R. A. (1984). Variational calculation of the dynamics of a two level system interacting with a bath. *J. Chem. Phys.*, 80(6), 2615.

[97] Smadici, S., Abbamonte, P., Bhattacharya, A., Zhai, X., Jiang, B., Rusydi, A., Eckstein, J., Bader, S., & Zuo, J.-M. (2007a). Electronic Reconstruction at $SrMnO_3$-$LaMnO_3$ Superlattice Interfaces. *Physical Review Letters*, 99(19), 196404.

[98] Smadici, S., Abbamonte, P., Taguchi, M., Kohsaka, Y., Sasagawa, T., Azuma, M., Takano, M., & Takagi, H. (2007b). Absence of long-ranged charge order in $Na_xCa_{2-x}CuO_2Cl_2$ (x=0.08). *Physical Review B*, 75(7), 075104.

[99] Smadici, S., Lee, J., Wang, S., Abbamonte, P., Logvenov, G., Gozar, A., Cavellin, C., & Bozovic, I. (2009). Superconducting Transition at 38 K in Insulating-Overdoped La_2CuO_4-$La_{1.64}Sr_{0.36}CuO_4$ Superlattices: Evidence for Interface Electronic Redistribution from Resonant Soft X-Ray Scattering. *Physical Review Letters*, 102(10), 107004.

[100] Sols, F. & Guinea, F. (1987). Bulk and surface diffusion of heavy particles in metals: A path-integral approach. *Physical Review B*, 36(15), 7775–7785.

[101] Stock, C., Cowley, R. A., Buyers, W. J. L., Frost, C. D., Taylor, J. W., Peets, D., Liang, R., Bonn, D., & Hardy, W. N. (2010). Effect of the pseudogap on suppressing high energy inelastic neutron scattering in superconducting $YBa_2Cu_3O_{6.5}$. *Physical Review B*, 82(17), 174505.

[102] Timusk, T. & Statt, B. (1999). The pseudogap in high-temperature superconductors: an experimental survey. *Reports on Progress in Physics*, 62(1), 61–122.

[103] Tranquada, J. M., Sternlieb, B. J., Axe, J. D., Nakamura, Y., & Uchida, S. (1995). Evidence for stripe correlations of spins and holes in copper oxide superconductors. *Nature*, 375(6532), 561–563.

[104] Tranquada, J. M., Xu, G., & Zaliznyak, I. A. (2014). Superconductivity, antiferromagnetism, and neutron scattering. *Journal of Magnetism and Magnetic Materials*, 350, 148–160.

[105] Tsutsui, K., Tohyama, T., & Maekawa, S. (1999). Momentum Dependence of Resonant Inelastic X-Ray Scattering Spectrum in Insulating Cuprates. *Physical Review Letters*, 83(18), 3705–3708.

[106] Tsutsui, K., Tohyama, T., & Maekawa, S. (2003). Mott Gap Excitations and Resonant Inelastic X-Ray Scattering in Doped Cuprates. *Physical Review Letters*, 91(11).

[107] Valla, T., Fedorov, A. V., Lee, J., Davis, J. C., & Gu, G. D. (2006). The ground state of the pseudogap in cuprate superconductors. *Science (New York, N.Y.)*, 314(5807), 1914–1916.

[108] van den Brink, J. & van den Brink, J. (2005). New light on magnetic excitations: indirect resonant inelastic X-ray scattering on magnons. *Europhysics Letters*, 80, 4.

[109] Vernay, F., Moritz, B., Elfimov, I., Geck, J., Hawthorn, D., Devereaux, T., & Sawatzky, G. (2008). Cu K-edge resonant inelastic x-ray scattering in edge-sharing cuprates. *Physical Review B*, 77(10), 104519.

[110] Vershinin, M., Misra, S., Ono, S., Abe, Y., Ando, Y., & Yazdani, A. (2004). Local Ordering in the Pseudogap State of the High-Tc Superconductor $Bi_2Sr_2CaCu_2O_{8+\delta}$. *Science*, 303(5666), 1995–1998.

[111] Vignolle, B., Vignolles, D., LeBoeuf, D., Lepault, S., Ramshaw, B., Liang, R., Bonn, D., Hardy, W., Doiron-Leyraud, N., Carrington, A., Hussey, N., Taillefer, L., & Proust, C. (2011). Quantum oscillations and the Fermi surface of high-temperature cuprate superconductors. *Comptes Rendus Physique*, 12(5-6), 446–460.

[112] Vojta, M. (2009). Lattice symmetry breaking in cuprate superconductors: stripes, nematics, and superconductivity. *Advances in Physics*, 58(6), 699–820.

[113] Žitko, R. (2011). SNEG – Mathematica package for symbolic calculations with second-quantization-operator expressions. *Computer Physics Communications*, 182(10), 2259–2264.

[114] Wakimoto, S., Yamada, K., Tranquada, J., Frost, C., Birgeneau, R., & Zhang, H. (2007). Disappearance of Antiferromagnetic Spin Excitations in Overdoped $La_{2-x}Sr_xCuO_4$. *Physical Review Letters*, 98(24), 247003.

[115] White, S. & Scalapino, D. (2000). Phase separation and stripe formation in the two-dimensional t-J model: A comparison of numerical results. *Physical Review B*, 61(9), 6320–6326.

[116] Wilkins, S., Spencer, P., Hatton, P., Collins, S., Roper, M., Prabhakaran, D., & Boothroyd, A. (2003). Direct Observation of Orbital Ordering in $La_{0.5}Sr_{1.5}MnO_4$ Using Soft X-ray Diffraction. *Physical Review Letters*, 91(16), 167205.

[117] Yao, H., Lee, D.-H., & Kivelson, S. (2011). Fermi-surface reconstruction in a smectic phase of a high-temperature superconductor. *Physical Review B*, 84(1), 012507.

[118] Yarkony, D. & Silbey, R. (1976). Comments on exciton phonon coupling: Temperature dependence. *J. Chem. Phys.*, 65(3), 1042.

[119] Yeh, N.-C. & Beyer, A. D. (2009). Unconventional low-energy excitations of cuprate superconductors. *International Journal of Modern Physics B (IJMPB)*, 23(22), 4543–4577.

[120] Zaanen, J. & Gunnarsson, O. (1989). Charged magnetic domain lines and the magnetism of high-T_c oxides. *Physical Review B*, 40(10), 7391–7394.

[121] Zaanen, J. & Sawatzky, G. (1990). Systematics in band gaps and optical spectra of 3D transition metal compounds. *Journal of Solid State Chemistry*, 88(1), 8–27.

[122] Zegkinoglou, I., Strempfer, J., Nelson, C., Hill, J., Chakhalian, J., Bernhard, C., Lang, J., Srajer, G., Fukazawa, H., Nakatsuji, S., Maeno, Y., & Keimer, B. (2005). Orbital Ordering Transition in Ca_2RuO_4 Observed with Resonant X-Ray Diffraction. *Physical Review Letters*, 95(13), 136401.

[123] Zeyher, R. & Greco, A. (2013). Self-energy effects in electronic Raman spectra of doped cuprates due to magnetic fluctuations. *Physical Review B*, 87(22), 224511.

[124] Zhou, K.-J., Huang, Y.-B., Monney, C., Dai, X., Strocov, V. N., Wang, N.-L., Chen, Z.-G., Zhang, C., Dai, P., Patthey, L., van den Brink, J., Ding, H., & Schmitt, T. (2013). Persistent high-energy spin excitations in iron-pnictide superconductors. *Nature communications*, 4, 1470.